DECENTRALIZED MODEL PREDICTIVE CONTROL OF A MULTIPLE EVAPORATOR HVAC SYSTEM

A Thesis

by

MATTHEW STUART ELLIOTT

Submitted to the Office of Graduate Studies of
Texas A&M University
in partial fulfillment of the requirements for the degree of

MASTER OF SCIENCE

August 2008

Major Subject: Mechanical Engineering

DECENTRALIZED MODEL PREDICTIVE CONTROL OF A MULTIPLE EVAPORATOR HVAC SYSTEM

A Thesis

by

MATTHEW STUART ELLIOTT

Submitted to the Office of Graduate Studies of
Texas A&M University
in partial fulfillment of the requirements for the degree of

MASTER OF SCIENCE

Approved by:

Chair of Committee,	Bryan Rasmussen
Committee Members,	Charles Culp
	Alan Palazzolo
Head of Department,	Dennis O'Neal

August 2008

Major Subject: Mechanical Engineering

ABSTRACT

Decentralized Model Predictive Control of a

Multiple Evaporator HVAC System. (August 2008)

Matthew Stuart Elliott, B.S., Texas A&M University

Chair of Advisory Committee: Dr. Bryan Rasmussen

Vapor compression cooling systems are the primary method used for refrigeration and air conditioning, and as such are a major component of household and commercial building energy consumption. Application of advanced control techniques to these systems is still a relatively unexplored area, and has the potential to significantly improve the energy efficiency of these systems, thereby decreasing their operating costs.

This thesis explores a new method of decentralizing the capacity control of a multiple evaporator system in order to meet the separate temperature requirements of two cooling zones. The experimental system used for controller evaluation is a custom built small-scale water chiller with two evaporators; each evaporator services a separate body of water, referred to as a cooling zone. The two evaporators are connected to a single condenser and variable speed compressor, and feature variable water flow and electronic expansion valves. The control problem lies in development of a control architecture that will chill the water in the two tanks (referred to as cooling zones) to a desired temperature setpoint while minimizing the energy consumption of the system.

A novel control architecture is developed that relies upon time scale separation of the various dynamics of the system; each evaporator is controlled independently with a model predictive control (MPC) based controller package, while the compressor reacts to system conditions to supply the total cooling required by the system as a whole. MPC's inherent constraint-handling capability allows the local controllers to directly track an evaporator cooling setpoint while keeping superheat within a tight band, rather than the industrially standard approach of regulating superheat directly. The compressor responds to system conditions to track a pressure setpoint; in this configuration, pressure serves as the signal that informs the compressor of cooling demand changes. Finally, a global controller is developed that has knowledge of the energy consumption characteristics of the system. This global controller calculates the setpoints for the local controllers in pursuit of a global objective; namely, regulating the temperature of a cooling zone to a desired setpoint while minimizing energy usage.

DEDICATION

To my teachers

ACKNOWLEDGEMENTS

I would first thank Dr. Bryan Rasmussen, for his guidance and support—financial and moral—during the development of the contents of the following pages, as well as Professors Alan Palazzolo and Charles Culp for serving on my advisory committee. Thanks also to all of my professional mentors throughout my years in industry; without their wisdom and instruction much of what follows would have not been possible, or at least much more difficult.

Additionally, I would like to thank my colleagues/comrades/partners in crime from the Thermo-Fluids Controls Laboratory, for much enjoyable discussion and fellowship, as well as for their seemingly limitless patience and tolerance for gallons of spilled water, earsplitting compressor noise, and the occasional wrench thrown across the room in frustration.

Finally, thanks go to my family and friends, for their love, encouragement, and understanding. If this makes you proud, then indeed I am well satisfied.

TABLE OF CONTENTS

Page

CHAPTER Page

LIST OF FIGURES

Page

Page

Page

Page

Page

LIST OF TABLES

Page

CHAPTER I

INTRODUCTION

Energy is a key foundation upon which the world's economy and the modern way of life are built. The presence of electricity in modern life allows people to conveniently preserve food with refrigeration, cool their homes and offices via air conditioning, and operate electronic devices in the pursuit of both profit and leisure. As the developing world continues to grow, mankind's ever-increasing appetite for energy ensures that the cost of the modern electricity-driven lifestyle will continue to increase. This economic reality, combined with the effects of man's energy related activities on the climate of our planet, creates an important opportunity to develop methods of energy consumption that are efficient, flexible, and reliable.

Vapor compression cooling (VCC) cycles—air conditioning and food refrigeration—accounted for over 30% of household electricity consumption in 2001, which is the last year for which official US Dept of Energy statistics are available [1]. VCC costs are a significant part of the expenses of managing a large building or operating a refrigerated truck. Control techniques for these cycles have traditionally consisted of simple electromechanical devices and on/off control strategies;

This thesis follows the style of *IEEE Transactions on Control Systems Technology*.

technological advances such as variable speed compressors, electronically controlled expansion valves, and improved computing speed now allow more precise control and efficient operation.

This thesis contributes an approach to controlling multiple evaporator systems with a two-level control architecture. Each evaporator has a self-contained controller directly tracking evaporator cooling to a setpoint and maintaining superheat within a band. Further, the compressor controls the first evaporator's pressure, and a discharge valve on the secondary evaporator controls its pressure. The pressure and cooling setpoints are generated by a global controller, which seeks to minimize tracking error and energy consumption.

The Control Problem

The central problem that this thesis addresses is the design of a controller that will regulate the temperature of multiple separate cooling zones independently. This is a common scenario that can be found in many applications, such as different apartments in an apartment building, different rooms in a house, or even a household refrigerator with freezer. In this case, the cooling zones are two individual volumes of water.

This controller will meet the desired temperatures of the cooling zones, and regulate the vapor compression cycle in such a way that energy efficiency is maximized as this task is completed. These are two competing control objectives; if the objective were only to consume minimal amounts of power, a minimum of cooling would be performed and the cooling zone temperatures would take an unacceptable amount of time to reach their setpoints. Similarly, if the controller ignores energy consumption, the

system will run at maximum capacity; the setpoints would be reached quickly but the process would be relatively expensive in terms of power consumption (note that this is essentially the approach taken by traditional mechanical controls for HVAC systems). Therefore, the controller must be tunable so that different weights can be placed on the competing objectives, depending upon the relative importance placed on each objective by the user. In addition, the controller should respect the limitations of the physical system being controlled. Figure 1.1 shows the control problem configuration.

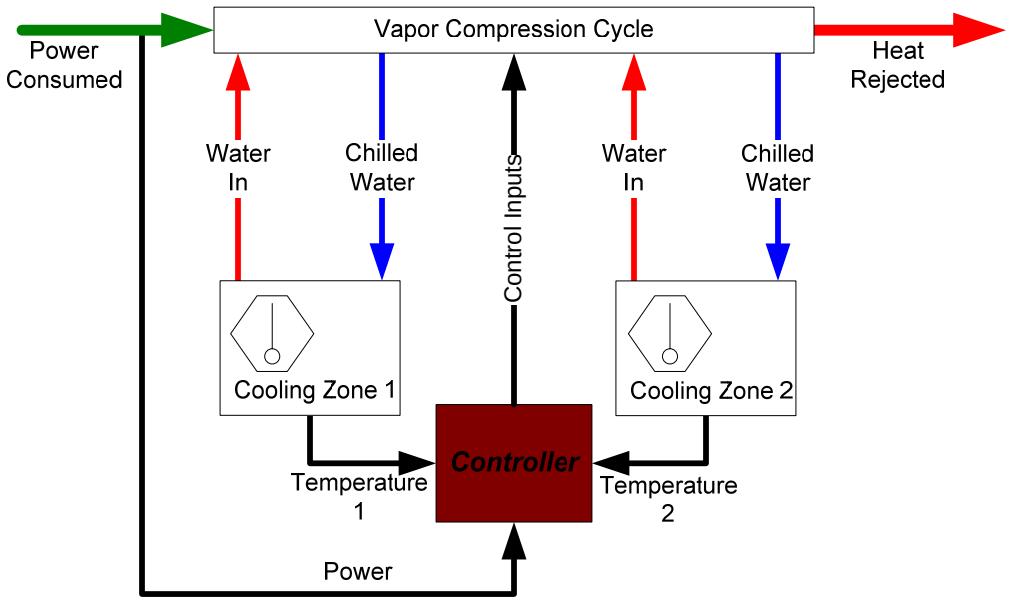

Fig. 1.1 Control problem configuration

Multiple-Evaporator Vapor Compression Systems

The research in this thesis is performed on a multiple evaporator water chiller. This chiller features a suite of evaporators, each servicing a different cooling zone, and linked to a single condenser. The reader should note that this system is intended to mimic a system where the refrigerant evaporation directly cools the air in the room or cabin, and not a system where chilled water is used to cool the various cooling zones. The compressor is variable speed, which allows it to deliver only the cooling required by the system; since the compressor is typically the single largest consumer of energy in the system, variable capacity control allows energy optimal operation. Figure 1.2 is a schematic of a general multiple evaporator system with *n* evaporators; this is adapted from a single evaporator system detailed in [2].

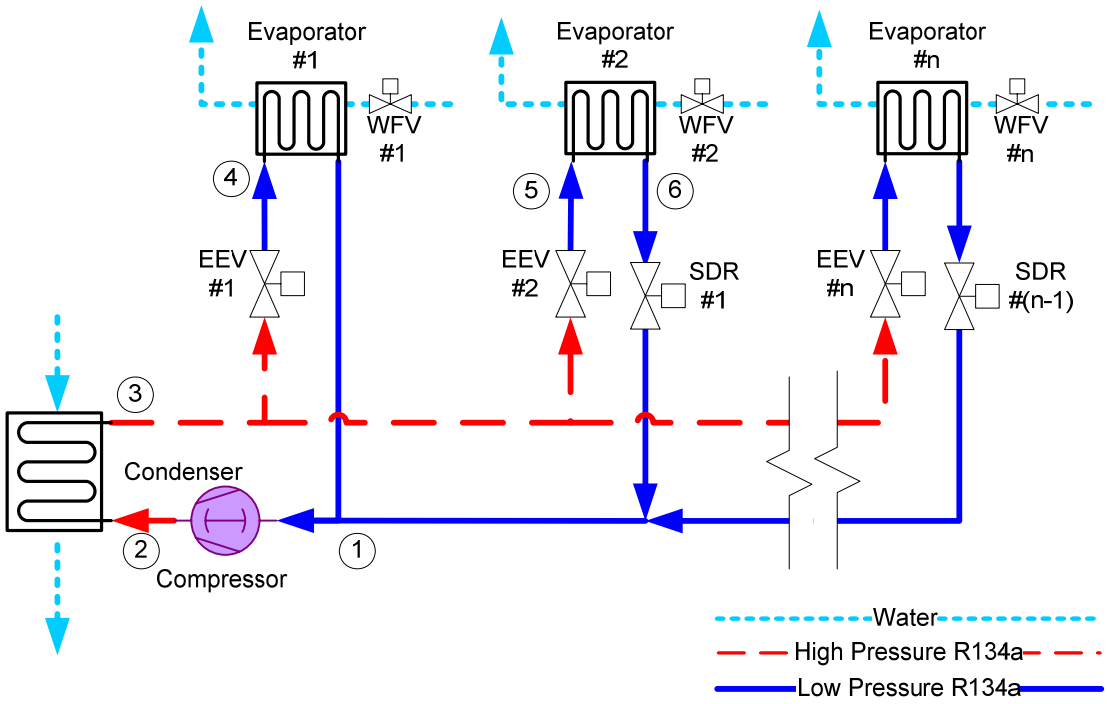

Fig. 1.2 General multi-evaporator system with designated states

The first stage of the thermodynamic cycle is at the inlet of the compressor, where refrigerant is in a low pressure, gaseous state, denoted as state 1 in Figure 1.2. The compressor adds energy to the fluid by compressing it to a high pressure, high temperature gas (state 2). This gas passes into the condenser, where heat energy is rejected from the refrigerant to the secondary fluid (water or air). This causes the refrigerant to condense to a high pressure liquid. A receiver at the end of the condenser ensures that the refrigerant becomes a saturated liquid (state 3). This saturated liquid is fed into a set of electronic expansion valves (EEVs), which meter the refrigerant flowing into their respective evaporators. The refrigerant is now a two-phase fluid (states 4 and 5). This two phase fluid absorbs heat from the water entering the evaporators, chilling the water and causing the refrigerant to evaporate. This low pressure gas exits the evaporators and returns to the compressor. The discharge valve (SDR) on the secondary evaporators creates a pressure differential between evaporators, thus allowing them to provide cooling at different saturation temperatures; at the inlet of the SDR, the refrigerant will be superheated at a higher pressure than that of the primary evaporator (state 6). After the refrigerant passes through the SDR, it will be at the same state as the refrigerant at the exit of the primary evaporator (state 1). The water flow valves (WFVs) regulate the flow of secondary fluid across each of the evaporators; they are equivalent to variable speed fans in an air-based system. Figure 1.3 shows the pressure-enthalpy (P-h) diagram of the cycle superimposed on the refrigerant vapor dome.

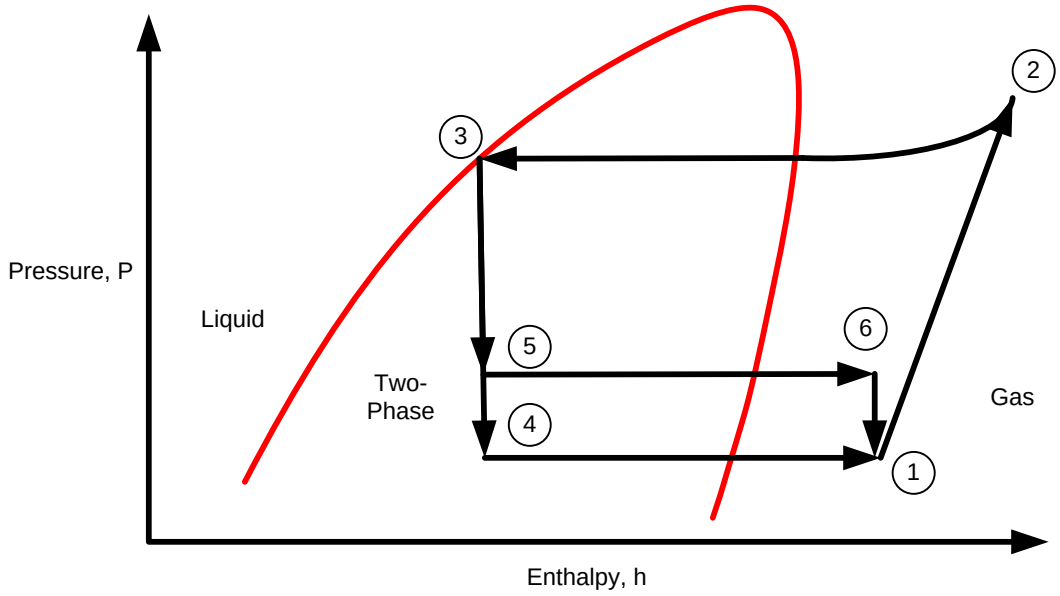

Fig. 1.3 P-h diagram for two-evaporator system

Model Predictive Control

VCC systems have many inherent constraints—minimum evaporator pressures, maximum compressor speeds, valves cannot open past 100%, et cetera. In addition, the dynamics of these systems are enormously complex and feature a large amount of cross-coupling. The presence of these constraints and dynamic coupling implies that a multiple-input, multiple-output (MIMO) control approach is desirable. This is especially true for a system with multiple evaporators, where each cooling zone has an individual evaporator to meet its cooling needs, and the entire system is serviced by a single compressor and condenser. In light of the constraint handling and controller parameter

tuning requirements set forward in the previous section, model predictive control is an ideal choice for the control of multiple evaporator systems.

Model predictive control (MPC) is an overarching term for a suite of control strategies mostly developed in industry during the 1970s. A controller based upon one of these strategies selects control inputs via the online optimization of a predefined cost function at discrete time intervals. MPC allows for explicit handling of input, output, and state constraints—if a set of control inputs violate a constraint as predicted by the dynamic model, that set of inputs is discarded as a possible choice. MPC is also well suited for multiple-input, multiple-output (MIMO) control. Therefore, closely-coupled dynamics in the plant can be controlled with a single controller, whereas a group of single-input, single-output (SISO) controllers will frequently interfere with each other. Furthermore, since the cost function can be changed online to match changes in global or external conditions, MPC-based controllers can have a high level of flexibility in meeting general operational goals as the operating conditions change.

MPC is also referred to as receding horizon control, since the horizon for which prediction is performed moves ahead in time at each sampling instant. There are two important horizons in MPC, both of which are expressed in terms of sampling instants. The prediction horizon is the span of time for which the plant outputs are predicted. The control horizon is the number of control inputs that are calculated in the prediction computation, and is always smaller than the prediction horizon. The size of the prediction horizon is generally limited by computation speed; it is important to choose

the control horizon such that the difference between the control and prediction horizons is as least as long as it takes for all dynamics in the system to settle out [3].

Generic MPC Example

As an example of a generic MPC controller, consider Figure 1.4. At the current sampling instant, $k = 0$, the input $u = 0.375$ and the output $y = 0$. As shown on the left hand plot, the control horizon is 3 sampling instants and the prediction horizon is 5 sampling instants. Assume that the three input profiles u_1, u_2, and u_3 are the possible input combinations to the plant, with their respective open loop dynamic responses y_1, y_2, and y_3 shown on the right side of the figure. The desired output (setpoint) is 0.333. The resulting cost function value for each scenario is given by *J*, next to the output plots. This cost function can be assumed to be dependent upon the weighted tracking errors at each sampling instant over the prediction horizon, as well as each weighted control input at each sampling instant over the control horizon:

$$J = \sum_{i=1}^{Ny} \lambda_e (y_{set} - y_{actual})_i + \sum_{j=1}^{Nu} \lambda_u \Delta u_j$$

In this equation, *Ny* is the prediction horizon, λ_e is the weight placed on error, *Nu* is the control horizon, λ_u is the weight placed on changes in control, and Δu is the change in input.

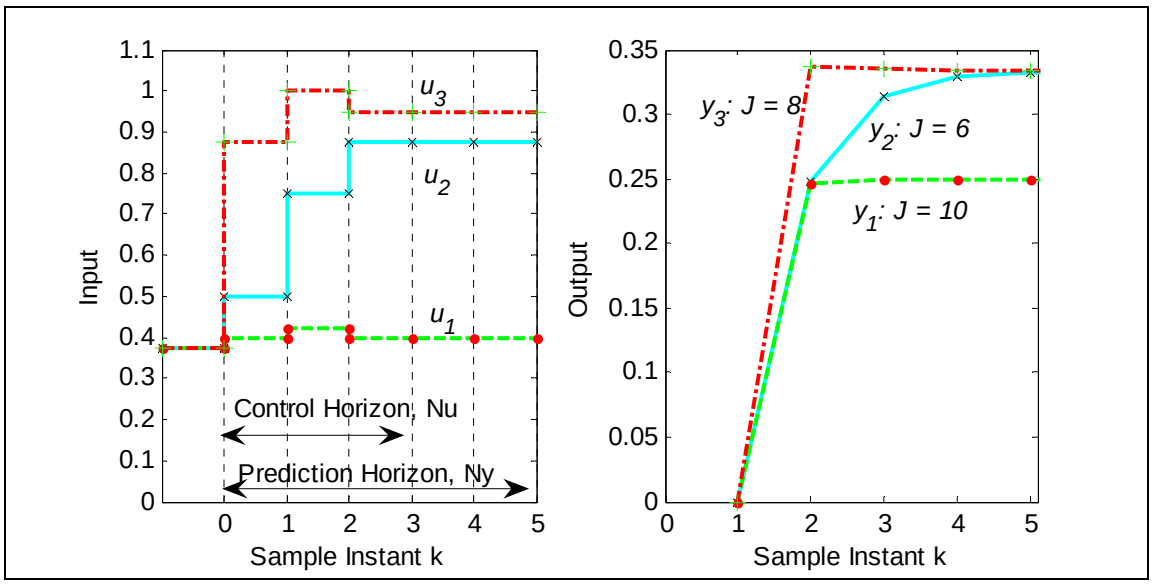

Fig. 1.4 MPC example inputs and outputs

Note that in calculating the command profiles, *Nu* changes in the input are calculated. After the time is larger than *Nu*, i.e. from $k = 3$ through $k = 5$, the value of the input is held constant. In this case, since the cost function is minimized for the response to input profile u_2, the first value only of u_2 (i.e., $u = 0.5$) is input to the plant at the current sampling instant. At the next sample instant, this process is repeated: the horizons are moved forward by one sample time, an optimal solution is computed, and the first control input of the optimal command profile is applied.

If a constraint were placed on the input so that it could not be larger than 0.9, u_3 would no longer be a valid input, and only u_1 and u_2 would be considered. Similarly, if the output were constrained to be less than 0.3, then u_2 and u_3 would no longer be valid inputs, since their output responses would violate the specified output constraint. In this case u_1 would be chosen, even though it is not the optimal choice in the unconstrained

case. Similarly, if a large weight were placed on controller action in the cost function calculation, and a very small weight placed upon error, it is possible that the cost function for u_1 would be the minimum case and would be chosen as the command profile, even though the setpoint is never met for this case. Clearly, careful selection of the constraints and tuning parameters is an important part of any MPC implementation.

Literature Review

The beginnings of refrigerant flow control are rooted in mechanical expansion and metering devices such as the thermal expansion valve (TEV). The TEV is a very widely used mechanical feedback device that regulates superheat at the evaporator exit; however, it tends to exhibit a limit cycle behavior commonly referred to as valve hunting, wherein the evaporator superheat oscillates without settling to a steady state value. Broerson and van der Jagt used a linearized dynamic model of an evaporator to show that this hunting behavior is due to interactions between the TEV with the evaporator dynamics [4]. Gruhle and Isermann also modeled the TEV and evaporator system, and discuss the conflict between efficient operation—a small superheat—with safe operation—keeping superheat above a minimum value [5]. They explored using an EEV with a PI control loop to control superheat, with improved results over the TEV. Additional modeling work on the TEV with evaporator has been done by Ibrahim in [6], and James in [7], although no experimental validation is provided in these researches. More recently, Chen, et al., explored the phenomenon of minimum stable superheat, and offered an explanation for the onset of hunting due to sudden changes in heat transfer

characteristics [8]. These widely observed problems with valve hunting led to exploration of the use of automatic controls with refrigeration and air conditioning systems.

The application of classical control theory to variable refrigerant flow systems has generally involved using the EEV to control superheat, analogous to the thermal expansion valve used in purely mechanical control systems. As mentioned earlier, Gruhle and Isermann compared the performance of a PID controller favorably to that of a TEV in [5]. In addition, other single-input, single-output controllers have been implemented that use the EEV to control superheat. In [9], Outtagarts compared the use of PID with that of optimal qualitative regulation. Finn and Doyle compare PID performance with that of a TEV, and explore using adaptive PID control to improve performance [10]. Larsen, Thybo, and Rasmussen applied a nonlinear evaporator model and cascaded PID loops to the superheat control problem, where an outer loop calculated the necessary mass flow for a desired superheat setpoint, and fed this as a setpoint to an inner PID controller, which directly controlled the EEV [11].

Due to the cross-coupled dynamics of VCC systems, purely SISO control approaches are severely limited, as shown by He, Liu, and Asada in [12]. Even a decoupled approach, where the EEV and variable compressor speed control different output variables, can have unacceptable results if not structured correctly, as found by Parnitzki in [13]. He, Liu, and Asada applied an advanced model-based control technique, Linear Quadratic Gaussian (LQG) control, in a multi-input, multi-output (MIMO) configuration to regulate superheat and evaporator temperature using a

variable-speed compressor and EEV [14]. In [15] and [16], He and Asada developed a control architecture implementing a nonlinear observer to perform feedback linearization, allowing a PI controller to control compressor speed. Lin and Yeh decoupled the control of a similar system, taking advantage of the difference in time scales of the dynamics to use the compressor to control evaporator pressure and the EEV to control superheat, with the evaporator pressure setpoint generated by a function of the difference between actual and desired room temperature [17]. In [18], the authors applied multi-variable indirect adaptive Linear Quadratic Regulator (LQR) control to an automotive air conditioning system, using the expansion valve and air fan speed to control evaporator pressure and superheat. Singh et al. also applied multivariable adaptive LQR control effectively, but to a two-zone fan coil heating system instead of a VCC system [19]. The interested reader can find descriptions of LQR, LQG, and other modern multivariable control methods in [20].

The primary weakness of most advanced control techniques with respect to VCC systems is the same as that of classical control: inability to account for constraints explicitly in the controller design, leading to a lower level of performance [21]. MPC has been used to solve many control problems in the chemical and refining industries [22]. Indeed, these industries specifically developed MPC to operate complex multivariable systems near constraints without violating them, since the most economic operating conditions in chemical processing are typically at intersections of constraints [23]. Academic research followed after successful industrial implementation, in a reversal of the usual theory/application gap; many of the MPC controllers in wide use

are proprietary algorithms [23]. Advancements in the study of stability in the presence of constraints and robustness have been made; Mayne provides a useful survey of the work performed in [24]. These academic advancements have been applied to systems varying from industrial chemical test stands [25] to air quality control in livestock barns [26]. Rawlings published a tutorial that provides an excellent reference in learning to use MPC [27]. In addition, widely referenced textbooks have been published by Camacho [21] and Rossiter [3], and Clarke published a collection of MPC papers describing advances in robustness, stability, and applications [28]; these are readily available resources for the reader wishing to learn more.

While the linear MPC problem has been heavily addressed, the control of nonlinear systems is still an open problem. Processes with a higher degree of process nonlinearity and where market forces require frequent changes in operating conditions, such as polymers and gas plants, are still not widely controlled with MPC [29]. Algöwer provides a collection of literature on the nonlinear model predictive control (NMPC) problem in [30]. The use of multiple model predictive control (MMPC) is a widely pursued avenue of interest; in MMPC a suite of linear models are developed: one for each linearized operating point deemed necessary by the user, and the controller switches among the individual models as operating conditions change [31].

Direct application of MPC to VCC cycles is still limited, although researchers have used MPC-based approaches to control airflow in the air handling units of large building cooling systems. These approaches have either used an MPC algorithm to directly control the system actuators as in [32], or used an MPC algorithm to set gains

for local PID controllers as in [33] and [34]. Another common approach is to use an MPC algorithm to perform controller self-tuning, whether for commissioning or to adapt to changing conditions, seen in [35] and [36]. Sousa et al. used MPC with fuzzy logic to control water valves in radiative heating systems [37]. He et al. extended this fuzzy model approach to the control of an HVAC air handling unit (AHU), such as that found in a large building HVAC system [32]. Leducq et al. applied a MIMO MPC algorithm to a single-evaporator water chiller system using a nonlinear model, controlling cooling and temperatures using compressor speed and water flow [38]. Even in this latter approach, however, the EEV was used with a PI loop to control superheat. One of the thrusts of this research will be to explore the idea of using the EEV for other purposes; since the EEV is at the entrance of the evaporator and superheat is measured at the end of the evaporator, there is significant dynamic behavior between the actuator and the controlled variable.

This research will involve a system with two evaporators, simulating a cooling system with multiple cooling zones. An internet search of multiple evaporator systems reveals many patents and commercial developed products, although academic research into dynamic controls of these systems is still limited, creating much potential for future exploration. They have not been implemented widely in the United States, despite their popularity elsewhere and their potential for energy savings over traditional water loop based configurations [39]. In their research into multiple-evaporator systems, Choi and Kim showed that using the EEVs and compressor in combination to modulate the capacity of each evaporator can result in better operating efficiencies, although each

EEV has a strong effect on the other evaporator [40]. Park et al. also explored this combination, calculating optimum EEV for a given compressor speed and load ratio [41]. In neither case is the design of a dynamic controller considered, although they reference the work of Fujita, who investigated using a PID loop with an EEV and variable speed compressor to control superheat and cooling capacity in a multi-evaporator system. Asada and He explored using feedback linearization in a PI loop controlling the compressor speed with a multiple-evaporator system, although simulation results only were presented [42]. Kim et al. investigated using MPC to control a multiple evaporator heat pump; in this case, the EEV was used to control the evaporator temperature. This method was shown to have performance improvements over using PI loops [43]. Shah et al. performed modeling work of a multi-evaporator system and explored control techniques; as expected, a MIMO approach was found to be superior to SISO techniques for control, due to the complexity of system dynamics [44]. Finally, Chiou et al. applied fuzzy control techniques to energy savings for small scale household air conditioners with multiple evaporators, and found better temperature regulation than could be had with traditional on/off techniques [45].

Figure 1.5 illustrates the potential for research in the confluence of several different fields of endeavor. While advanced controls—including MPC—have been applied to HVAC systems (both refrigerant flow and air handling elements), very little work has been done applying MPC to the refrigerant cycle itself. Additionally, the investigation of applications of advanced control techniques to multiple evaporator

systems has barely been explored by either the controls or HVAC communities, and therefore the potential for progress in this area is great indeed.

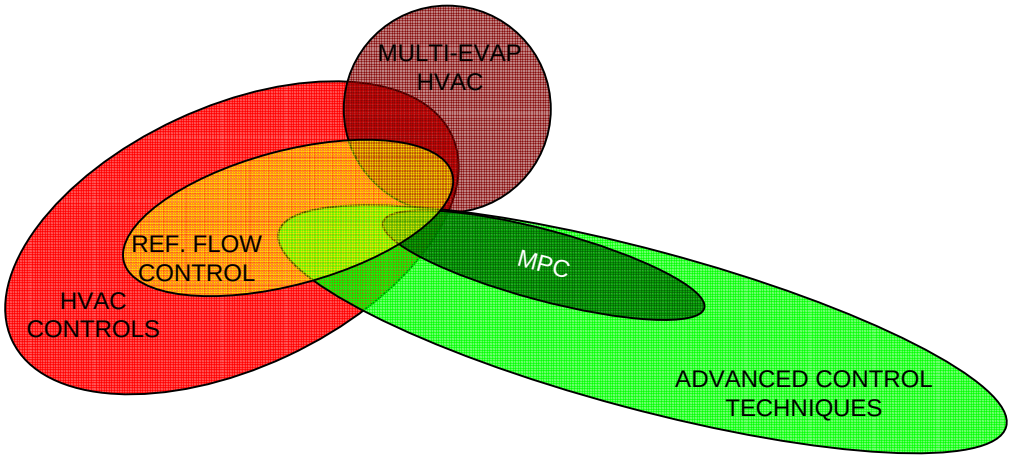

Fig. 1.5 Areas of research

Organization of Thesis

Experimental validation is important to any new control architecture; Chapter II of the thesis details the custom-built experimental system constructed for this purpose. A dynamic analysis was performed in order to develop an understanding of the dynamic relationships between the control inputs and the system states. This effort is described in Chapter III. The information from the dynamic analysis was used to design a two-level control architecture; development of the local controllers are described in Chapter IV and that of the global controller in Chapter V. A concluding discussion of the results is presented in Chapter VI.

CHAPTER II

EXPERIMENTAL SYSTEM

Overview

Justification and Organization

The experimental system used for the research presented in this thesis is a custom-built, small-scale two-evaporator water chiller. This system is intended for dynamic model validations, control development, fault detection, and other research for the Thermo-Fluids Control Laboratory. These uses and the desire for modularity and flexibility were the primary considerations during the process of component selection and system construction. This chapter first gives an overview of the flow logic and construction of the primary (refrigerant) system and the secondary (water) system. Construction details of the heat exchangers are given. Details of the individual components for the primary and secondary loops are explained. The sensors used in the system are described. Finally, the software and data acquisition systems are detailed. Wiring schematics for the electrical and electronic components can be found in the Appendix. Figure 2.1 is a photo of the entire system.

Fig. 2.1 Entire system

Primary System

The refrigerant or "primary" side of the system is constructed of copper tubing. Where possible, SAE 45° flare fittings are used to connect the tubing together, since they are economical and reusable. Wherever it was not practical to flare tubing, Swagelok brand compression fittings were used. For some components, such as at the compressor inlet and outlet ports, soldered connections were required. Nominal 1/4" tubing is used for lines carrying liquid, and 3/8" tubing is used for gas lines and lines carrying two-phase fluid (i.e., from the expansion valves to the evaporators). A liquid receiver is installed at the end of the condenser to ensure that saturated liquid is fed to the expansion valves. Manual shutoff valves are used throughout the system to allow retention of refrigerant while sections of the system are being worked upon as well as to provide manifolds to route refrigerant through different expansion devices or even to bypass the liquid receiver if so desired. The compressor is a variable speed compressor that has an integrated accumulator to prevent liquid from passing into the compression chamber. Figure 2.2 is a schematic of the primary side of the system. Component descriptions are provided later in the chapter; additionally, the Appendix contains a complete table of the schematic reference numbers (A2, MV8, etc.) and a description of the role played by each.

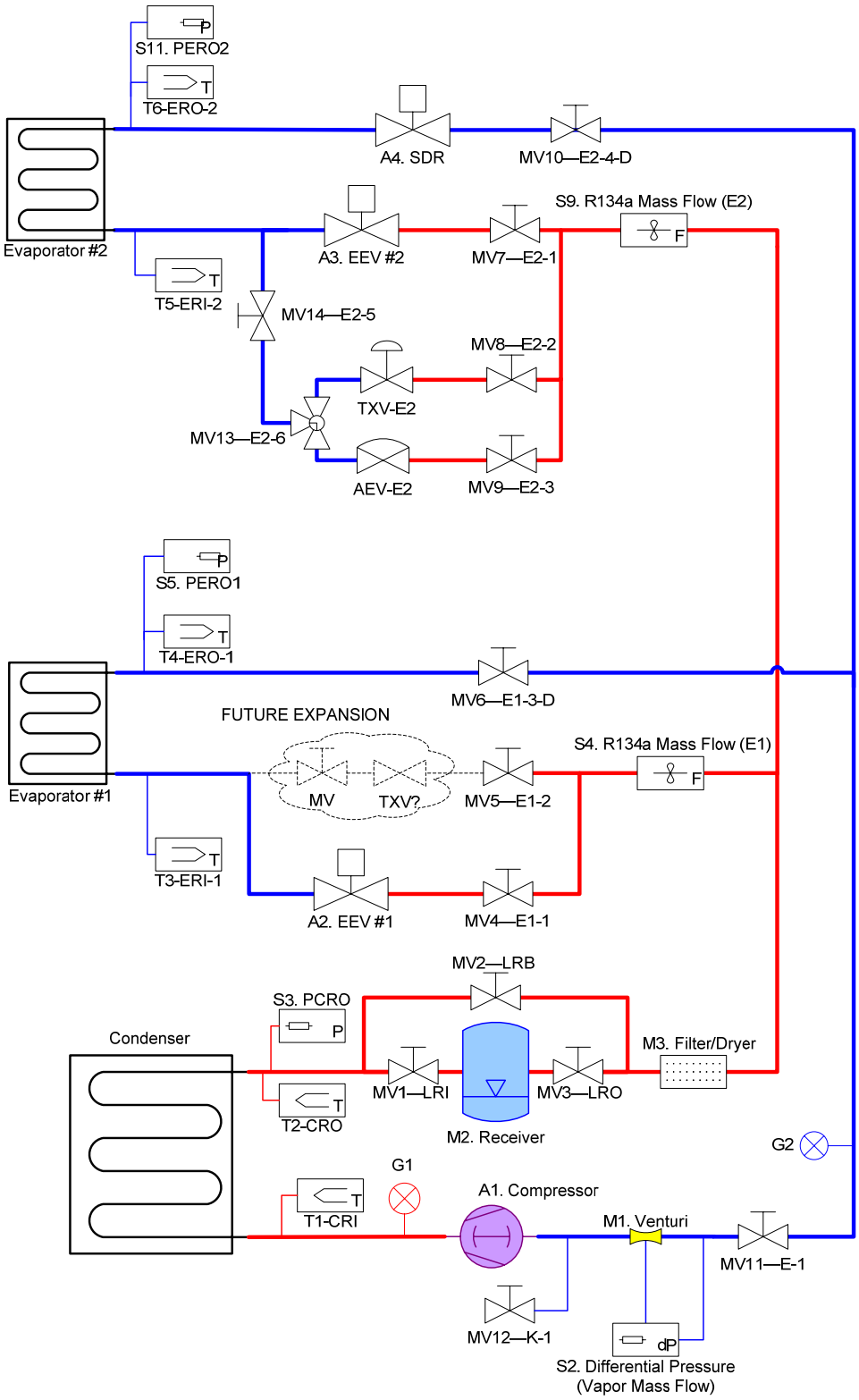

Fig. 2.2 Primary (refrigerant) loop

Secondary System

Water is used as the "secondary" working fluid in the heat exchangers, since the flow rate of water is much easier to measure and regulate than that of air. The water is fed via gravity to each of the three heat exchangers from water tanks. Each of these supply tanks has a pump inlet as well as an overflow outlet. Since the pumps delivering water to the supply tanks are by design pumping more water than is being fed to the heat exchangers, there is an excess of water supplied to the top tanks. This excess is removed from the supply tanks via the overflow lines, which flow into the return tanks at the bottom of the system. This arrangement guarantees that a constant head of water pressure (experimentally verified as within 1.8%) is present during system operations regardless of water flow to the heat exchangers. Figure 2.3 shows the overflow configuration; Figures 2.4 and 2.5 are photos of the top and bottom tanks, respectively.

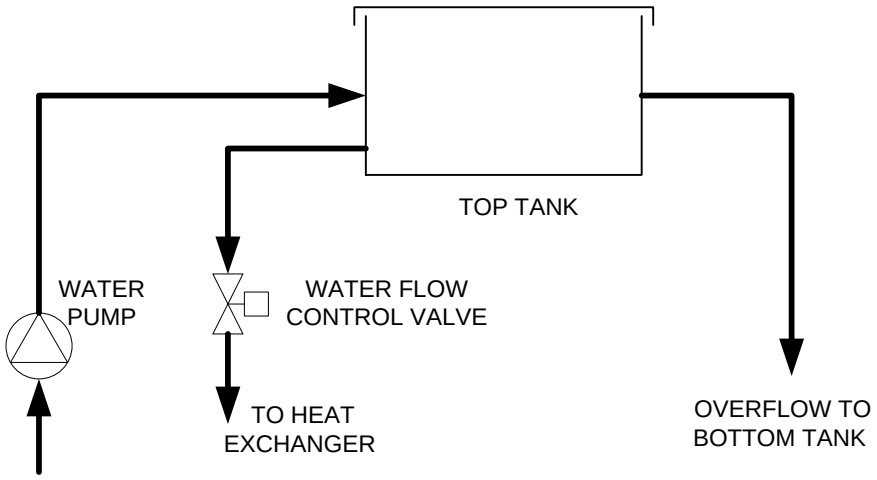

Fig. 2.3 Water overflow arrangement

Fig. 2.4 Top tanks

Fig. 2.5 Bottom tanks

After the water is heated by the condenser or chilled by the evaporators, it is fed into one of three return tanks. Each of the heat exchangers, therefore, has its own isolated water supply. This allows for simulations of controlling the temperature of a cabin or room. A valve manifold also allows for heated condenser water to be diverted into the evaporator tanks, which allows simulation of temperature disturbances and removes excess heat from the condenser water, since chilled water overflow from the evaporator return tanks is fed into the condenser return tank. Figure 2.6 is a photo of the condenser manifold. A modified window air conditioner is also used to remove the heat added to the condenser water, which helps to keep the condenser supply water temperature constant within a few degrees over the course of an experiment. Figure 2.7 is a photo of this arrangement. A valve manifold is also used with the water pumps so that water from any of the three bottom tanks can be pumped to any of the three top tanks. This feature, along with the return tanks' overflow lines, means that the water from the heat exchangers can be re-mixed during an experimental run, and that the water temperature fed into the heat exchangers can be held constant during a model validation run. This becomes especially important while mapping out system behavior over the range of operation, and also allows for application of load disturbances, as will be detailed later in the thesis. Figure 2.8 is a photo of the pump manifold. Figure 2.9 is a schematic of the entire secondary system.

Fig. 2.6 Condenser manifold

Fig. 2.7 Condenser water chiller

Fig. 2.8 Water pump manifold

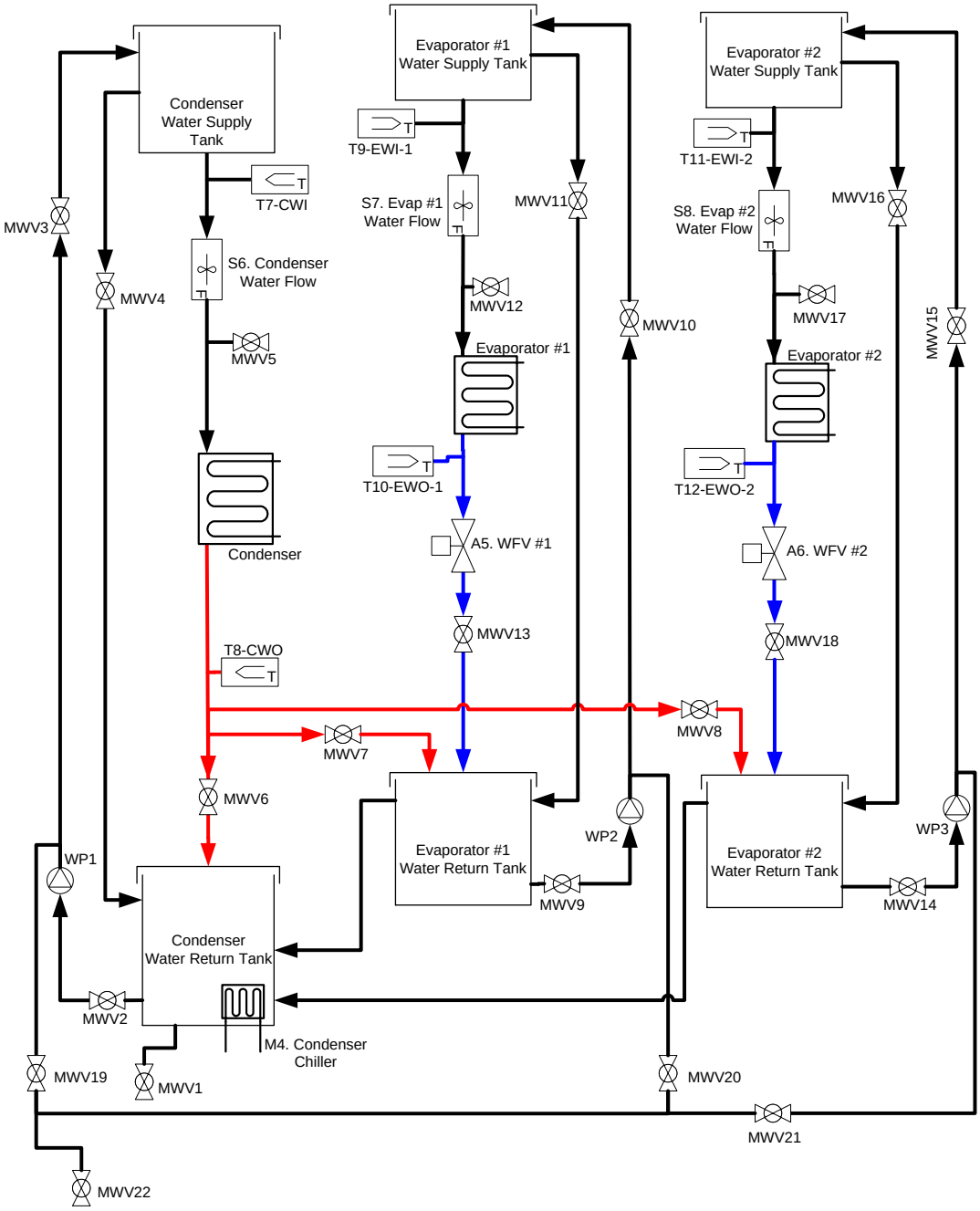

Fig. 2.9 Secondary loop schematic

Heat Exchangers

The three heat exchangers—two evaporators and one condenser—constructed for the system provide the interface between the primary and secondary loops and are the means by which energy is transferred within the system. Since the experimental rig is constructed for model validation as well as for the research presented in this thesis, each exchanger is of a different design.

The condenser, which is the largest of the three, consists of 3/8" copper tubing wound around a 2" Schedule 40 PVC pipe (all pipe sizes listed are nominal size unless noted otherwise). This is contained within a chamber constructed of 4" Schedule 40 PVC pipe. Three intake runners feed water into the chamber; the water comes into contact with the copper tubing, drawing heat from the refrigerant inside the tubing during the condensing process. Two exhaust runners allow the water to drain into the lower tank. The rationale behind this "cross-flow" style of construction was to attempt to simulate water and refrigerant flowing at right angles to each other in order to simplify the modeling assumptions used when modeling flow inside the condenser. The outer condenser shell is approximately 0.74 m long; the uncoiled length of tubing is approximately 8.38 m. Figure 2.10 is a photo of the condenser; figure 2.11 shows a cutaway view of the condenser construction.

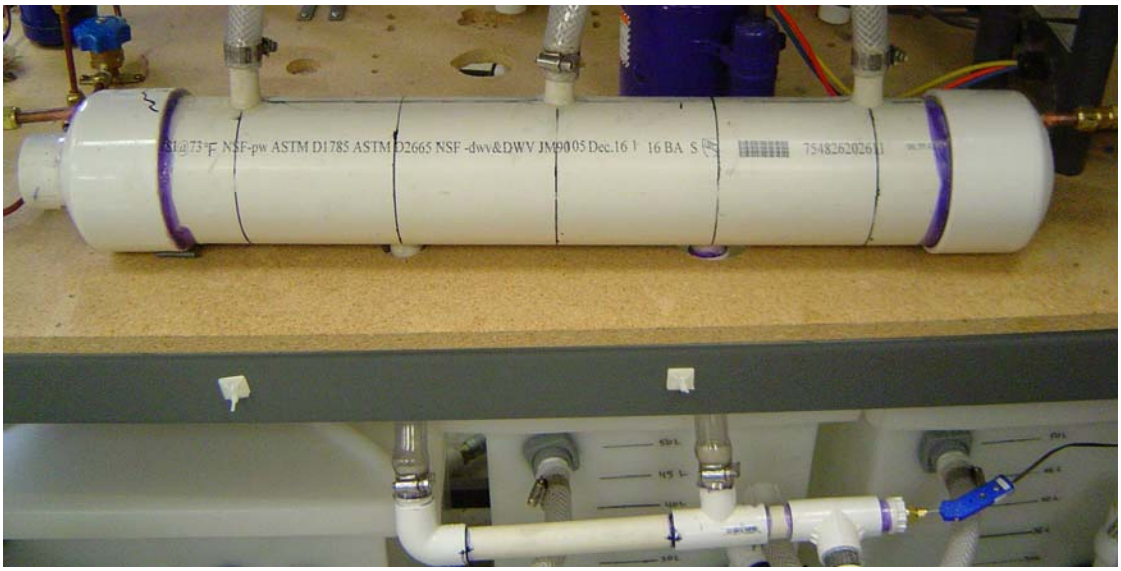

Fig. 2.10 Condenser

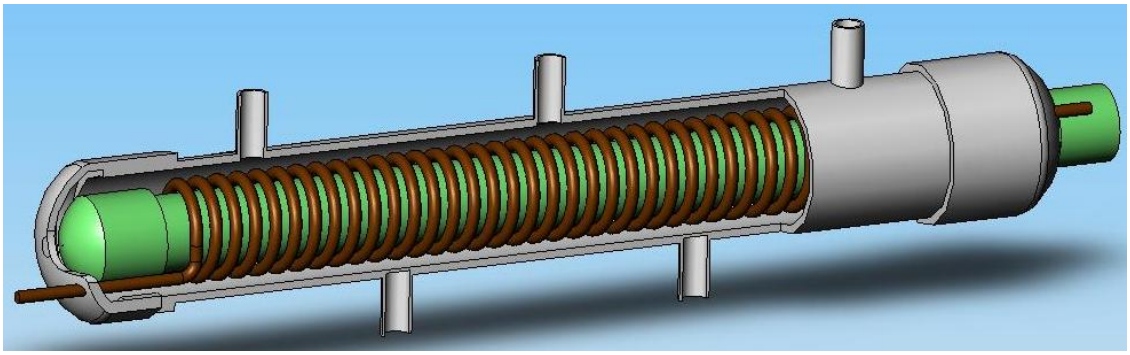

Fig. 2.11 Condenser construction

Both evaporators are of a simple shell and tube style construction, wherein the primary fluid flows in a center tube, and the secondary fluid flows around this center in an outside shell. The inner tube is a straight run of 1/2" copper refrigeration tubing, 1 m long; 1/2" to 3/8" adapter fittings are soldered onto the ends of the tube to interface with the 3/8" copper lines at the entrance and exit of the evaporator. The outer shell is 3/4" Drain/Waste/Vent (DWV) PVC pipe, 1 m long. The water enters via a tee fitting at one end of the pipe and exits the other end. Evaporator #2 is a counterflow heat exchanger; the refrigerant and water flow in opposite directions. Evaporator #1 is a co-flow heat exchanger, that is, the refrigerant and water flow in the same direction. While co-flow is not as efficient as counterflow, this arrangement allows for model validation of both styles of heat exchanger. Figure 2.12 is a photo of the evaporators; figure 2.13 shows the construction of the two evaporators.

Fig. 2.12 Evaporators

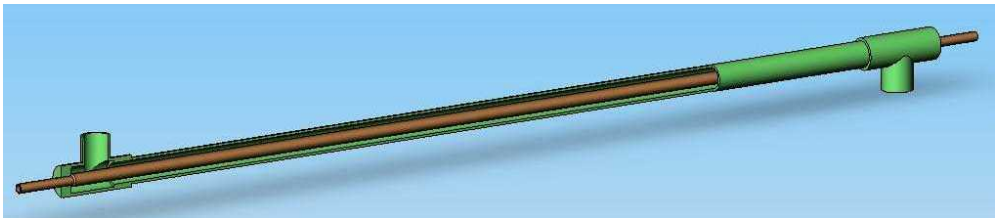

Fig. 2.13 Evaporator construction

Primary Loop Components

Refrigerant Valves

The expansion valves used in the system are electric expansion valves (EEVs) manufactured by Sporlan. Each valve is controlled by a Sporlan IB interface board. These boards accept a 4-20 milliamps (mA) command signal from the user and position the valve proportionally according to the signal using the step motor integral to the valve assembly. They have a resolution of 1596 steps at 200 steps per second, for a total travel time of approximately 8 seconds from completely open to completely closed. Figure 2.14 is a photo of the expansion valve.

Fig. 2.14 Electronic expansion valve (EEV)

In order for the second evaporator to operate at a higher pressure than the first evaporator, a discharge control valve must be placed at the end of the second evaporator. For this purpose a Sporlan SDR valve was selected. It is also controlled with a Sporlan IB board and a 4-20 mA signal in exactly the same manner as the expansion valve. Figure 2.15 is a photo of the discharge valve (hereinafter referred to as the SDR). The stepper motor has exactly the same characteristics as that of the EEV.

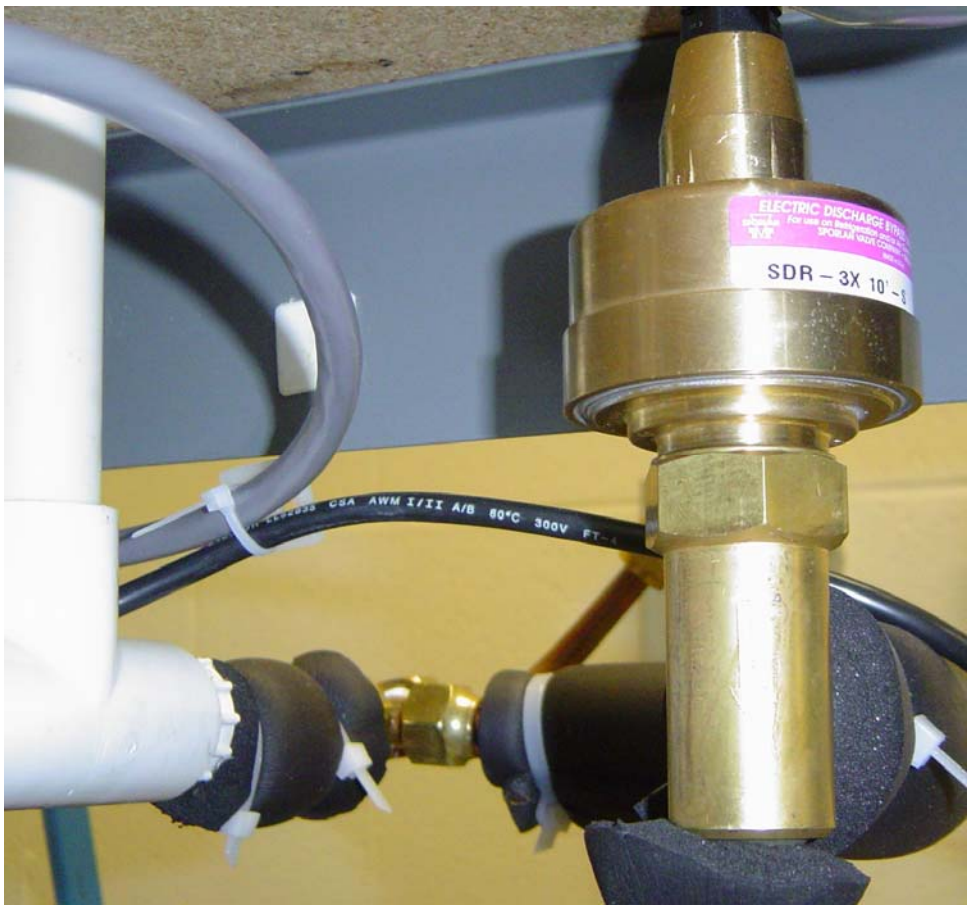

Fig. 2.15 Discharge valve (SDR)

Manual shutoff valves are also installed at various places in the system; this allows one of the evaporators to be shut off, or for a section of the primary loop to be closed off while another section is being worked on. This way the majority of the refrigerant in the system can be stored in the liquid receiver while the system is being worked on, resulting in a minimum of refrigerant loss. Figure 2.16 is a photo of one of these valves.

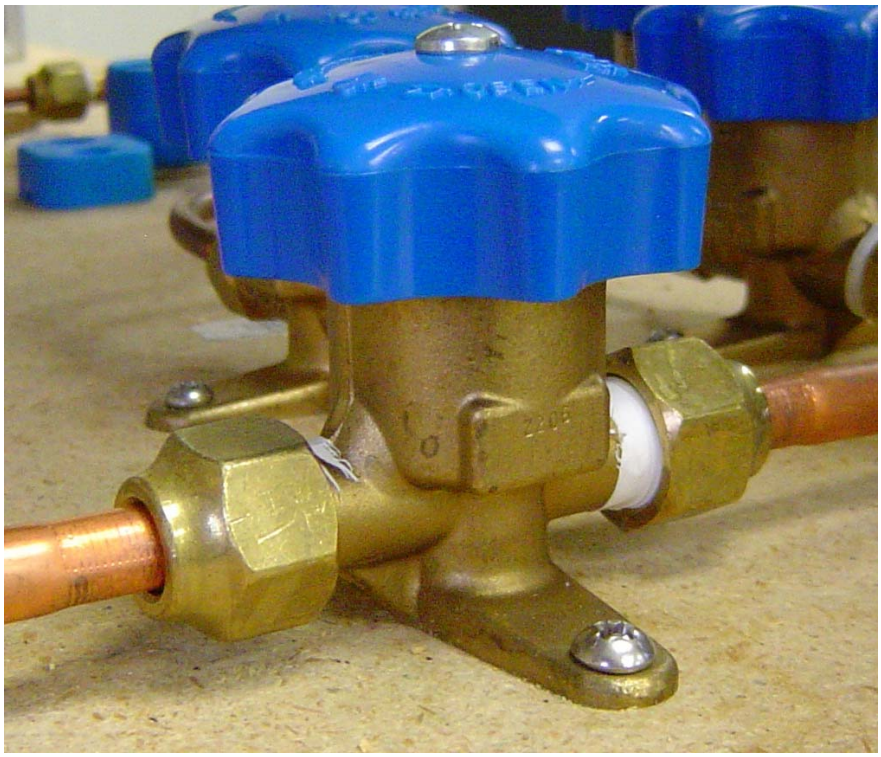

Fig. 2.16 Manual shutoff valve

In addition to the EEVs, the second evaporator has two auxiliary selectable expansion devices for model validation or other experimental purposes not related to the research presented in this thesis. These two devices are a Thermal Expansion Valve (TXV) and an Automatic Expansion Valve (AEV). The desired auxiliary valve is selected using a 3-way L-type ball valve; there is a shutoff manual valve at the end of the selection manifold for when the EEV is used. Figure 2.17 is a photo of this arrangement.

Fig. 2.17 Auxiliary expansion device manifold, evaporator #2

Compressor

The compressor for the system is a Sierra model manufactured by Masterflux. This is a scroll-type variable speed compressor that uses a 48V DC power supply and is designed to operate with R134a refrigerant. This voltage is fed into a compressor control module included by the manufacturer, which accepts control signals from the user and regulates the compressor speed. The control module allows for a manual switch to turn the power on and off, outputs a tachometer signal, the current consumed, and accepts a 0-5 volt signal to control compressor speed. The compressor speed varies from 1800 to 6500 RPM. Total compressor capacity is approximately 1.5 tons of cooling. Figure 2.18 is a photo of the compressor.

Fig. 2.18 Masterflux compressor

Liquid Receiver

A liquid line receiver made by Henry Technologies is placed at the end of the condenser. This receiver serves as a safety measure to ensure that only liquid is fed into the expansion valves, thus decreasing the risk of choking the valves. Using a receiver also ensures that the liquid will be saturated rather than subcooled, which enables some assumptions with regards to enthalpy calculations and system conditions. Figure 2.19 is a photo of this component.

Fig. 2.19 Liquid receiver

Filter/Drier

A filter/drier is placed in the refrigerant flow stream after the liquid receiver manifold in order to protect the expansion devices; in addition, a sight glass is also located here to allow the operator to verify that only liquid refrigerant is being passed to the valves. Figure 2.20 is a photo of these components.

Fig. 2.20 Filter drier with sight glass

Venturi

A converging-diverging nozzle or Venturi is placed in the fluid flow immediately before the compressor. This is used with a differential pressure transducer to measure vapor mass flow into the compressor, although is not used for the research presented in this thesis. Figure 2.21 is a photo of this component.

Fig. 2.21 Venturi

Pressure Gages

Pressure gages are installed on the low and high pressure sides of the refrigerant loop. These provide a visual check that the system is working properly and give a comparison to the pressure transducers. Additionally, a Ranco pressure cutoff switch kills the power to the compressor if the high or low pressures exceed constraints. Figure 2.22 shows one of the pressure gages. Table 2.1 gives a brief description of each of the primary loop components; a list of supplier information can be found in the Appendix.

Fig. 2.22 Pressure gage

Table 2.1 Primary loop system components

Description	Qty	Manufacturer	Part Number	Notes	Schematic Reference
Electric Expansion Valve (EEV)	2	Sporlan	SEI 0.5-10-S	R134a expansion	A2, A3
Discharge Valve (SDR)	1	Sporlan	SDR-3X	Evaporator 2 pressure regulation	A4
Manual Shutoff Valve, 1/4"	8	Mueller	A14833	Refrigerant routing	MVx-xx-x
Manual Shutoff Valve, 3/8"	4	Mueller	A14835	Refrigerant routing	MVx-xx-x
3-way Ball Valve, 3/8"	1	ValveWorx	536503	Auxilary valve selector	MV13-E2-6
Compressor	1	Masterflux	Sierra 03-0982Y3	--	A1
Liquid Receiver	1	Henry Technologies	S-8060	--	M2
Filter Drier	1	Alco	EK-032	--	M3
Sight Glass	1	Emerson	AMI 1FM2	1/4" female X male SAE	--
Venturi	1	Lambda Square	VU-0.5-0.148	1/2" size; 0.148" throat	M1
High Pressure Gage	1	Omega	PGC-25L-300	0-300 psig range	G1
Low Pressure Gage	1	Omega	PGC-25L-160	0-160 psig range	G2
Pressure Shutoff Switch	1	Ranco	012-1594-70	--	--

Secondary Loop Components

Water Valves

The water flow for each evaporator is controlled by an electrically actuated valve manufactured by Erie. The control unit accepts a 4-20 mA signal that opens and closes the valve proportionally based upon the command signal. These valves require a 24VAC power supply; a transformer is used to supply this voltage to both valves. Fuses are installed on the primary and secondary windings of this transformer. Figure 2.23 is a photo of the water flow valves (WFVs). In addition, ¾" PVC ball valves are used throughout as shutoff valves for the water supply, and ½" PVC ball valves are used to bleed air out of the water lines. These valves are standard plumbing components readily available at any hardware store.

Fig. 2.23 Water flow valves

Water Pumps

The pumps for the secondary loop are manufactured by Laing. These are sealed centrifugal pumps and are not self priming. The inlet and outlet connections are ¾" male National Pipe Thread (NPT). These pumps are capable of 10 gallons per minute of flow with 8 feet of head and require standard 120 VAC power. Figure 2.24 is a photo of the pumps. Table 2.2 gives a brief description of the secondary loop components.

Fig. 2.24 Water pump

Table 2.2: Secondary loop system components

Description	Qty	Mfr.	Part Number	Notes	Schematic Reference
Water Flow Valve (WFV)	2	Erie	APA23A000	water flow control	A5, A6
Transformer, 24 VAC	1	Honeywell	AT72D-1683	Provides power for WFV	N/A
Manual Water Valves	19	various	various	standard 3/4" PVC ball valves	MWVxx
Manual Water Valves	3	various	various	1/2" PVC ball valves used for air bleed	MWV5, MWV12, MWV17
Water Pumps	3	Laing	SM-1212-T-26	--	WPx
Condenser Water Chiller	1	Haier	HWF05XC5T	5000 BTU/hr rating	M4
Condenser Water Tanks	2	Tamco	6314	34 gallon	N/A
Evaporator Water Tanks	4	Tamco	6305	15 gallon	N/A

Transducers

Water Mass Flow

The transducers used to measure water flow, seen in Figure 2.25, are volumetric turbine-style flowmeters manufactured by Kobold Industries. These transducers output a square wave signal from an NPN transistor whose frequency corresponds linearly to the volumetric flow of the fluid. This signal is converted to a voltage with a signal conditioning module which is fed into the data acquisition board on the system computer.

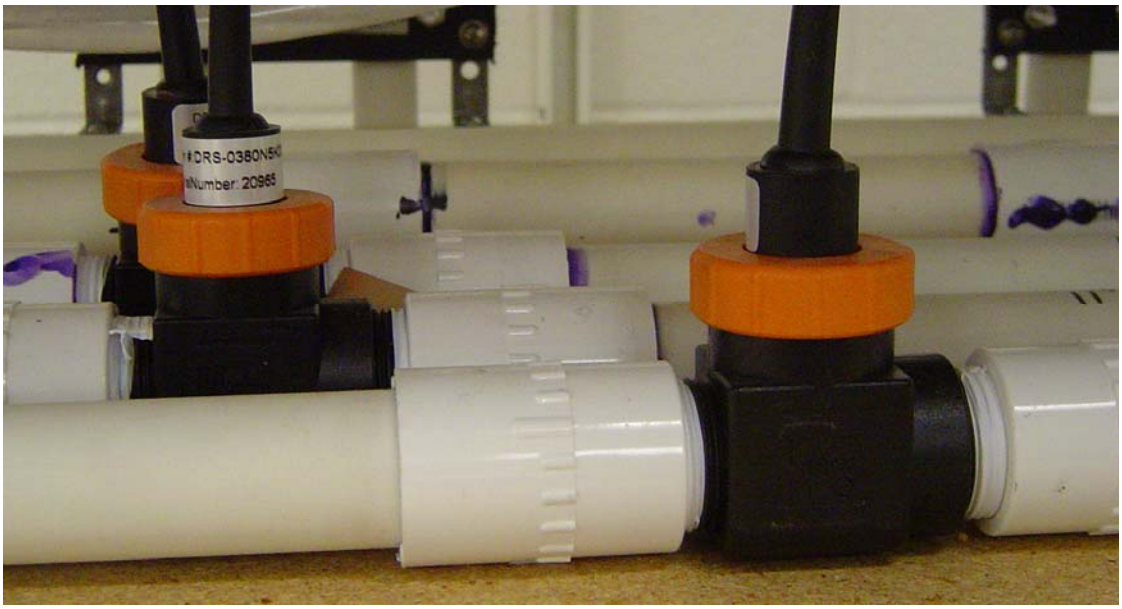

Fig. 2.25 Water flow transducers

Thermocouples

Temperature measurements are made with type T thermocouples immersed in the tested fluid. These thermocouples have ungrounded sealed tips and are of the low-noise variety. The thermocouples are immersed in the measured fluid; a Swagelok tube fitting grips the shaft of the thermocouple, sealing the measured fluid from the air. Figure 2.26 is a photo of this arrangement. The thermocouples are wired into a thermocouple terminal board with built-in cold junction compensation; this board is connected to a PCI thermocouple board on the computer.

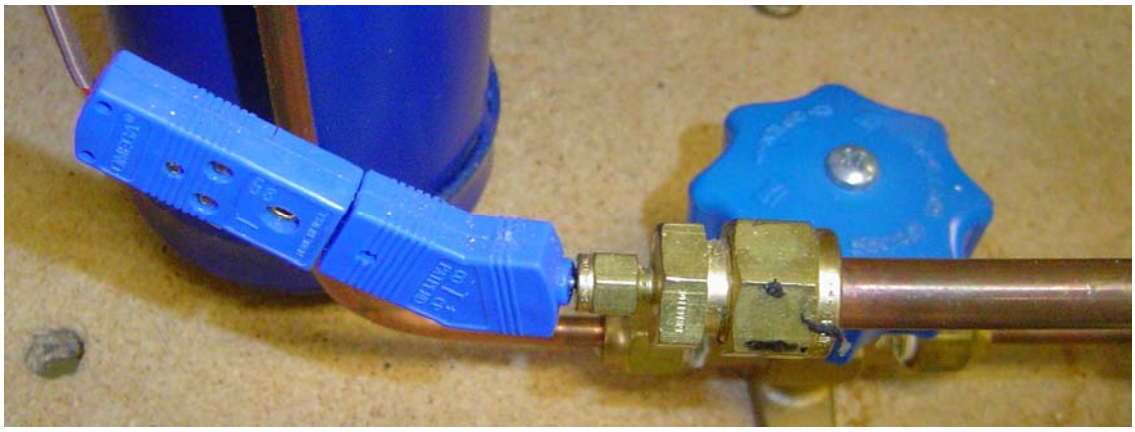

Fig. 2.26 Immersion thermocouple

Pressure Transducers

Pressure measurements of the refrigerant are made using sealed stainless steel diaphragm-type pressure transducers manufactured by Cole-Parmer. A transducer with maximum pressure of 300 psi is used to measure pressure at the outlet of the condenser, and transducers with maximum pressure rating of 100 psi are used at the outlets of the two evaporators. All of these transducers output a 1-5 V signal proportional to the pressure, which is fed into the data acquisition boards without processing. Figure 2.27 is a photo of the 300 psi transducer.

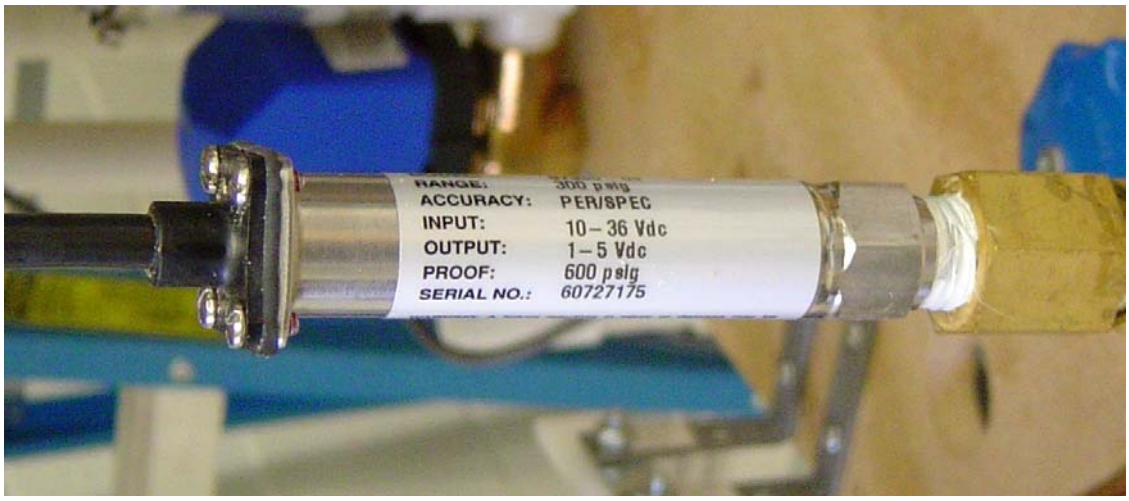

Fig. 2.27 Pressure transducer

A differential pressure transducer is installed on the Venturi described earlier. This transducer outputs a 4-20 mA signal proportional to the pressure drop through the Venturi. The purpose of this arrangement is to allow investigation of fluid flow dynamics of the compressor for model verification purposes, although it is not used in the research presented in this thesis.

Refrigerant Mass Flow

The transducers used to measure refrigerant flow, seen in Figure 2.28, are volumetric turbine-style flowmeters manufactured by McMillan. These transducers output a 0-5V signal, which is fed directly into the data acquisition board without signal conditioning.

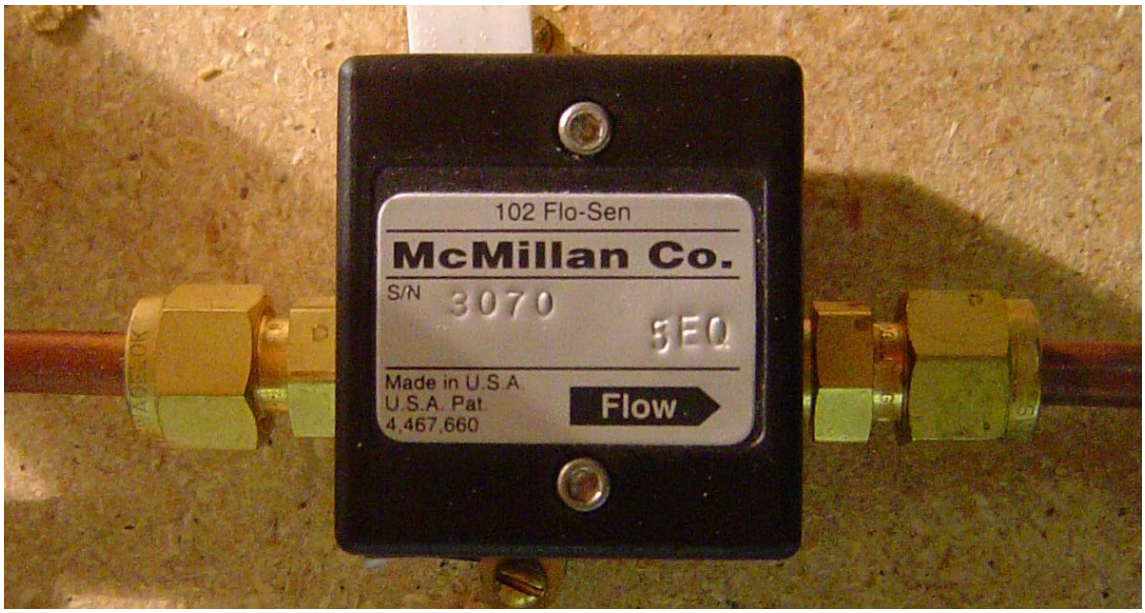

Fig. 2.28 Refrigerant flow transducer

Current Transducer

The current consumed by the compressor is measured with a current transducer made by CR Magnetics. This transducer uses the Hall Effect to measure DC current passing through the wire to the compressor electronics; it outputs a 0-5V signal proportional to the current.

Tachometer

The compressor electronics output a square wave signal whose frequency is proportional to the measured compressor speed. This square wave is fed into a signal conditioning module, which converts the signal to a 0-5V DC voltage that the data acquisition board can accept. Table 2.3 gives a brief description of each of the transducers in the experimental system.

Table 2.3 Transducers

Description	Qty	Mfr.	Part Number	Operating Range	Output	Listed Accuracy, +/-	Schematic Reference
Water Flow	3	Kobold	DRS-0380-N5-K000	2-40 LPM	0-320 Hz	1.5% FS	S6, S7, S8
Thermocouples	12	Omega	GTMQSS-062U-6	-270-400 °C	TC	0.5 °C	Tx-xxx-x
Evaporator Pressure	2	Cole-Parmer	07356-03	0-100 psig	1-5 V	1.0% FS	S5, S11
Condenser Pressure	1	Cole-Parmer	07356-04	0-300 psig	1-5 V	1.0% FS	S3
Differential Pressure	1	GE General Eastern	Modus W30-31E-1-T	1-6 psid	4-20 ma	1.0% FS	S2
Refrigerant Flow	2	McMillan	102-5-E-Q-B4-NIST	50-500 mL/min	0-5 V	3.0% FS	S4, S9
Compressor Current	1	CR Magnetics	CR5210	0-50 amps DC	0-5 V	1.0% FS	S10
Tachometer	1	Masterflux	--	1800-6500 RPM	0-2600 Hz	none	S1

Comments on Sensor Accuracy

Since the primary thrust of this thesis is design of a control algorithm, less emphasis is placed on the accuracy of the transducer measurements than if the research was geared towards design of an experimental system, or comparison of the behavior of

different systems. Any measurement biases from the actual values of pressure, superheat, et cetera, are not as important to this work as are the trends that these measurements follow. In other words, if the controller is asked to regulate pressure at 275 kilopascals (kPa), and it performs such that the sensor readings track 275 kPa, the controller is considered to be successful, even if the actual pressure is 20% higher. If the setpoint is then changed to 245 kPa, and the controller responds by seeking to decrease the measured pressure by the appropriate amount, this level of accuracy will be considered sufficient for the purposes of controller design. In the case where there is a severe change in the qualitative behavior of the system, such as during a loss of superheat, this will be reflected in the overall behavior and can be detected by all of the sensors acting together. As a measure of validation for the sensor measurements, an energy balance was checked wherein the heat transfer measured at the water passing through the evaporator is compared to that of the refrigerant; ideally, these properties would be equal. Figure 2.29 shows this comparison. Although there is as much as a 15% difference between the two properties, the dynamics track each other quite well. This implies that the measurement accuracies are good enough for the purposes of this control research.

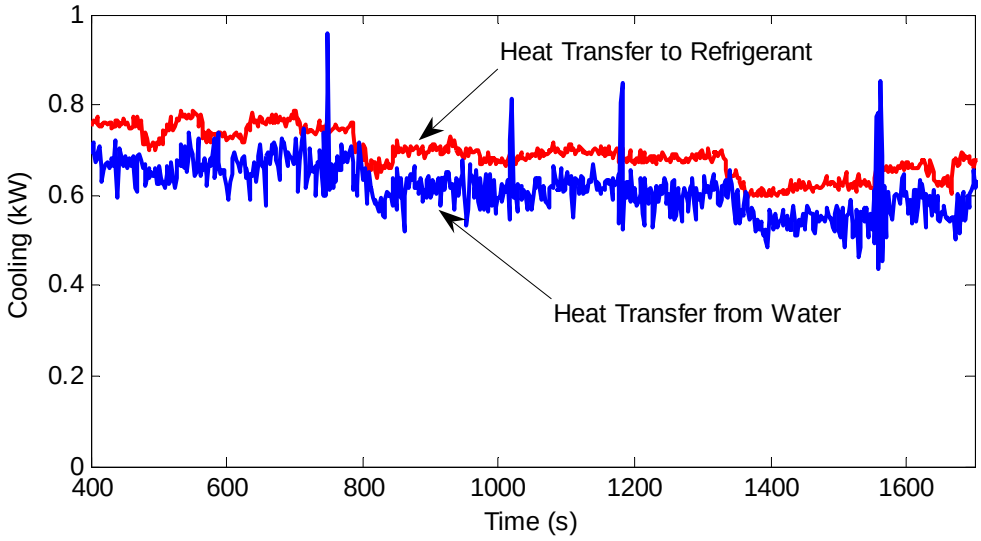

Fig. 2.29 Energy balance comparison

Power Components

The compressor is powered by two 800 Watt DC power supplies. These power supplies accept a 208VAC supply and output up to 16 amps at 48 VDC each. They are connected in parallel to deliver the power needed to run the compressor and are individually switched.

Power supplies for the transducers and signal conditioning equipment are also used. The 24VDC power supply is used to power the pressure, refrigerant flow, compressor current, and differential pressure transducers. The 12 VDC power supply is used to power the water mass flow transducers and the cooling fans for the compressor control unit and the 48V power supplies.

Each Sporlan Interface Board (IB)—one for each EEV and SDR—is powered by an individual 24 VAC transformer made by Honeywell. The IB manufacturer recommends that in order to protect the boards metal oxide varistors (MOVs) are placed across the 120V AC power supply (from the mains) and ground. As an additional measure of safety, fuses on the primary and secondary windings of the transformers are installed. An identical transformer is used to power the WFVs in the secondary system. Table 2.4 describes the power components; wiring schematics for all power components can be found in the Appendix.

Table 2.4 Power components

Description	Qty	Mfr.	Part Number	Components Powered	Rating
Transformer, 24 VAC	1	Honeywell	AT72D-1683	Provides power for WFV	40VA
Transformer, 24 VAC	3	Honeywell	AT72D-1683	Provides power for IB	40VA
Power Supply, 48 VDC	2	Cotek	800S-P048	Compressor; requires 208VAC suuply	800W
Power Supply, 24 VDC	1	Traco	TML 15124C	Sensors	15W
Power Supply, 12 VDC	1	Control Engineering Co.	31053	Water flow, cooling fans	18W
Power Supply, 5 VDC	1	Traco	TML 15105C	Signal Conditioning	15W

Data Acquisition

The data acquisition (DAQ) system is centered around four on-board DAQ boards installed on a PC. Temperature measurements are performed using the type T thermocouples detailed earlier and recorded and logged using a Measurement Computing thermocouple board, model PCI-DAS-TC. This board includes cold junction compensation and is capable of handling sixteen thermocouples. For this system arrangement, twelve thermocouples are used. Analog output signals to control

compressor speed, valve positions, et cetera, are output by a Measurement Computing PCI-DDA-08 board. This is a 12-bit board that has up to eight channels of analog output. Other sensor measurements (pressure, mass flow, et cetera) are logged using a pair of National Instruments E-Series boards, model number E-6023. These boards have eight channels when connected in differential mode. They also have up to eight channels of digital output and two channels of analog output each.

A pair of Analog Devices signal conditioning backplanes is also used in the system. All analog output channels are processed through optical isolators. These isolators serve the dual purpose of separating the analog output board from the high-powered system electronics, thus protecting the PC, and they also convert the PC output signals into the appropriate signals for the various actuators (e.g., 0-5 VDC to 4-20 ma for the EEVs). For transducers with outputs other than 0-5 VDC, these signals are also processed into a 0-5 VDC signal. For example, the NPN square wave output of the water mass flow transducers is converted into a 0-5 VDC signal, proportional to the frequency of the square wave. Table 2.5 details the signal conditioning provided by the backplanes and modules.

Table 2.5 Signal conditioning

Signal	Analog Input or Output	Mfr.	Part Number	Input	Output
Tachometer	AI	Omega	OM5-IKI-3K-C	0-3000 Hz	0-5V
Evaporator 1 Water Flow	AI	Analog Devices	5B45-01	0-500 Hz	0-5V
Condenser Water Flow	AI	Dataforth	SCM 5B45-01	0-500 Hz	0-5V
Evaporator 2 Water Flow	AI	Dataforth	SCM 5B45-01	0-500 Hz	0-5V
Differential Pressure	AI	Omega	OM5-11-4/20-C	4-20 ma	0-5V
Compressor	AO	Omega	OM5-IV-10B-C	-10 to +10V	0-5V
EEV 1	AO	Analog Devices	5B39-01	0-5V	4-20 ma
EEV 2	AO	Analog Devices	5B39-01	0-5V	4-20 ma
SDR	AO	Dataforth	SCM5B39-01	0-5V	4-20 ma
WFV 1	AO	Dataforth	SCM5B39-01	0-5V	4-20 ma
WFV 2	AO	Dataforth	SCM5B39-01	0-5V	4-20 ma

Software

The data logging and control functions are performed with WinCon 5.0, a software package by Quanser that provides a convenient interface with MatLab and Simulink. A Simulink model is created and compiled into a program that WinCon executes in real time. Additionally, gains and many other parameters can be varied while the program is running, which is very convenient when tuning controllers or performing experiments. Unfortunately, the selection of available DAQ boards that WinCon supports is very limited. A set of drivers for the thermocouple board and the analog output board was developed by the Alleyne Research Group at the University of Illinois at Urbana-Champaign; these drivers were modified and implemented for the experimental PC. The analog input boards are supported by WinCon, so no driver development was required for these boards.

CHAPTER III

DYNAMIC ANALYSIS OF WATER CHILLER SYSTEM

Justification

Implementation of a massive multi-input, multi-output (MIMO) controller to regulate an entire multi-evaporator system is theoretically possible, but is also difficult to achieve in practice and is computationally expensive, especially as the number of evaporators increases. Therefore, decoupling of the system dynamics as much as possible will aid in the design and implementation of a complete control system; ideally, each cooling zone—and hence each evaporator—will have its own independent control package, with the compressor responding to the cooling demands placed on the system as a whole.

Comments on Frequency Response

A complete understanding of the effects of each actuator on the various system conditions is necessary in order to design a control approach; the need for this understanding motivates an investigation of the relationships between control inputs (e.g., compressor speed, EEV opening) and system outputs (e.g., evaporator pressure, cooling), as well as the interaction between evaporators. If two different actuators have similar effects on the same system output, it is difficult to separate the actuators into two separate controllers, since the controllers may fight each other. Two actuators can have effects on the same outputs and still be separated, however, if the time scales of the

responses are very different from each other. As an example, consider the illustrative MIMO plant shown in Figure 3.1. This plant has two inputs (u_1 and u_2) and two outputs (y_1 and y_2). Three sets of possible dynamic responses will be considered to illustrate the possibilities of controller separation: uncoupled dynamics, coupled dynamics, and coupled dynamics that are separable due to differences in time scale.

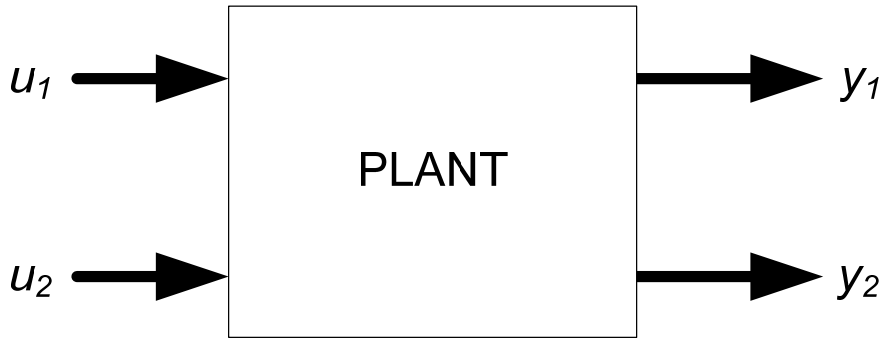

Fig. 3.1 Illustrative example plant

Figure 3.2 shows a possible frequency response plot of the two inputs to the two outputs. Note that the response of y_1 to u_2 and the response of y_2 to u_1 are both very weak, since the low-frequency gains of these responses are very small. The responses of y_1 to u_1 and y_2 to u_2, however, are very strong. This implies that the dynamics of the plant are not coupled, and control of this plant can be separated into two SISO controllers. Figure 3.3 illustrates this control architecture.

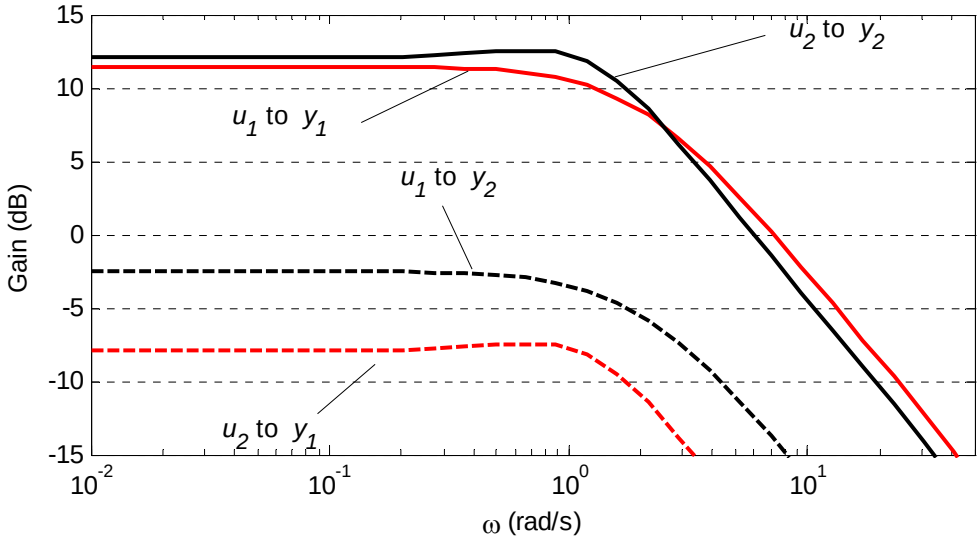

Fig. 3.2 Frequency response for uncoupled dynamics

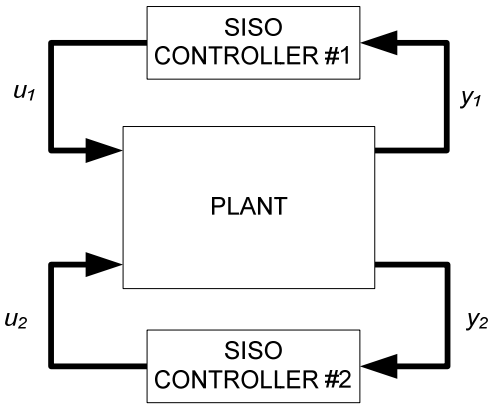

Fig. 3.3 SISO Control architecture for MIMO plant

Figure 3.4 shows another possible set of frequency responses for the plant in Figure 3.1. As in the earlier example, the input u_1 and u_2 have strong effects on y_1 and y_2, respectively. However, input u_1 also has a very strong effect on output y_2, and input u_2 has a non-negligible effect on y_1. This implies that if the controllers were separated as

in the earlier case, any movement in u_1 would impact y_2; since the bandwidth of u_1 to y_2 is about the same as that of u_2 to y_2, and the DC gain is larger, y_2 might not be able to control u_2 at all. At the very least, the controllers would end up fighting each other and would not be able to track setpoints properly. This situation is the usual justification for implementation of a MIMO controller as shown in Figure 3.5.

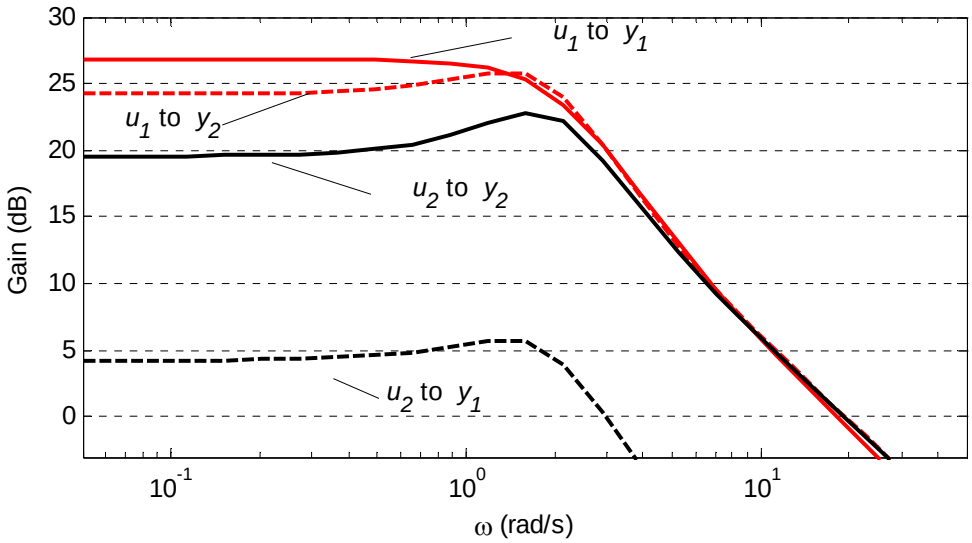

Fig. 3.4 Frequency response for significantly coupled dynamics

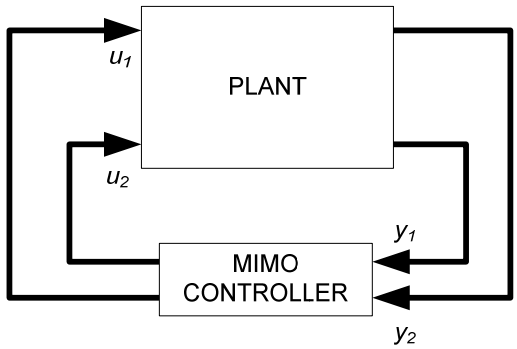

Fig. 3.5 MIMO control architecture for MIMO plant

Figure 3.6 shows a final possible set of frequency responses for the plant in Figure 3.1. Note that both inputs u_1 and u_2 have a strong steady state gain effect on output y_1 in this configuration, but the y_1 to u_1 response curve has a larger bandwidth than that of y_1 to u_2, and hence y_1 reacts much faster to changes in u_1 than to changes in u_2. This allows a controller configuration where u_2 controls y_2 and u_1 controls y_1 in a SISO configuration, as shown in Figure 3.3. The "fast" controller does affect both dynamics, but the slow moving controller treats these changes as instantaneous, and free of dynamics. Similarly, the fast controller can treat the dynamics of the slow controller as steady state, and therefore has sufficient time to respond. Hence, the controllers can be separated out due to a difference in the time scale of the responses of the outputs to the two inputs.

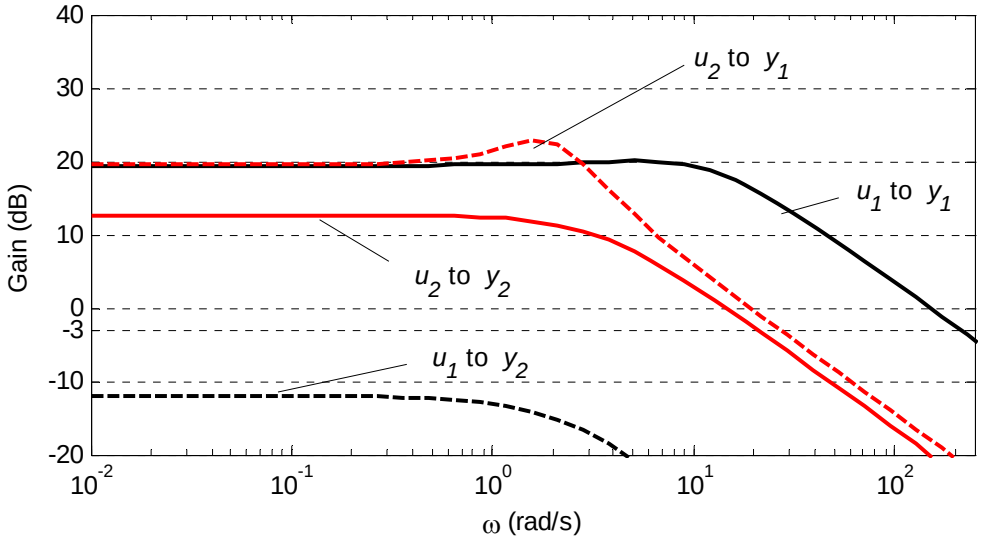

Fig. 3.6 Frequency response for coupled dynamics separable by bandwidth

Single-Input, Single-Output System Identification

In order to investigate the presence of these sorts of dynamic relationships in the experimental system, a set of experimentally derived linear models was created at selected operating conditions using standard system identification (ID) techniques [46]. The system was allowed to come to steady state operation, and then excited with a pseudo-random binary signal (PRBS) input. This procedure was then repeated; the first run was used for model identification, and the second run used for model validation. Because of the differing units and disparate scaling, the inputs and outputs were normalized before constructing empirical models, allowing the effects of each input into each output to be compared accurately [20]. This normalization consisted of removing the steady state values from the data and dividing by the maximum absolute values that resulted; hence, each input and output is at zero when at steady state and the maximum value in each vector is at one.

The models developed were discrete time state space models derived with the prediction error method (PEM); these models are of the form:

$$x(t+T_s) = Ax(t) + Bu(t) + Ke(t)$$
$$y(t) = Cx(t) + Du(t) + e(t)$$

State space models have a structure that maintains a close relationship to physically-based models; this gives them a particular advantage over other identification methods such as ARMAX, ARX, et cetera [46]. The PEM algorithm first makes an initial guess using the N4SID subspace algorithm detailed in [47], and then refines the prediction error fit by minimizing a quadratic prediction error criterion. The interested

reader can find a general reference on system identification in [46]. All model identification and validation was performed using the MatLab System Identification Toolbox.

The first step to selecting the models used in the graphs is generating 1st through 8th order PEM state space models for each input/output pair. For each of these models, the program calculates the quality of the fit as a percentage, according to the following formula found in [48]:

$$\% = \frac{1 - \|y_m - y_a\|}{\|y_a - mean(y_a)\|}$$

In this equation, y_a is the vector of actual output data points recorded for a recorded set of inputs, and y_m is the vector of data points that the model outputs when the same input is used. A perfect fit would result in a value of 100%.

In general, the model with the best fit is chosen; however, if there is a lower order model that comes within 10% of the best model's fit, the lower order model is chosen instead. For example, if the 6th order model has a fit quality of 82.96%, but the 2nd order model has a fit of 80.29%, the second order model is chosen, since the additional model complexity of the higher order option does not yield significant additional improvement. If at least a 10% quality of fit is not achieved for any of the models derived, then a first order model is used—this only tends to happen if the gain between the input and output is very small, such as the effect of the first water flow valve on the pressure of the second evaporator.

The following figures illustrate this process, and show some examples of the system identification results. Figure 3.7 shows the initial results from a system identification run: the compressor speed is the input, and the pressure and superheat of evaporator 1 are the example outputs. Figure 3.8 shows this same data run normalized as described.

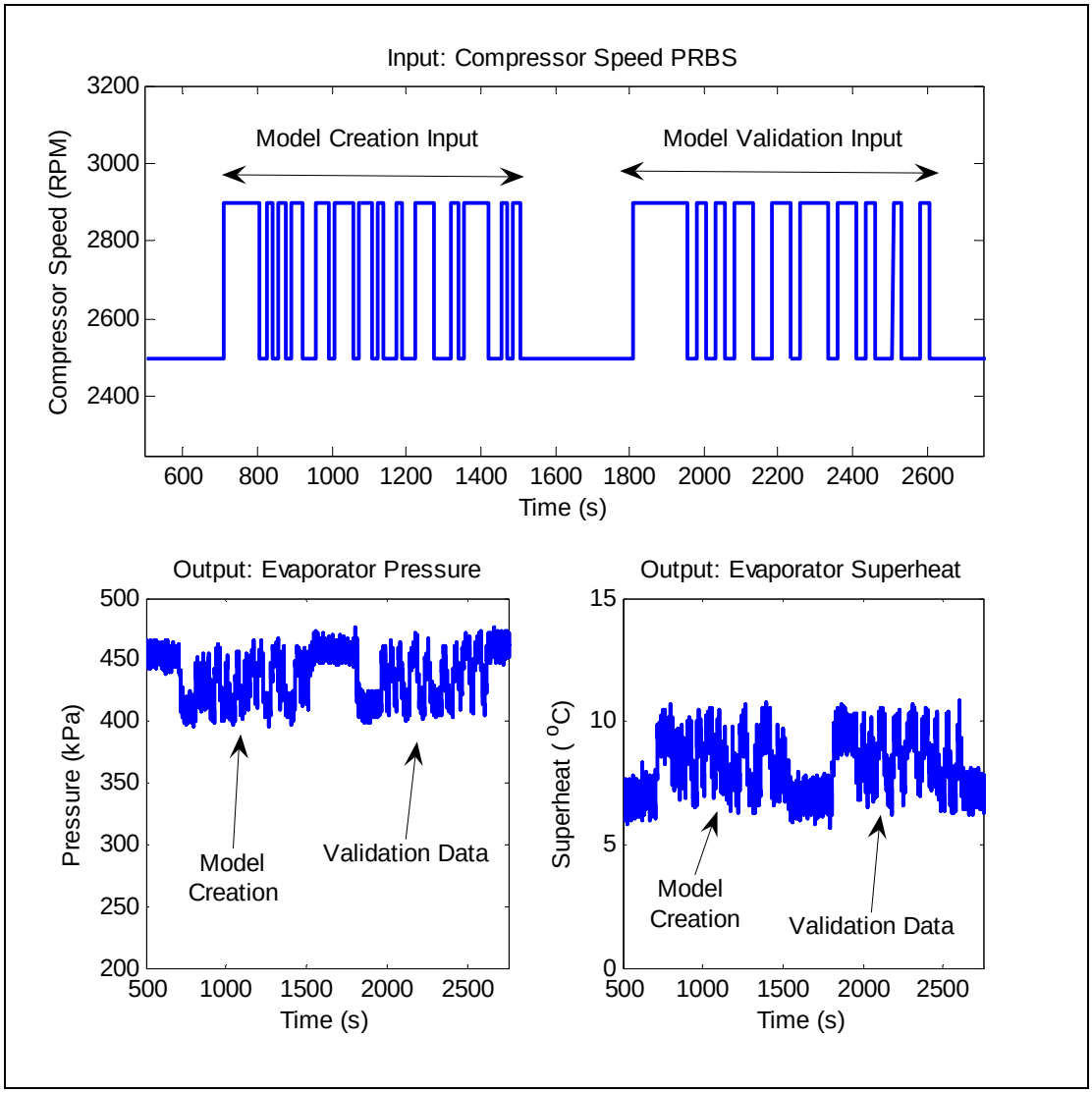

Fig. 3.7 Identification data run

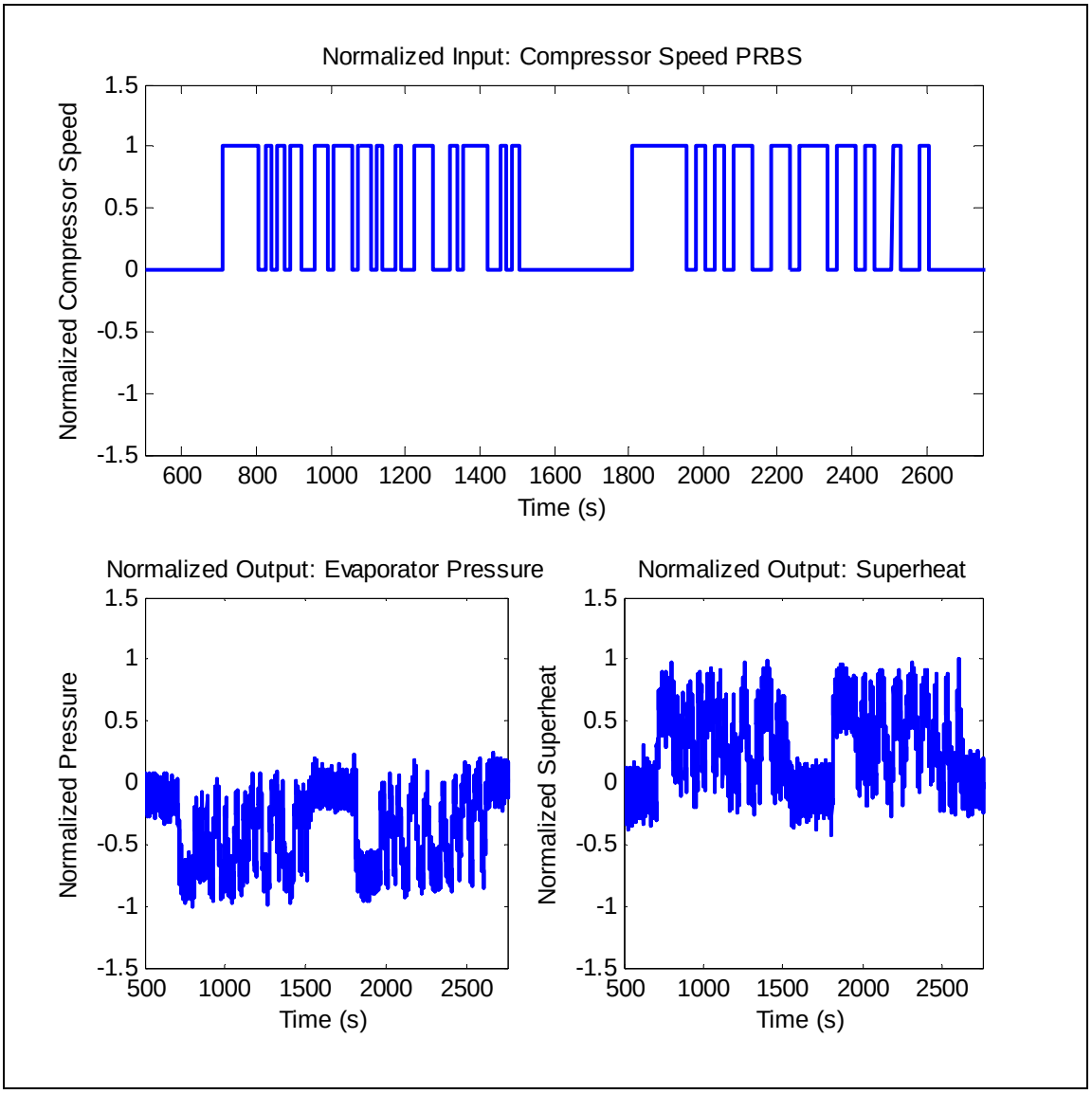

Fig. 3.8 Normalized data

From the "model creation" section of the normalized data, 8 models are created for each input-output pair. Table 3.1 shows the models for each pair, as well as the quality of fit for each model when compared to the validation data set.

Table 3.1 Model orders and qualities of fit

RPM to Pressure		RPM to Superheat	
Model Order	Fit	Model Order	Fit
1	68.84%	1	62.35%
2	63.88%	2	54.42%
3	26.74%	3	69.97%
4	71.88%	4	70.22%
5	67.07%	5	70.23%
6	28.18%	6	70.20%
7	67.12%	7	70.24%
8	36.92%	8	70.08%

According to the selection algorithm set out earlier, a 1st order model is selected for the RPM to Pressure 1 model and a 3rd order model is selected for the RPM to Superheat 1 model. Recall that these models are in the following form:

$$x(t+T_s) = Ax(t) + Bu(t) + Ke(t)$$
$$y(t) = Cx(t) + Du(t) + e(t)$$

For RPM to Pressure 1, the matrix values are:

$$A = [0.9909]; \quad B = [-0.0003]; \quad C = [25.749];$$
$$D = [0]; \quad K = [0.0061]; \quad T_s = 0.1$$

For RPM to Superheat 1, the matrix values are:

$$A = \begin{bmatrix} 1.1264 & 0.1303 & -0.0404 \\ -0.0196 & 1.0487 & 1.0725 \\ -0.0735 & -0.0971 & 0.6476 \end{bmatrix}; \quad B = \begin{bmatrix} 0.0001 \\ 0.0010 \\ -0.0004 \end{bmatrix};$$

$$C = \begin{bmatrix} 22.1040 & -4.1532 & 4.5679 \end{bmatrix};$$

$$D = [0]; \quad K = \begin{bmatrix} 0.0089 \\ -0.0151 \\ 0.0012 \end{bmatrix}; \quad T_s = 0.1$$

As a visual check, the model outputs of the selected models can be compared to the validation set. Figures 3.9 and 3.10 show these validation checks.

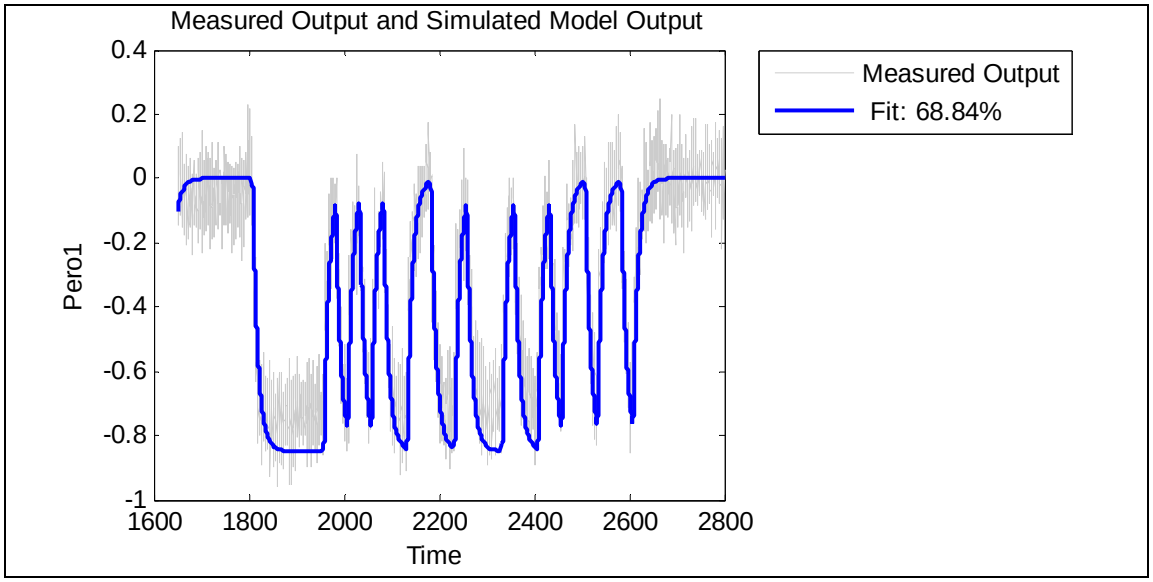

Fig. 3.9 Model validation—compressor RPM to evaporator 1 pressure

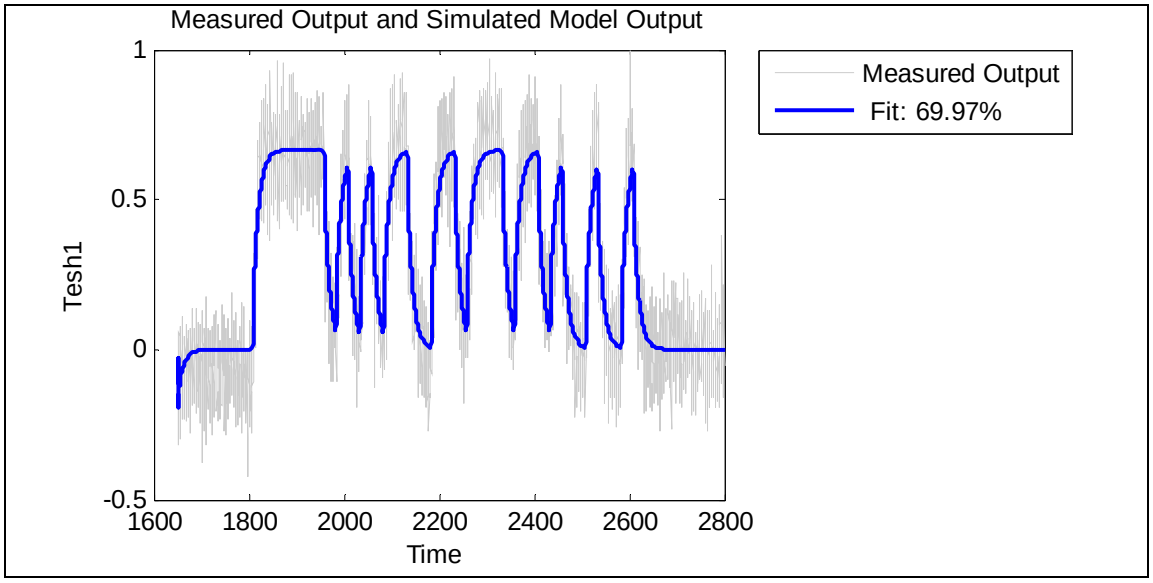

Fig. 3.10 Model validation—compressor RPM to evaporator 1 superheat

This approach was applied to the various inputs and outputs of interest in the system: compressor speed, EEV, SDR, and WFV as inputs, and pressure, superheat, and cooling for both evaporators as the outputs. Frequency response plots were generated for these models as will be shown in the next section; from these curves insight can be gained into the dynamic responses of the system.

Frequency Responses of Experimental System

Figure 3.11 shows the frequency responses of the models derived by stepping the compressor speed. Clearly, compressor speed has a strong effect on evaporator pressures and superheats. This effect is stronger at lower speeds. However, the effect on cooling when the compressor alone is varied is weak. While this may at first seem counterintuitive, consider that increasing compressor speed increases superheat, condenser pressure, and decreases evaporator pressure, but if the valve does not open to permit additional refrigerant flow, the effect on cooling performed by the evaporator will be negligible.

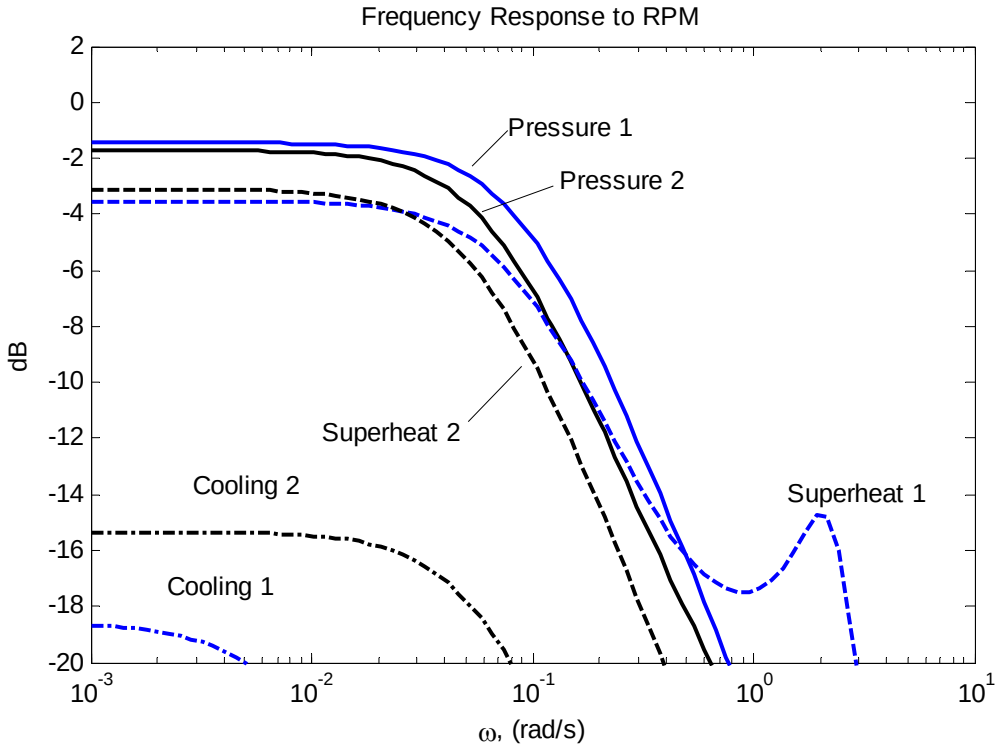

Fig. 3.11 Normalized frequency responses to step changes in RPM

Figure 3.12 shows the effects of the first EEV. The EEV has a strong effect on the pressure and superheat of both evaporators at all operating conditions. The strength of this relationship is reflected in the success that users of EEVs have had in using these devices to control the conditions of superheat and pressure. The effect of the EEV on the first evaporator's cooling has the strongest and fastest response; one can surmise that upon changing the valve, the first response is the change in refrigerant flow, before pressures and superheats have a chance to respond. Note that the effect of the first EEV on the second evaporator's cooling is negligible.

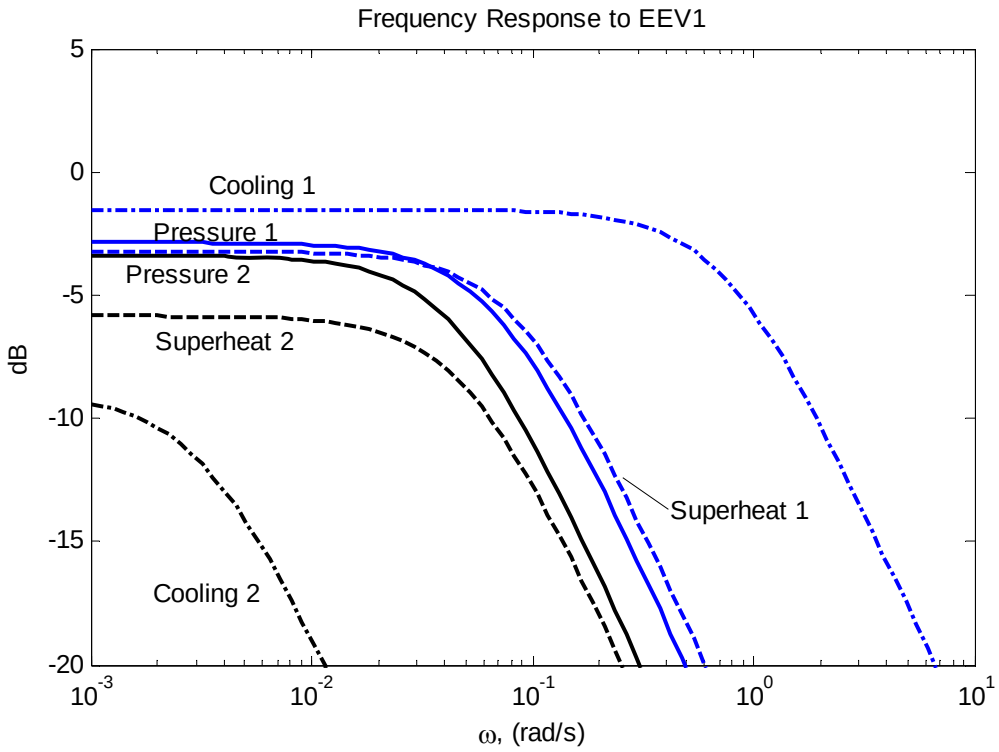

Fig. 3.12 Normalized frequency responses to step changes in EEV 1

Figure 3.13 details the responses to changes in the discharge valve (SDR). It has a strong effect on the pressure of the second evaporator, and therefore its superheat. The SDR does not affect the steady state operation of the first evaporator at steady state, though there are some transient effects, as evidenced by the hump in the response curves at approximately 0.1 rad/s. This is evidence of the coupling of the dynamics of the two evaporators. The effects on cooling were negligible so they are omitted.

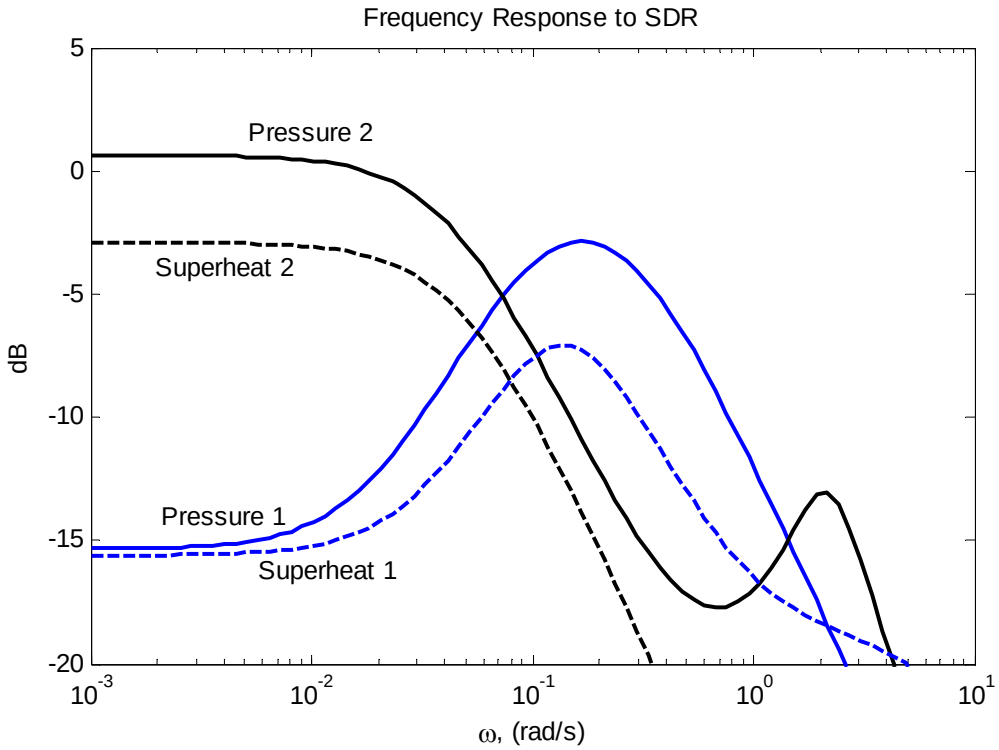

Fig. 3.13 Normalized frequency responses to step changes in SDR

Figure 3.14 details how the system responds to changes in water flow of the first evaporator via step changes in water flow valve (WFV) #1. It has a strong effect on superheat and a smaller effect on cooling. WFV #1 does not have any effect on the second evaporator.

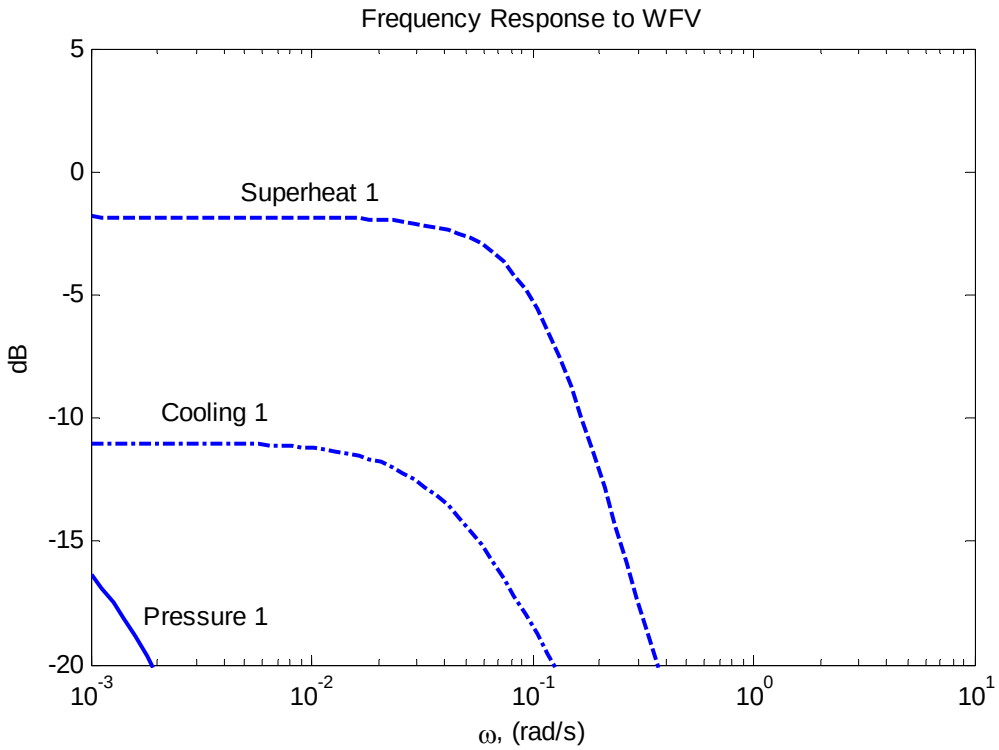

Fig. 3.14 Normalized frequency responses to step changes in WFV 1

Clearly, the individual EEVs have a strong effect on the pressure of both evaporators; this suggests a strong dynamic coupling between the two evaporators. However, the actual cooling performed by each evaporator is unaffected by the other's EEV. As noted earlier, the evaporators' cooling is also only minimally affected by changing the compressor speed alone. If the valve does not open to permit additional refrigerant flow, increasing compressor speed has the primary effect of increasing the ratio of condenser pressure to evaporator pressure (hereinafter referred to as the pressure ratio). The additional energy delivered to the system by the compressor is rejected into the condenser water, in effect wasting the extra power consumed by the compressor. Figure 3.15 shows the system response to just such a change in inputs; the compressor speed is increased but the valve position remains fixed; the pressure ratio and superheat increase, but cooling remains fixed. Figure 3.16 shows the condenser water temperature during this same test, illustrating that the system is dumping additional heat into the condenser water when the compressor is stepped up.

This suggests that the compressor can change its speed to deliver the energy system necessary to meet changes in cooling demand in one cooling zone without affecting cooling performed in other zones. For example, if evaporator 1 needs additional cooling, the compressor can increase speed to provide it without greatly affecting the cooling in evaporator 2.

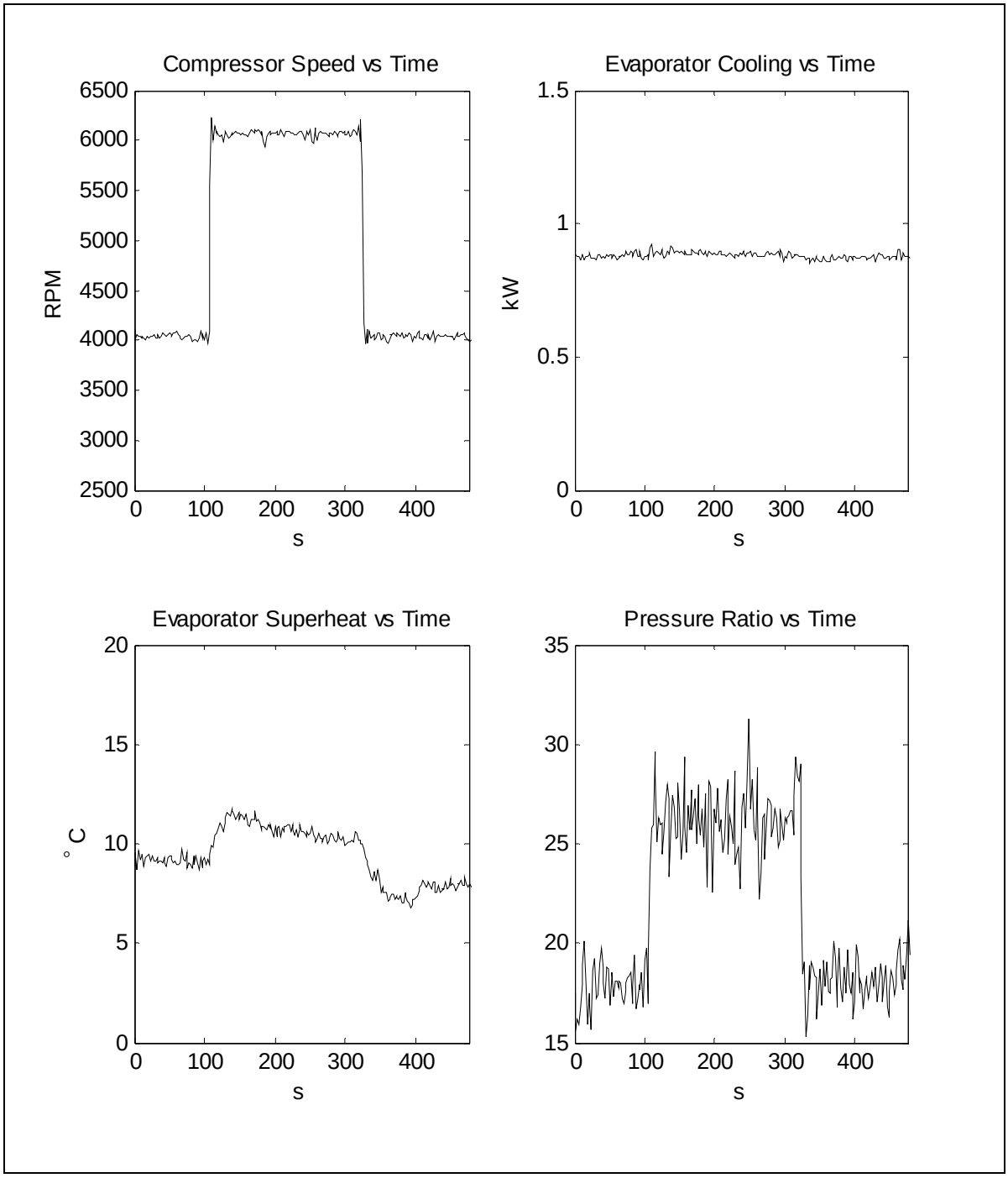

Fig. 3.15 Effect of compressor speed changes (no valve changes)

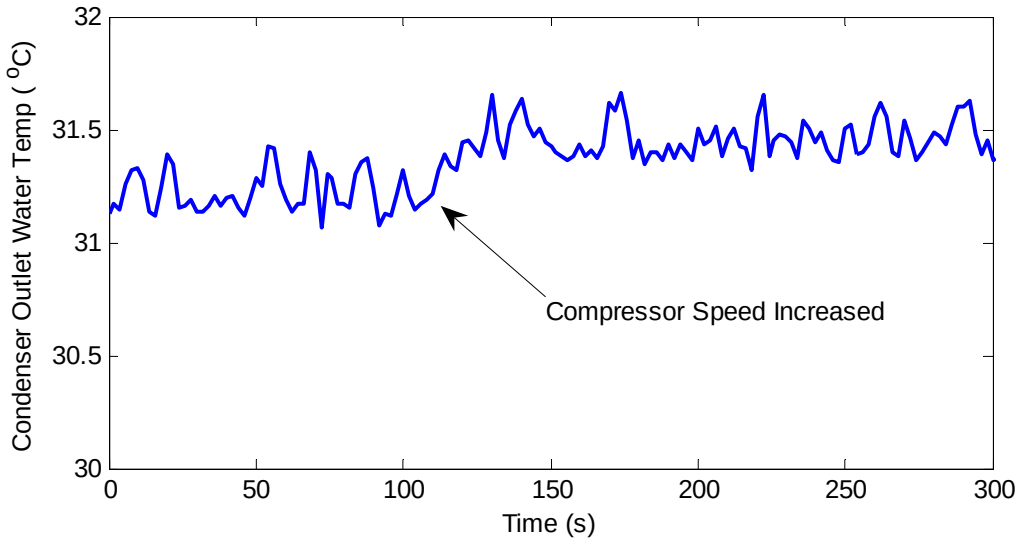

Fig. 3.16 Increased heat rejection to condenser from compressor step

An observation made from Figure 3.13 is that the SDR does not affect the steady state operation of the first evaporator, which suggests that control of the first evaporator can be separated from the SDR. Furthermore, the SDR can control the pressure of the second evaporator without affecting the steady state pressure of the first.

Finally, the first WFV does not have any effect on the second evaporator; this suggests that the water flow for each evaporator can be controlled without affecting the other. The WFV does have an effect on cooling and superheat of the first evaporator, however, so it can be an effective control component, much like a variable speed fan in a commercially available air conditioning system.

Figure 3.17 shows the frequency responses of superheat (SH) to compressor speed (RPM), EEV, and WFV. The steady state gain of EEV and RPM are about the same, and the WFV has a stronger impact. The WFV is considerably slower than the

other two, especially the EEV. This graph confirms the intuitive guess that all three actuators have a strong effect on evaporator superheat.

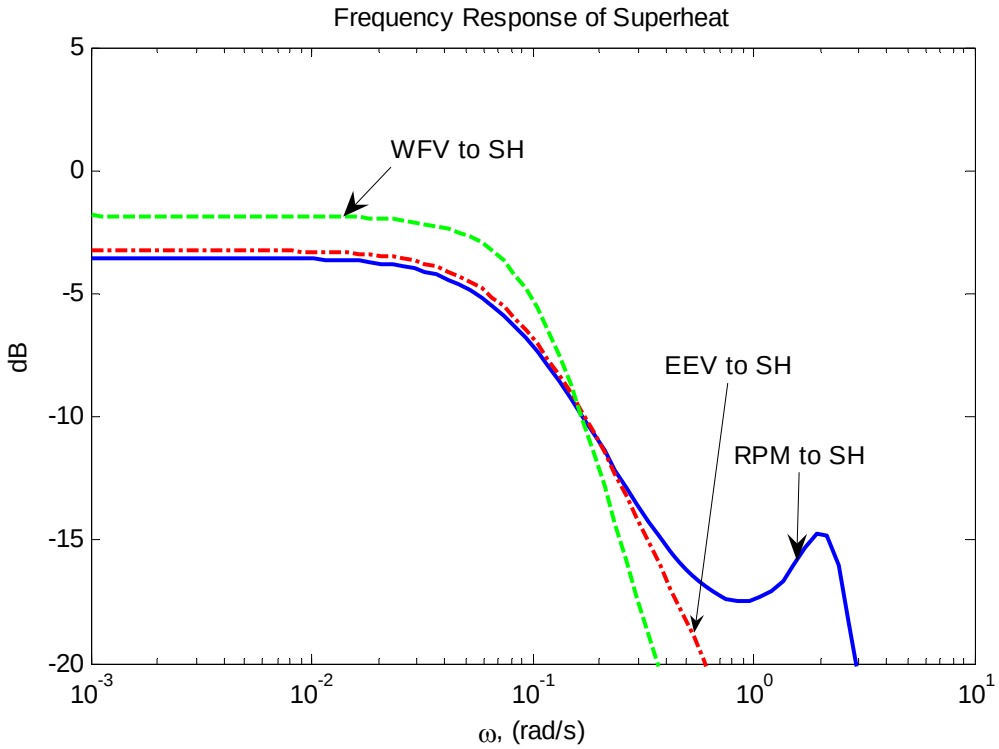

Fig. 3.17 Frequency responses of superheat to various inputs

Similarly, Figure 3.18 shows the response of pressure to the EEV and RPM. The compressor has both a faster and stronger effect on pressure, although the EEV affects the pressure as well. This agrees with the faster response of superheat to RPM shown in Figure 3.17.

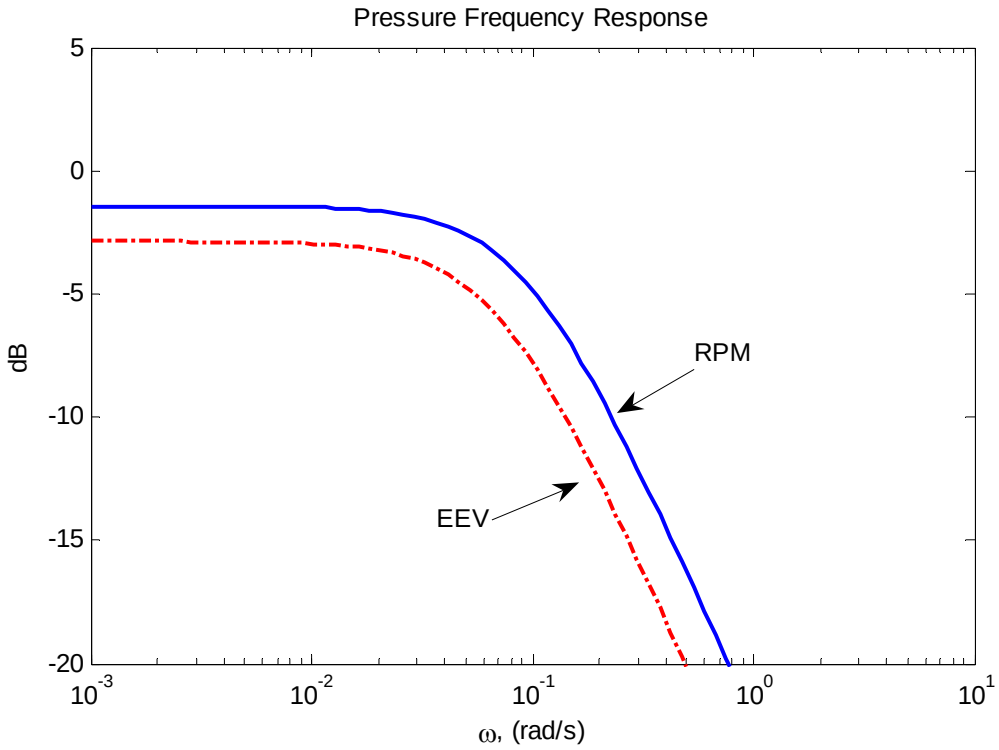

Fig. 3.18 Frequency responses of pressure to various inputs

Finally, Figure 3.19 shows the response of cooling (Q) to the same inputs. Clearly, the EEV is the best choice to control cooling. This insight, plus the relative strength and speed of pressure response to RPM, point towards using the compressor to control pressure in some manner while regulating cooling with the EEV.

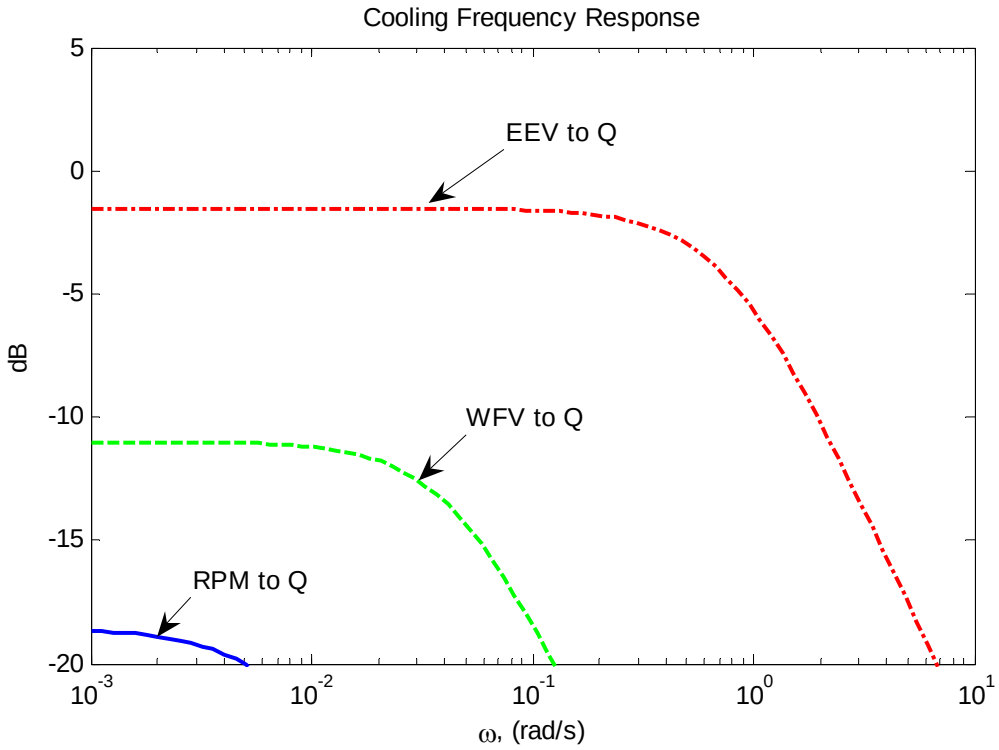

Fig. 3.19 Frequency responses of cooling to various inputs

Conclusion

The results of this dynamic analysis suggest that control of the system can indeed be broken down into a suite of individual controllers for each component or subsystem. Each evaporator can be controlled by its respective actuators with a degree of independence from the other; this implies that cooling zones can be established and maintained for a large system. Further, the compressor can be controlled to deliver the energy needed for the precise cooling demands of the system, suggesting that a high-level controller can be designed to ensure that the needs of the individual cooling zones

can be simultaneously met in the most energy-efficient manner possible. The design and implementation of the lower-level component controllers are detailed in the next chapter.

CHAPTER IV

DESIGN AND IMPLEMENTATION OF LOCAL CONTROLLERS

Overview

In Chapter III of this thesis, the exploration of the effects of the various system actuators on the thermodynamic system conditions was detailed. The motivation behind this exploration was development of a control architecture that decouples the system dynamics as much as possible; implementing MIMO control only when necessary simplifies the control problem significantly, while simultaneously avoiding the pitfalls of competing SISO controllers. This chapter details the design and implementation of an MPC-based control architecture that combines MIMO and SISO controllers; the overall goal is an architecture that is modular in approach. Each evaporator should have its own isolated control package that delivers the required amount of cooling—tracking a setpoint—while ensuring safe operation (i.e., the presence of superheat). The compressor should be controlled such that it delivers only the necessary energy into the system for the total cooling demand. Moreover, the behavior of the compressor should be independent of the total number of evaporators as well as the proportion of total cooling load for which each evaporator is responsible.

Traditional control of VCC systems has primarily depended upon simple electromechanical devices and on/off strategies, such as a bimetallic thermostat or a mercury switch. Mechanical valves were used as expansion devices and primarily

regulated evaporator pressure (Automatic Expansion Valve, or AEV) or evaporator superheat (Thermostatic Expansion Valve, or TXV). As noted earlier, application of completely variable expansion devices, such as the electronic expansion valves (EEVs) used in the experimental apparatus, has usually involved an extension of these sorts of approaches to both classical and modern control techniques, e.g., PID and LQG, respectively. In these approaches, the EEV is generally used to control evaporator pressure or superheat.

Comments on Superheat Control

When controlling superheat, the most critical requirement is that superheat is present. Once this condition is met, the primary advantage of a close regulation of superheat is that as superheat is driven down to a minimum value, the evaporator operates with increasing efficiency. Traditionally, this regulation has been performed mechanically with the TXV, and the EEV has been implemented in a similar manner. As the conditions of the system change, the expansion device opens or closes to regulate superheat; this indirectly provides a means to control refrigerant flow as more or less cooling is required. For example, with a two-stage compressor, if the compressor speed is increased, superheat will also increase, leading the valve to open to return superheat to its setpoint; this allows more refrigerant to flow, and hence more cooling is performed.

With the combination of variable speed compressors and EEVs, however, cooling and evaporator pressure setpoint regulation can be performed regardless of the amount of superheat present. Therefore, from the perspective of cooling and pressure control, strict regulation of superheat to a setpoint is unnecessary, as long as superheat

stays above a minimum value to protect the compressor. However, excessive superheat is undesirable, since a large amount implies that a great deal of heat transfer is occurring when the refrigerant is in a gaseous state, which is much less efficient than the heat transfer that occurs during refrigerant evaporation. If every kilowatt (kW) of cooling is "bought" by a certain amount of power consumed by the compressor, an energy-optimal control arrangement will ensure that the maximum amount of heat transfer occurs for a given amount of power consumption. In the case of the evaporator, this implies that the vast majority of cooling must occur during the evaporation process, and as small a portion of the cooling that is safe and practical occur after the refrigerant has boiled off. This idea is illustrated by Figure 4.1 seen below.

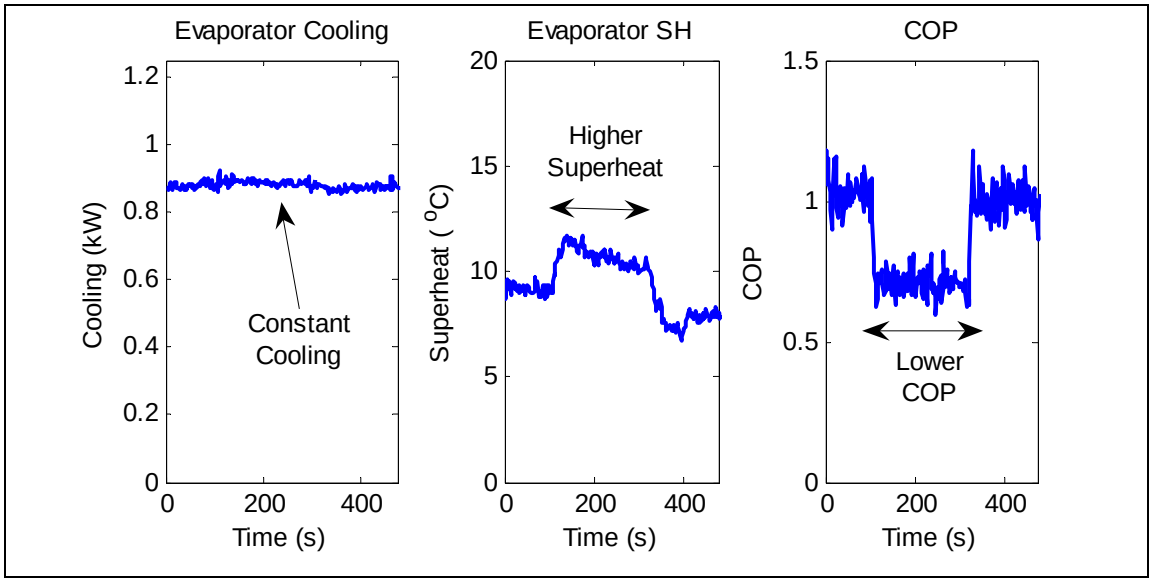

Fig. 4.1 Evaporator efficiency

Figure 4.1 revisits the experimental run shown in Figure 3.11. Recall that the evaporator cooling remains constant throughout the process as shown, and the expansion

valve does not change. A step increase in the compressor leads to more superheat; simultaneously the Coefficient of Performance (COP) decreases, implying less efficient operation. COP is calculated as the cooling performed by the system divided by the compressor power consumption (fan work is ignored in this example). Clearly, for a given amount of cooling, as superheat decreases, the cost of each kW of cooling also decreases due to more efficient evaporator operation. However, as noted earlier, superheat must be present to avoid damaging the compressor. Therefore the task at hand is to keep superheat above a safety-mandated minimum while not allowing it to grow too large, which would decrease operating efficiency. For the research detailed in this thesis, superheat is calculated as:

$$SH_n = T_{en,ro} - T_{sat,en}$$

Where:

SH_n ≡ Superheat of the n^{th} evaporator, °C

$T_{en,ro}$ ≡ Exit R134a temperature of n^{th} evaporator, °C

$T_{sat,en}$ ≡ R134a saturation temperature at n^{th} evaporator pressure, °C

Model Predictive Control

In addition to tracking cooling setpoints and keeping superheat within a reasonable band, the controller should not exceed the physical constraints of the actuators, since the valves cannot open past 100% or close past 0%. Therefore, a control strategy is required that respects the physical limits of the actuators, will regulate cooling to a specific value, and will keep superheat within a defined band of operating conditions without exerting unnecessary controller effort. This leads naturally to adopting a model predictive control approach.

As noted in Chapter I, all MPC algorithms use an explicit model of the physical system to derive the set of controller actions that minimize a cost function subject to a set of constraints. These constraints can be inherent to the actuators, e.g., a valve cannot open past 100% open or close past 0% open. While classical control techniques like PID loops can be modified with a saturation to ensure that actuator limits are not exceeded, MPC has the advantage of being able to foresee and plan for these limitations, which can improve system performance over the long term [21]. MPC also has the advantage that additional constraints can be defined by the user to keep the system operating in a safe range, e.g., keeping evaporator superheat within a desired band.

Baseline Case—PID Control

Before implementation of the final control architecture, a completely SISO approach was attempted in order to provide a baseline case and to verify that the dynamic analysis detailed earlier provided valid information. In this baseline case,

evaporator cooling will track a setpoint with a traditional PI loop using the EEV as the actuator. The idea behind this approach is that since cooling is largely dependent on the refrigerant flow, the valve can act to regulate the amount of refrigerant entering the evaporator. For the controllers implemented in this thesis, the cooling calculation is performed on the refrigerant side, since the small change in the water temperature as it passes across the evaporator during typical operation (approximately 2-3 °C) means that the calculation is highly susceptible to sensor noise and uncertainty. This cooling calculation can be done with temperature sensors and a "virtual" mass flow sensor relying on a manufacturer supplied mass flow function, but for this research cooling is calculated as shown:

$$\dot{Q}_n = \dot{m}_{ref,n}\left(h_{en,o} - h_{en,i}\right)$$

Where:

$\dot{Q}_n$ ≡ Cooling at the nth evaporator, kW

$\dot{m}_{ref,n}$ ≡ Mass flow of R134a for nth evaporator, kg/sec

$h_{en,o}$ ≡ Enthalpy of R134a at nth evaporator exit, kJ/kg

$h_{en,i}$ ≡ Enthalpy of R134a at nth evaporator inlet, kJ/kg

In order to find enthalpy at the evaporator inlet, the condenser outlet pressure is measured. Due to the presence of the liquid receiver, the refrigerant is assumed to be a saturated liquid at this state, and enthalpy can be obtained from the refrigerant property tables from the pressure only. Additionally, the expansion valve is assumed to be isenthalpic; under these assumptions, the enthalpy of the refrigerant at the evaporator

inlet will be same as that at the condenser outlet. The enthalpy at the evaporator outlet is found by measuring the pressure and temperature of the refrigerant at the evaporator outlet; assuming this refrigerant is superheated, the enthalpy can be found from the thermodynamic property tables.

Once the evaporator controller is implemented, the evaporators need a way to communicate to the compressor how much energy input is required to achieve the total desired cooling. Since the compressor has a large impact on evaporator pressure, and changes in the expansion valve to meet cooling demand change the evaporator pressure, pressure of the first evaporator is chosen as the signal to communicate this need to the compressor. The first evaporator pressure is chosen because the pressure differential between the two evaporators can be independently regulated by the SDR valve. With this approach, the pressure of the two evaporators can be regulated using two SISO PI loops. For example, as one of the EEVs opens to allow more mass flow and achieve the set cooling capacity, the pressure of the evaporator will rise. The compressor will speed up to drop the pressure. Meanwhile, the pressure differential between the two evaporators is regulated by the SDR in the second evaporator using a PI loop. Finally, superheat will be regulated using the WFVs. Figure 4.2 shows the completely SISO control architecture. Table 4.1 shows the controller gains used in each loop.

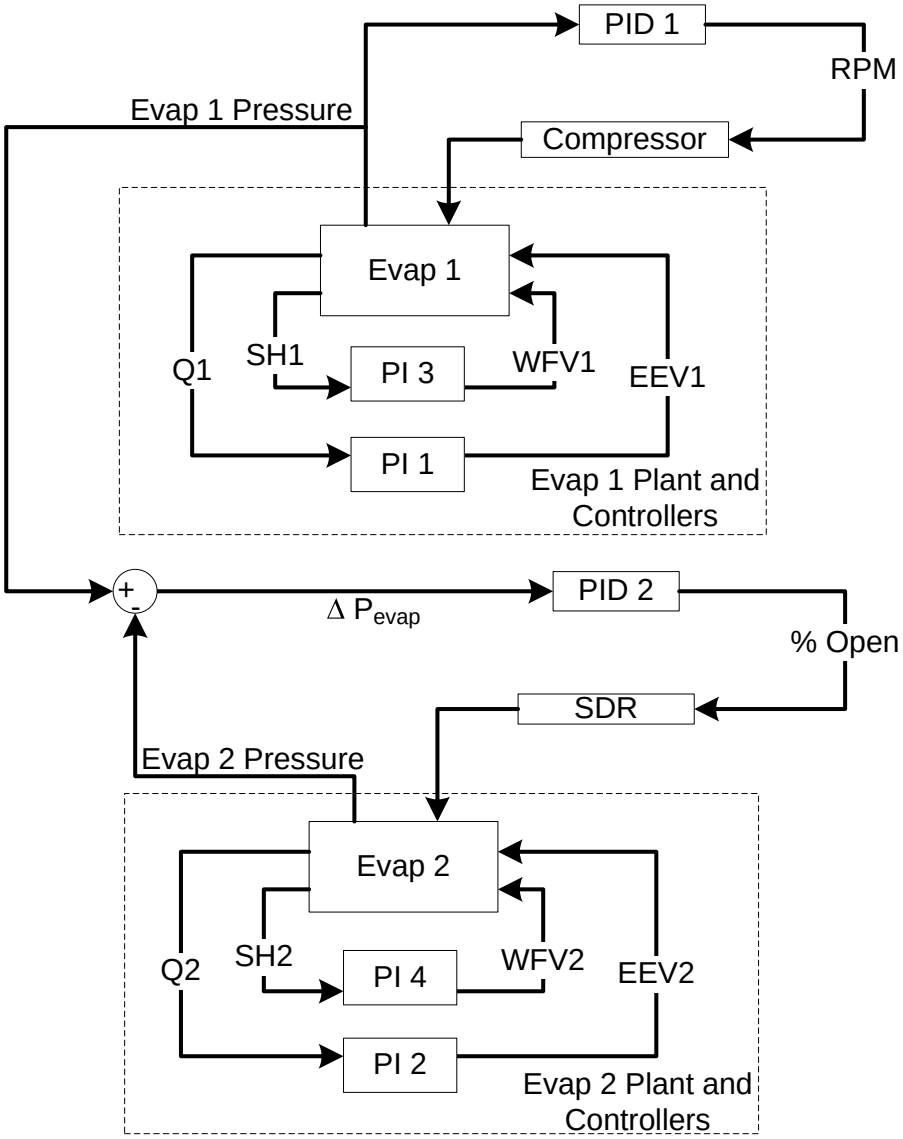

Fig. 4.2 SISO control architecture

Table 4.1: SISO control gains

Controller	Input (Actuator)	Output	K_P	K_I	K_D
PI 1	EEV #1	E1 Cooling	7.200	1.080	0.000
PI 2	EEV #2	E2 Cooling	7.200	1.080	0.000
PI 3	WFV #1	E1 Superheat	0.750	0.014	0.000
PI 4	WFV #2	E2 Superheat	0.750	0.014	0.000
PID 1	Compressor	E1 Pressure	6.000	2.000	3.500
PID 2	SDR	E2 Pressure	0.250	0.050	0.025

First, a test run using these controllers was performed. Superheat, cooling, and pressure setpoints were fed into the controllers. The results of this test run are shown in the following set of figures. Figure 4.3 shows the cooling setpoint tracking of the two evaporators. Figure 4.4 shows the pressure setpoint tracking—note that both evaporators are set to the same pressure, 325 kPa. Figure 4.5 shows the evaporator superheat during this test run.

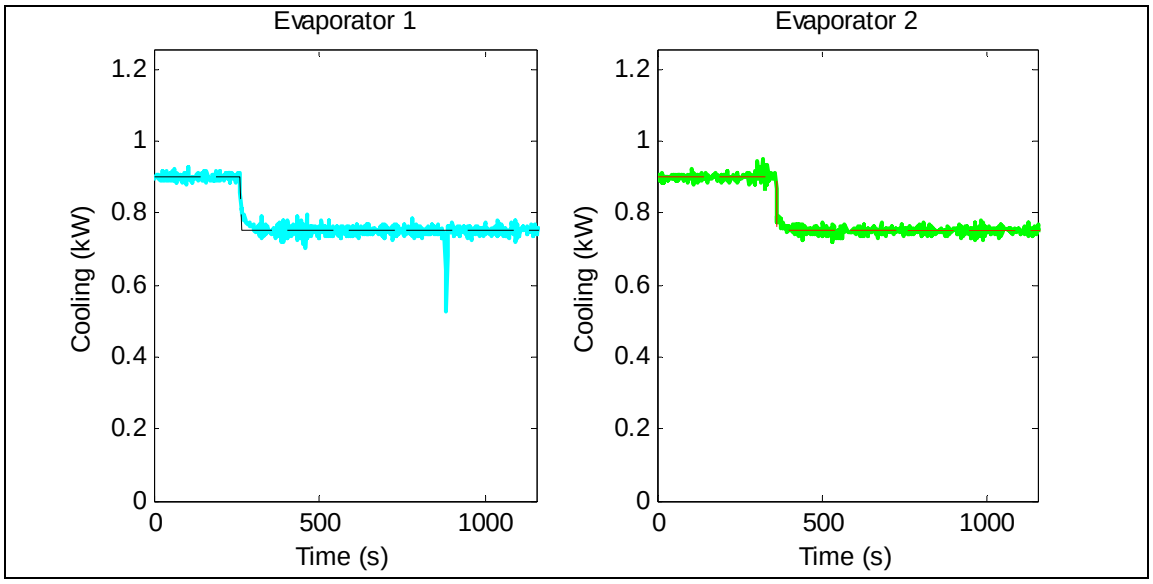

Fig. 4.3 Cooling setpoint tracking, SISO control

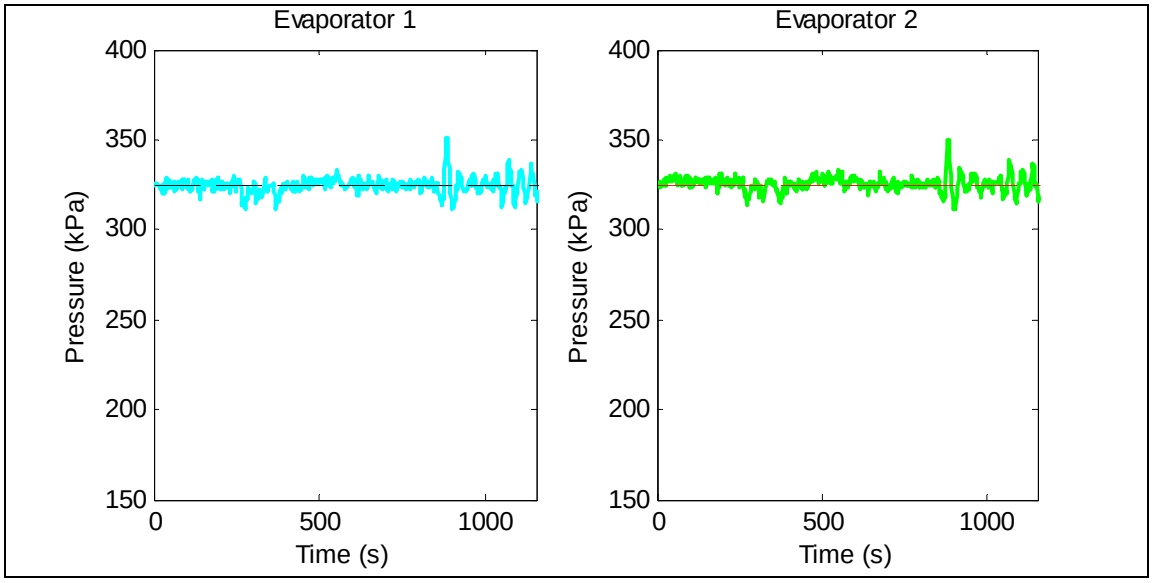

Fig. 4.4 Pressure setpoint tracking, SISO control

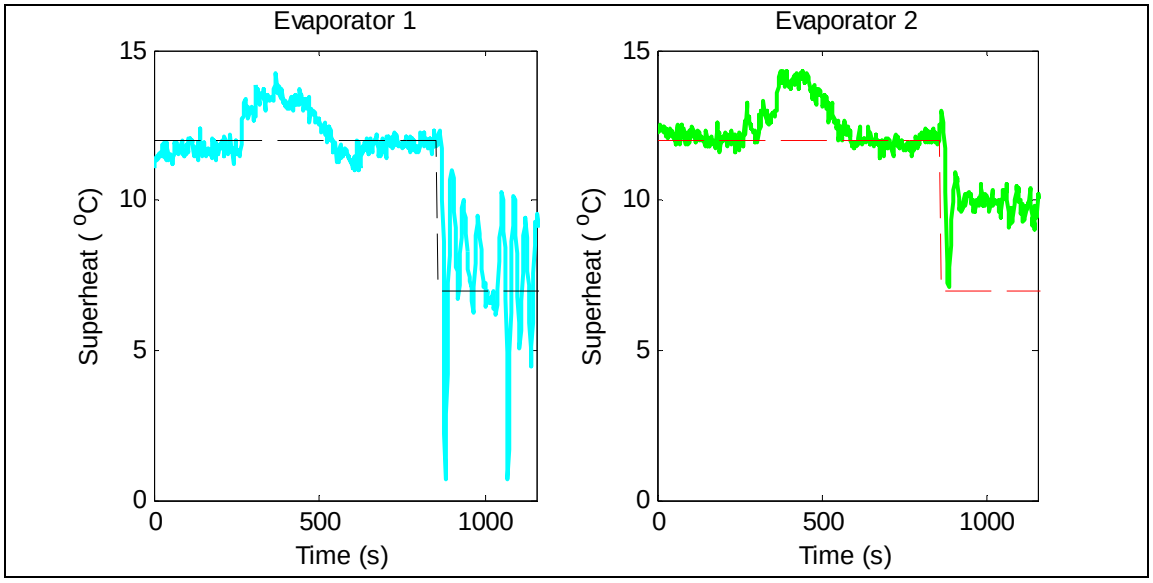

Fig. 4.5 Evaporator superheat, SISO control

This purely SISO-based scheme shows that the EEVs can indeed be used effectively to regulate cooling, and the compressor and SDR to regulate pressures. After the step decrease in cooling, the WFVs bring down superheat to the setpoint of 12°C.

However, when asked to regulate superheat at a lower value to obtain better system efficiency, the WFVs can not manage this task. Additionally, the EEVs also have a very strong effect on superheat; in the presence of a large change in cooling demand, the valve changes drastically, which changes pressure, occasionally resulting in a loss of superheat. The WFV has a strong effect on superheat, but its slew rate is too slow and the presence of quantization severely affects its ability to provide effective control. For the next set of runs, the water flow valves were maintained at a constant 100% open, to allow a demonstration of the EEVs regulating cooling while the compressor and SDR regulate evaporator pressures. Figure 4.6 shows the cooling for this case; Figure 4.7 shows evaporator pressures; Figure 4.8 shows superheat.

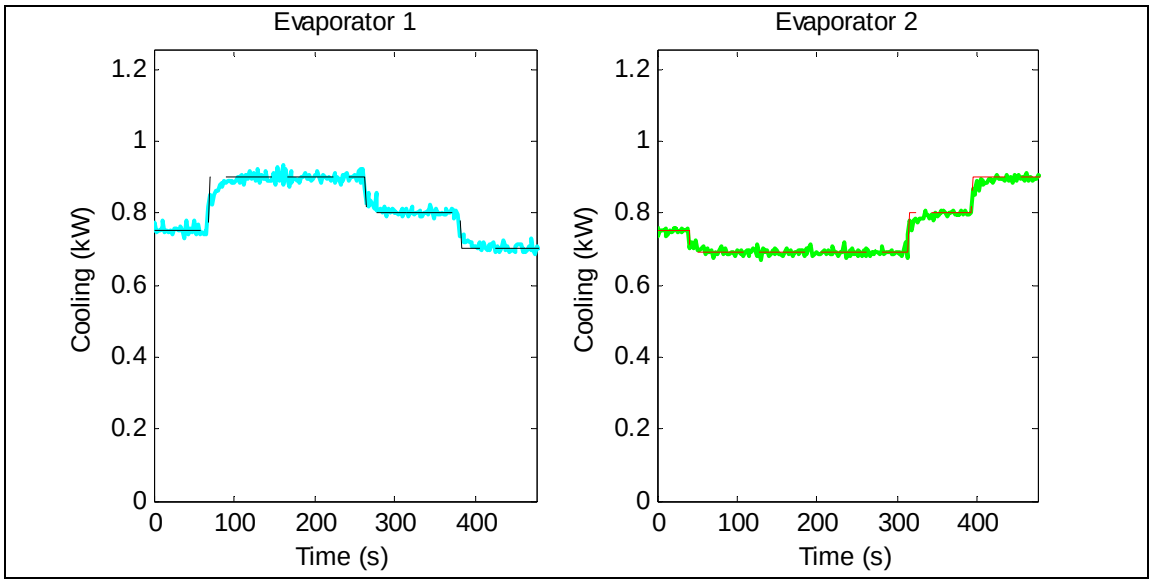

Fig. 4.6 Cooling setpoint tracking, SISO control, full water flow

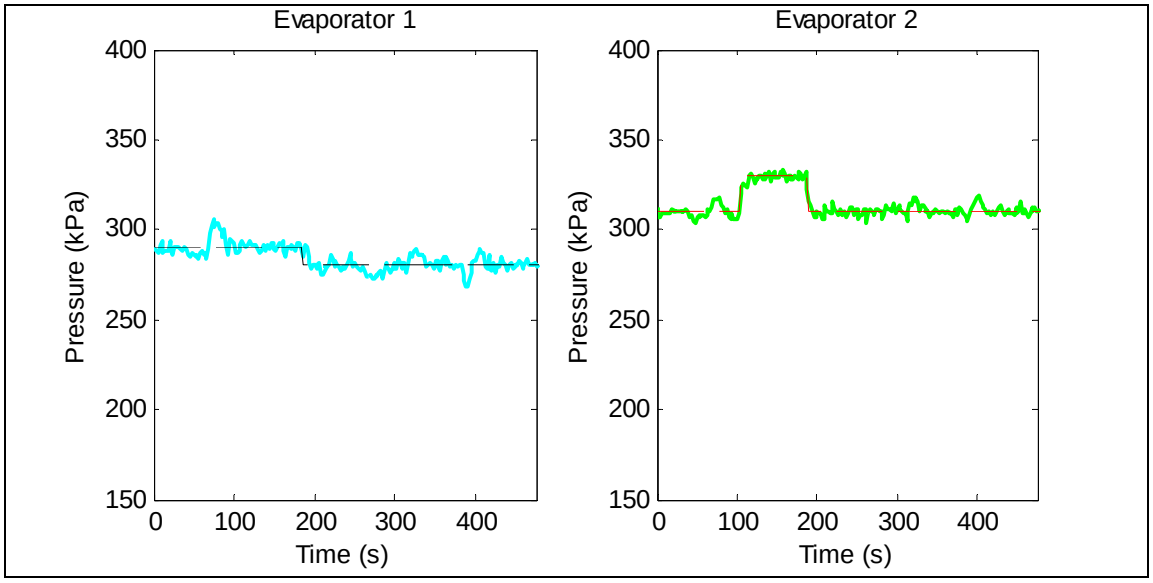

Fig. 4.7 Pressure setpoint tracking, SISO control, full water flow

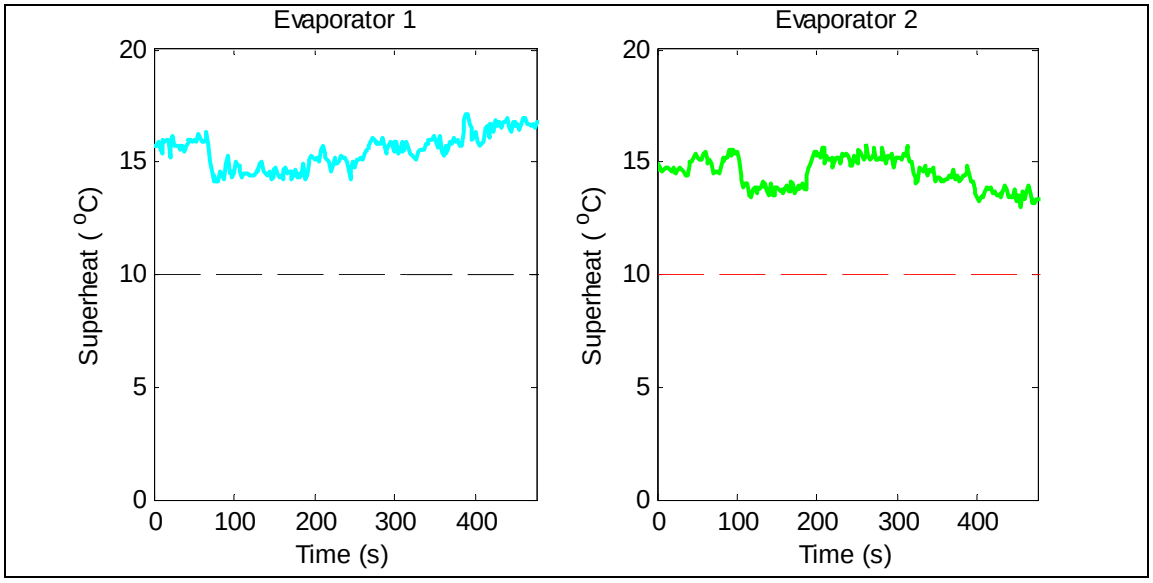

Fig. 4.8 Superheat, SISO control, full water flow

Again, the SISO loops are very successful at cooling and pressure setpoint tracking. However, in this case, superheat is very high and hence the system is not

operating as efficiently as it can. Since both the EEV and the WFV have a strong effect on superheat, and the EEV can regulate cooling, joining the two inputs and the two outputs into a MIMO plant is warranted. Ideally, the EEV would open or close to achieve the desired cooling; it would, however, also help to maintain superheat at a desirable level long enough for the WFV to catch up so that cooling can be delivered while retaining superheat. This configuration is very well suited for MPC, since the superheat constraint can be built directly into the controller.

In the proposed control architecture, the EEV and WFV for each evaporator will be coupled to regulate cooling (the primary control objective) and superheat, resulting in a 2-input, 2-output plant for each evaporator. This is different from the industrially standard approach of using EEVs to control evaporator superheat. This new approach also gives the additional benefit of being modular; it is expandable to any number of evaporators. The SISO loops controlling evaporator pressures will be retained from the baseline case. Figure 4.9 shows a block diagram of the proposed architecture.

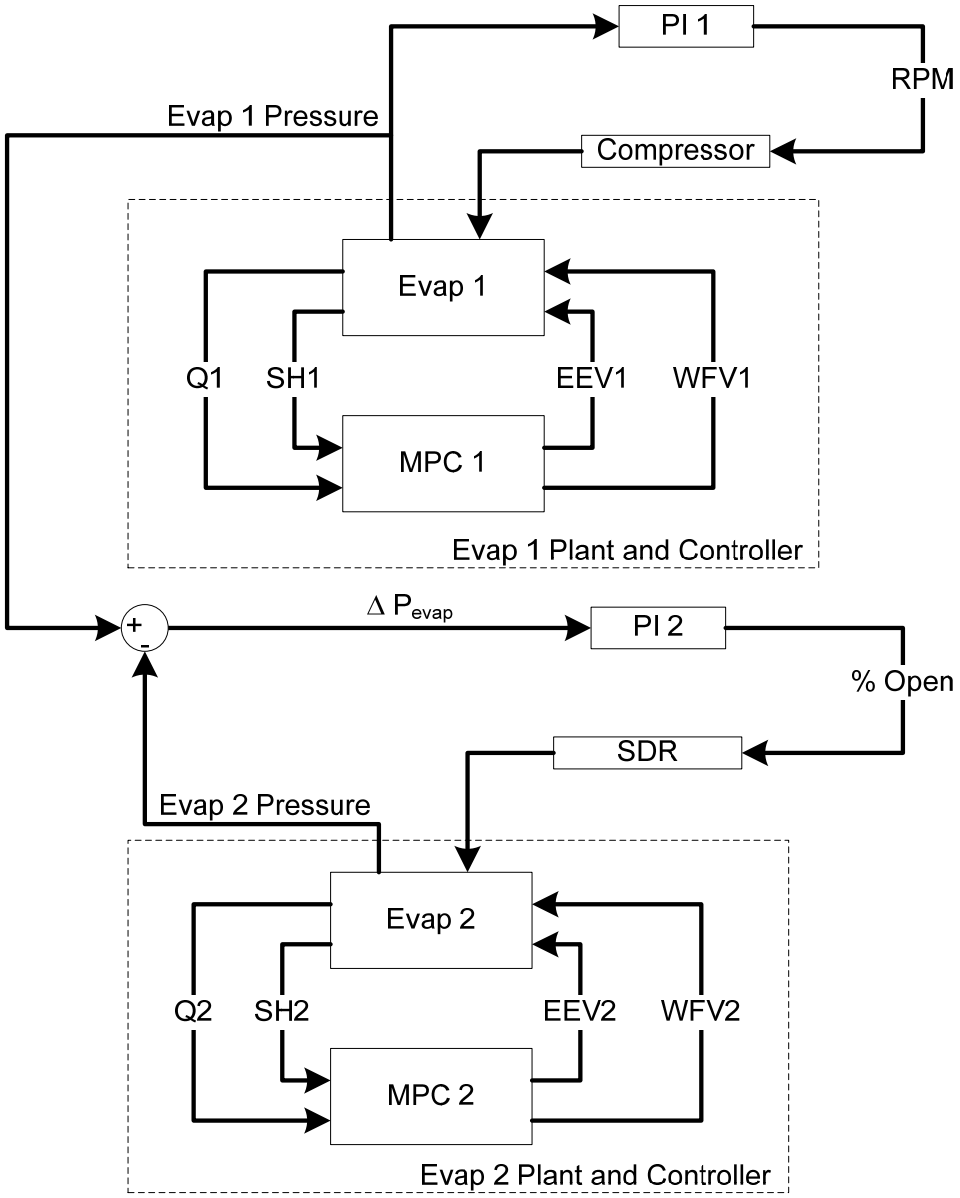

Fig. 4.9 Proposed local control architecture

Local Control Configuration

In the proposed configuration, six outputs—two evaporator pressures, two amounts of cooling, and two superheats—are regulated using two 2x2 MIMO plants and two SISO PID loops. One of the great advantages of this decentralized approach is that it is expandable to a large number of evaporators networked together over large physical distances, without the need for unreasonable increases in computing power.

The models used in the MPC controllers were experimentally derived using a step-response approach. The system was allowed to come to a steady state operating condition where each evaporator was performing 0.75 kW of cooling, at a pressure of 350 kPa, and approximately 9° C superheat. A step of 0.75% was applied to the EEV, then returned to 10%. Similarly, the WFV was increased from 27% to 31% and back. A first order response was assumed; from the graphs, time constants and steady state gains were calculated. Since the water flow rate has very weak effects on the evaporator cooling measured on the refrigerant side, this transfer function is assumed to be zero. This resulted in a 2-input, 2-output first-order model, shown below:

$$\begin{bmatrix} \dot{Q} \\ SH \end{bmatrix} = \begin{bmatrix} \frac{0.1467}{2.6s+1} & 0 \\ \frac{-1.333}{7.2s+1} & \frac{0.25}{18.9s+1} \end{bmatrix} \begin{bmatrix} EEV \\ WFV \end{bmatrix}$$

Figures 4.10 through 4.12 compare the model responses to the evaporator step responses recorded during the aforementioned data run. Figure 4.10 shows cooling response to changes in the EEV. Figure 4.11 shows the superheat response to the same

EEV changes. Finally, Figure 4.12 shows the superheat response to changes in the WFV. Although the EEV response shows evidence of second order behavior, the final settling time and steady state gain show good matching, so for the purpose of simplicity in implementing the local controller the first order models are used. All three models show good comparison to the recorded data.

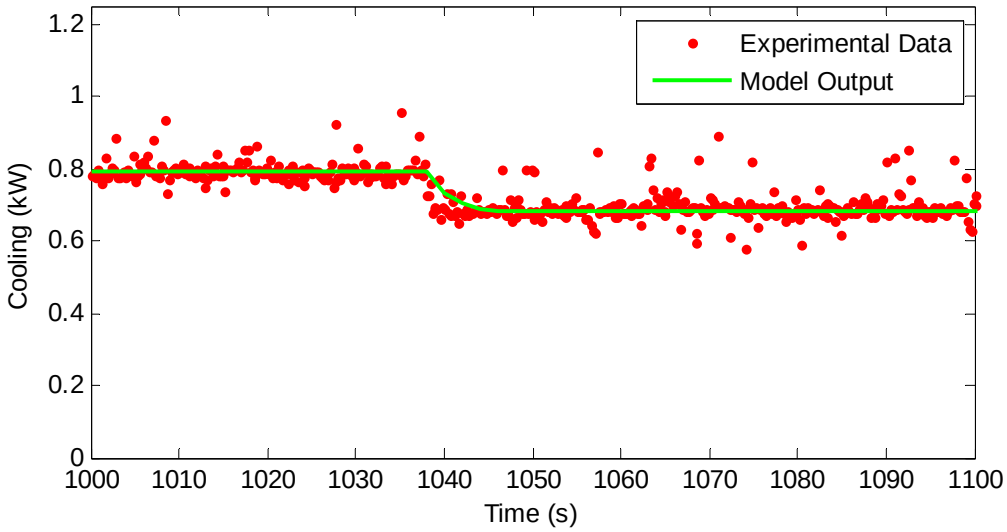

Fig. 4.10 EEV to cooling step response, model and experimental

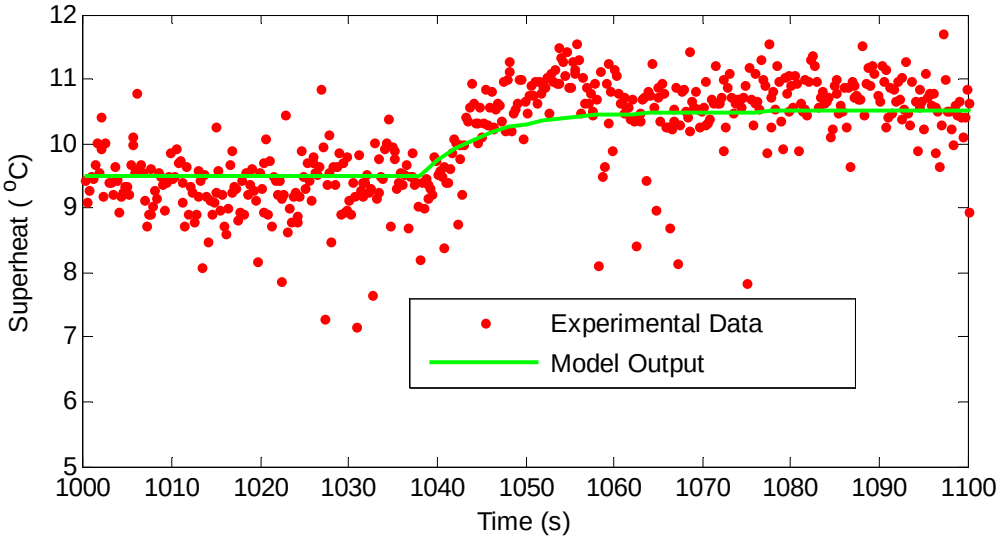

Fig. 4.11 EEV superheat step response, model and experimental

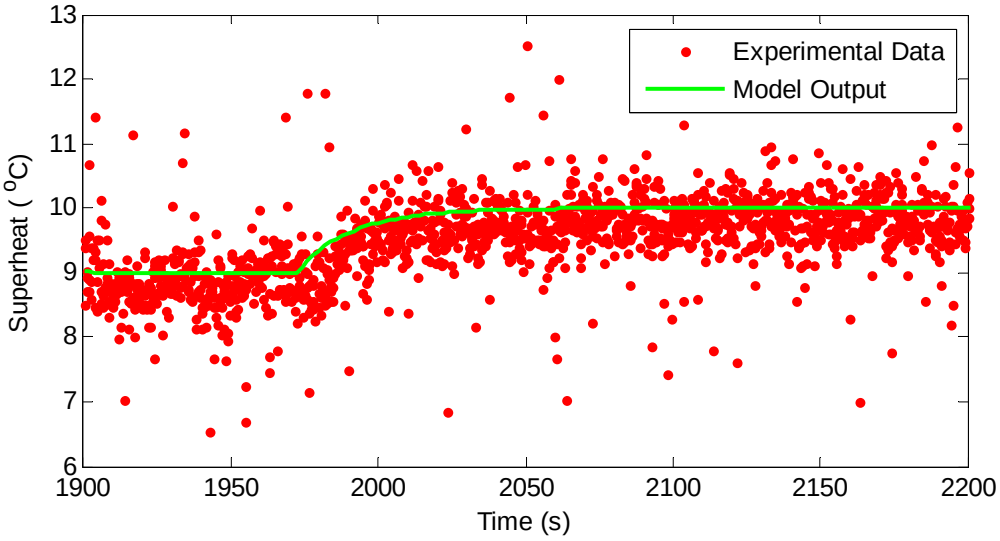

Fig. 4.12 WFV to superheat step response, model and experimental

Implemented Controller Performance

The proposed architecture was implemented on the experimental system, and was successful in regulating cooling and pressures, and keeping superheat within a desired band. The PID loops controlling the compressor and SDR have the same gains as those detailed in Table 4.1. These gains were developed using a Ziegler-Nichols tuning algorithm as detailed in [49]. Integrator anti-windup techniques are applied to the PID controllers as detailed in [50].

The MPC controller was implemented using the MatLab MPC Toolbox. The controller minimizes the following cost functions as detailed in [51]:

$$S_y(k) = \sum_{i=1}^{P} \sum_{j=1}^{n_y} \left\{ w_j^y \left[r_j(k+i) - y_j(k+i) \right] \right\}^2$$

$$S_{\Delta u}(k) = \sum_{i=1}^{M} \sum_{j=1}^{n_{mv}} \left\{ w_j^{\Delta u} \Delta u_j(k+i-1) \right\}^2$$

The first equation penalizes deviation of the outputs from the setpoints by computing the weighted sum of squared deviations, where:

$k \equiv$ current sampling interval

$k + i \equiv$ future sampling interval

$P \equiv$ prediction horizon

$n_y \equiv$ number of plant outputs

$w_j^y \equiv$ weight of output j

$r_j(k + i) - y_j(k + i) \equiv$ predicted deviation at future instant $k + i$

The second equation penalizes large changes in the actuators, and makes the controller more robust, by computing the weighted sum of controller adjustments, where:

$M \equiv$ control horizon

$k + i \equiv$ future sampling interval

$P \equiv$ prediction horizon

$n_{mv} \equiv$ number of manipulated variables (inputs)

$w_j^{\Delta u} \equiv$ weight of change in input j

$\Delta u_j(k + i - 1) \equiv$ predicted adjustment of input u_j at future instant $k + i - 1$

Local Controller Parameters

In the MPC controllers, output weights of 10,000 and 0 (w_j^y) were placed on the cooling and superheat, and rate weights of 1000 and 100 ($w_j^{\Delta u}$) were placed on the EEV and WFV, respectively. A control interval of 4 seconds was used, with a control horizon of 3 intervals (12 seconds) and a prediction horizon of 25 intervals (100 seconds). The EEVs were constrained between 8% and 14.5%; the WFVs were constrained between 22% and 50%. An output constraint was placed on superheat bounding it between 6° C and 12° C.

The weights placed on the output errors and actuator changes are an important part of tuning and implementing the MPC controller [3]. The output weights signify that the controller will seek to track the cooling setpoint, since a high weight is placed on cooling error, but the weight of superheat being set to zero implies that the controller

will ignore superheat unless the model predicts that superheat will exceed the specified constraints. An intuitive understanding of the rate weights on the actuators implies that the controller will view the EEV as ten times more expensive to change than the WVF, i.e. a 1% change in the EEV costs 1000 and a 1% change in the WFV costs 100. Likewise, if the cooling error is +/- 0.1 kW, this has the same weight as a 1% change in the EEV.

The role of the respective weight settings can be illustrated with an example. If the model predicts that the minimum superheat constraint will be violated during the prediction horizon, the controller's first "preference" will be to increase the water flow, since changing the WFV has a relatively low weight compared to tracking the cooling setpoint. Since the WFV is a slow actuator with a lower gain to superheat than the EEV, however, its change might not be sufficient to prevent the constraint violation during the prediction horizon. In this case, the EEV will also change to help prevent superheat violation, even though this will result in an increase in the cooling error—constraint violation supersedes all controller weights. After the WFV has changed sufficiently so that superheat can be retained within its constraints at the current cooling setpoint, the EEV will return to maintaining cooling. Intuitively speaking, the EEV tracks the cooling setpoint and the WFV seeks to keep the superheat inside the specified constraints; if the WFV is not able to perform this task, the EEV will help ensure that superheat stays in the desired range. Also, if the cooling setpoint is greater than the system's capacity at a given pressure, superheat cannot be kept above the lower constraint, and the controller will have the net effect of shedding the excess demand.

This approach is very different from the way that evaporators are generally controlled, in that the controller does not seek explicitly to control superheat. It can be argued that a TEV indirectly regulates cooling capacity by regulating superheat; however, the presence of evaporator dynamics creates the valve hunting problems noted earlier. Since valve hunting leads to a fluctuating flow of refrigerant, the cooling delivered by the evaporator also fluctuates. This new control architecture directly controls cooling capacity of the evaporator, ignoring superheat unless it threatens to exceed allowable limits. This is only possible due to exploitation of the capabilities of MPC. If the superheat band is set correctly, the controller and evaporator will deliver a steady amount of cooling and operate in a safe yet efficient manner.

Experimental Run with Local Controllers

An experimental run was performed using the designed local control architecture. In this experimental run, random setpoints for cooling and pressure were fed into the controllers. Note that this test run consists of tracking of randomly selected setpoints and is not intended to achieve optimal energy efficiency. Figure 4.13 shows the cooling setpoints and actual cooling vs. time for an experimental run using the local controllers; the control architecture tracks the setpoint. Figure 4.14 shows superheat for the two evaporators; although it does occasionally exceed the constraints set for the controller, the actuators respond quickly to rectify this, and superheat is never lost. Figure 4.15 shows the actuator inputs calculated by the MPC controllers.

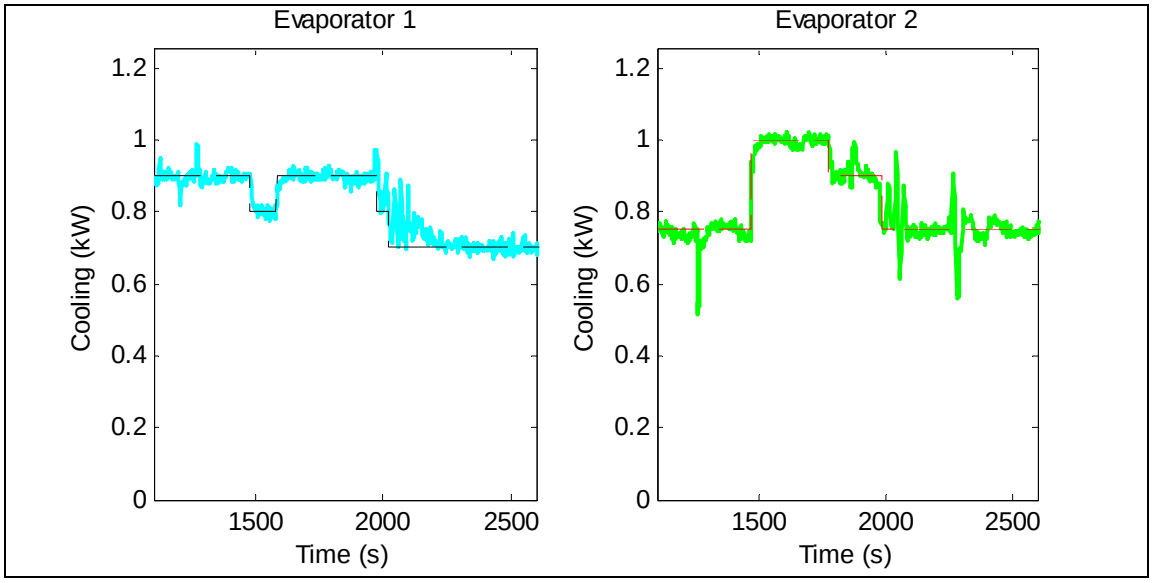

Fig. 4.13 Cooling setpoint tracking, local MPC architecture

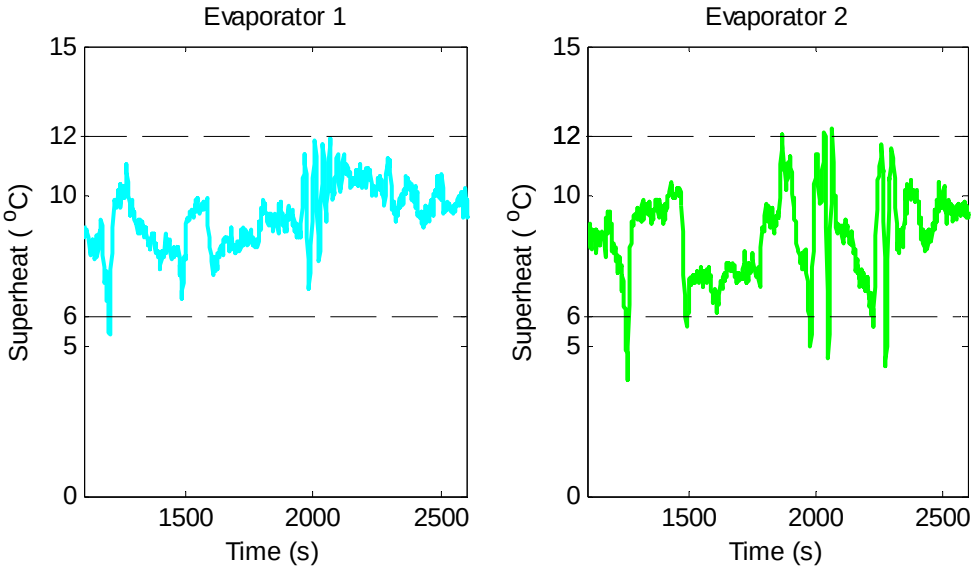

Fig. 4.14 Evaporator superheat, local MPC architecture

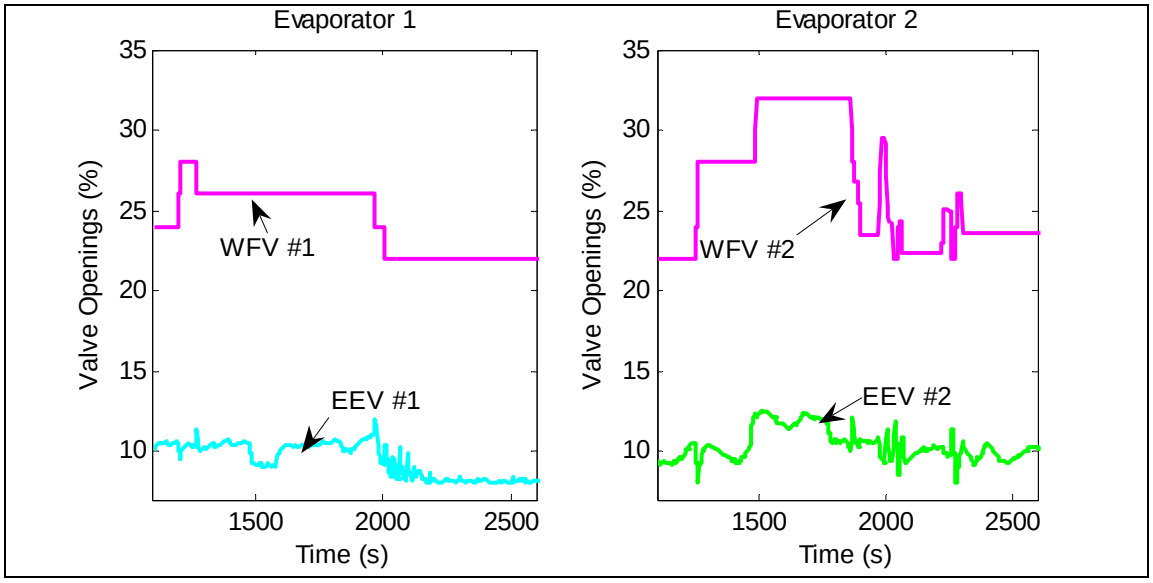

Fig. 4.15 MPC controller inputs

As more cooling is requested of either valve, it opens to permit the extra mass flow needed. Since the has the effect of increasing evaporator pressures, the compressor speed increases to keep pressure at the required setpoint; the net effect is that as more cooling is needed, the compressor increases the energy input to the system in order to achieve the desired cooling. For a decrease in cooling requirements, the reverse process occurs. Figure 4.16 shows the evaporator pressures during the same test run. The compressor response is seen in Figure 4.17.

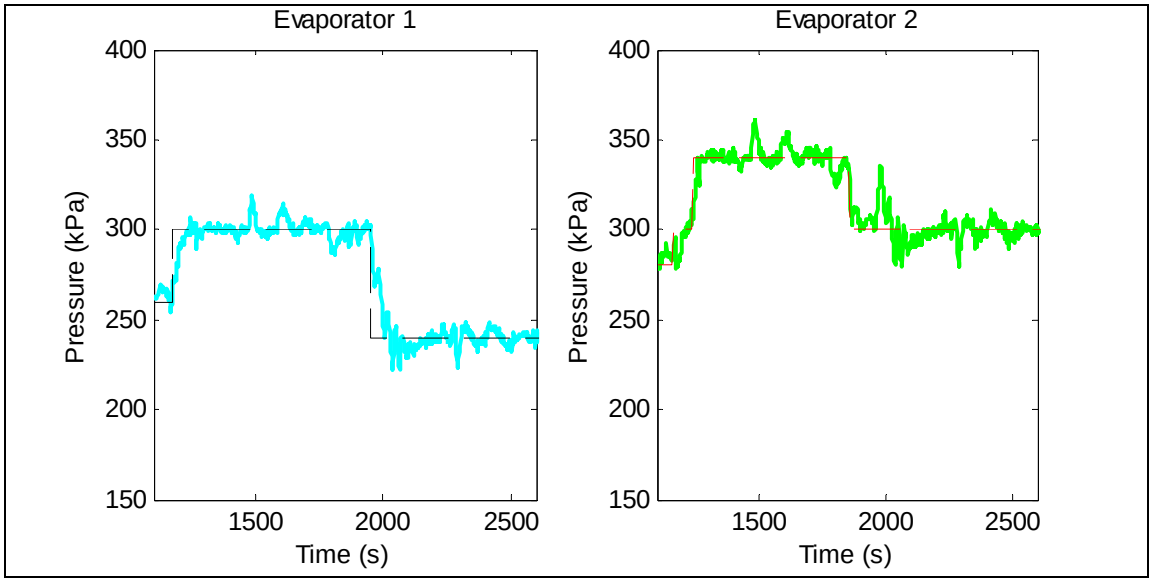

Fig. 4.16 Refrigerant pressures

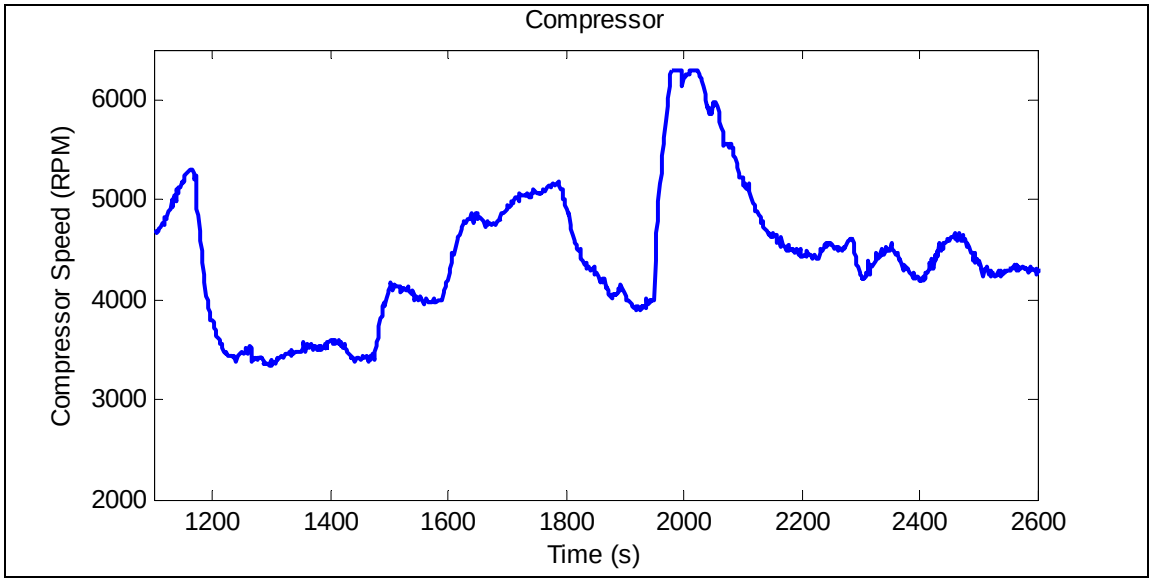

Fig. 4.17 Compressor speed regulating evaporator pressure

In conclusion, a novel control architecture using MPC has been designed and tested for this system in order to deliver a desired level of cooling and evaporator pressures, while keeping superheat within a set band. The next phase of the thesis will detail efforts to develop a global control law, which will calculate the cooling and pressure setpoints to meet a global cooling objective while maximizing energy efficiency.

CHAPTER V

DESIGN AND IMPLEMENTATION OF GLOBAL CONTROLLER

The Global Control Problem

In Chapter IV of this thesis, a suite of local controllers was developed to regulate cooling and pressure in each evaporator and ensure a minimum level of superheat. These controllers take desired pressure and cooling setpoints and meet them within the limits of operation of the system. Now we need a global controller to set the evaporator cooling and pressure setpoints to meet a desired global objective while maximizing energy efficiency. For the purposes of this research, the temperature of the evaporator water at the inlet is the chosen setpoint. This simulates regulating the temperature of a cooling zone in a commercial system. Since the water from the outlet of the evaporator is mixed with the water in the tank, the evaporator inlet water temperature is assumed to represent the temperature of the water in the tank—or cooling zone—as a whole. Figure 5.1 shows this configuration.

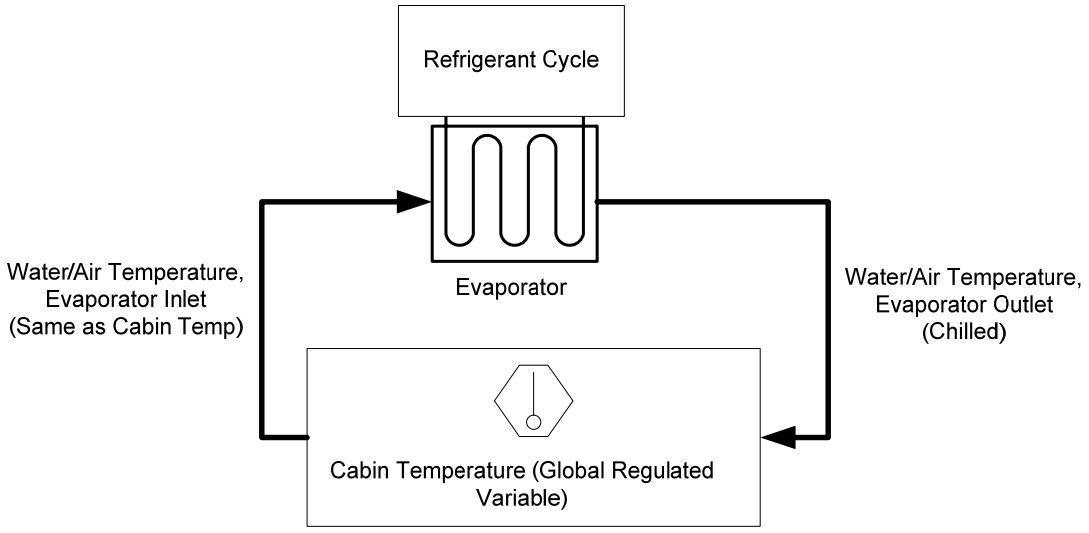

Fig. 5.1 Cooling zone configuration

The primary role of the global controller will be to govern the setpoints of the individual local controllers. This global controller will regulate the cabin temperatures as detailed in figure 5.1 while seeking to maximize the energy efficiency of the system as a whole. In order to achieve this, it must have knowledge of the system energy consumption characteristics and estimates of the volume of the cabins. In order to balance the competing goals of temperature regulation via cooling and maximizing energy efficiency, weights specified by the user will govern the controller decisions. For example, if a very large weight is placed on the water temperature error relative to the weight placed on energy consumption of the plant, the controller will make decisions that will bring the temperature to its setpoint as quickly as possible, regardless of energy consumption. Similarly, if energy consumption is specified as very "expensive," the controller will choose cooling and pressure setpoints that will minimize energy consumption and the zone temperatures will reach their setpoints slowly, or tolerate a

non-zero steady state error. In addition, this global controller must be easily expanded so that a similar approach could be used for systems with more than two evaporators. This continues the modular, networked approach pursued in the development of the local level controllers. Finally, the global controller must take into account the local level constraints of the various components; for example, the maximum amount of cooling that one evaporator is capable of delivering. The combination of tunable control weights and constraint handling again points toward adaptation of an MPC-based control algorithm for the global law. Figure 5.2 shows the overall system architecture that will be developed in this chapter.

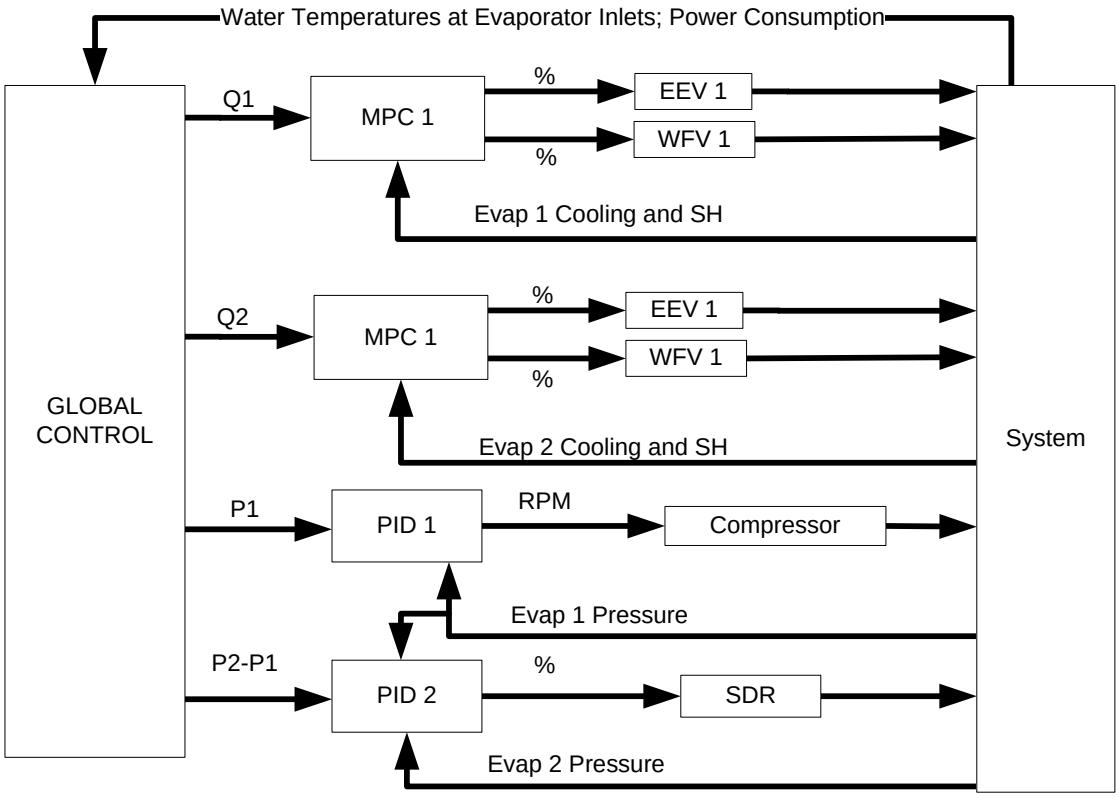

Fig. 5.2 Global control architecture

The first step in development of the global control law will be selecting an MPC framework for the controller. Then an energy efficiency function will be developed for the experimental system. A cooling zone temperature error function will be developed for use within the MPC framework. These two functions will be implemented into the MPC framework in order to create the global control law. Finally, some comments on implementation and test run results will be provided, along with discussion of the implementation results and exploration of the characteristics of the final controller.

MPC Framework for Global Law Development

The control law will seek to minimize a quadratic cost function of the form:

$$\underset{\min(x)}{J} = \frac{1}{2} x^T H x + f^T x$$

Where J is a scalar quantity to be minimized, $\boldsymbol{x}$ is the vector of length n that is to be varied to achieve the minimization, $\boldsymbol{H}$ is a constant $n \times n$ symmetric, positive definite matrix, and $\boldsymbol{f}$ is a constant vector of length n. Furthermore, this minimization is subject to the constraints:

$$Ax \leq b$$

$$x \geq x_{\min}$$

Where $\boldsymbol{x}$ is the vector of length n being varied (as before), $\boldsymbol{A}$ is a constraint matrix of dimension Nc x n, where Nc is the number of constraints, $\boldsymbol{b}$ is a constraint

vector of length *Nc*, and $\boldsymbol{x_{min}}$ is the vector containing the minimum values that each entry of $\boldsymbol{x}$ is permitted to take. This minimization problem is an adaptation of the Generalized Predictive Control approach developed by Clarke [52].

For this MPC controller the vector $\boldsymbol{x}$ is the vector of all control inputs over the MPC control horizon. Specifically, this vector will contain the changes in cooling and pressure setpoints from the setpoints at the current sampling instant:

$$x \equiv \Delta U = \begin{bmatrix} {}^{1}\Delta Q \\ {}^{2}\Delta Q \\ {}^{1}\Delta P \\ {}^{2}\Delta P \end{bmatrix} = \begin{bmatrix} {}^{1}\delta Q_{1} \\ \vdots \\ {}^{1}\delta Q_{Nu} \\ {}^{2}\delta Q_{1} \\ \vdots \\ {}^{2}\delta Q_{Nu} \\ {}^{1}\delta P_{1} \\ \vdots \\ {}^{1}\delta P_{Nu} \\ {}^{2}\delta P_{1} \\ \vdots \\ {}^{2}\delta P_{Nu} \end{bmatrix}_{4\,Nu\times 1}$$

Where *Nu* is the control horizon, ${}^{n}\delta Q_{i}$ is the change in cooling for the nth evaporator at the i^{th} future sampling instant, and ${}^{m}\delta P_{j}$ is the change in pressure for the m^{th} evaporator at the j^{th} future sampling instant. These subscript and superscript conventions will hold for the rest of this chapter. Figure 5.3 illustrates these quantities.

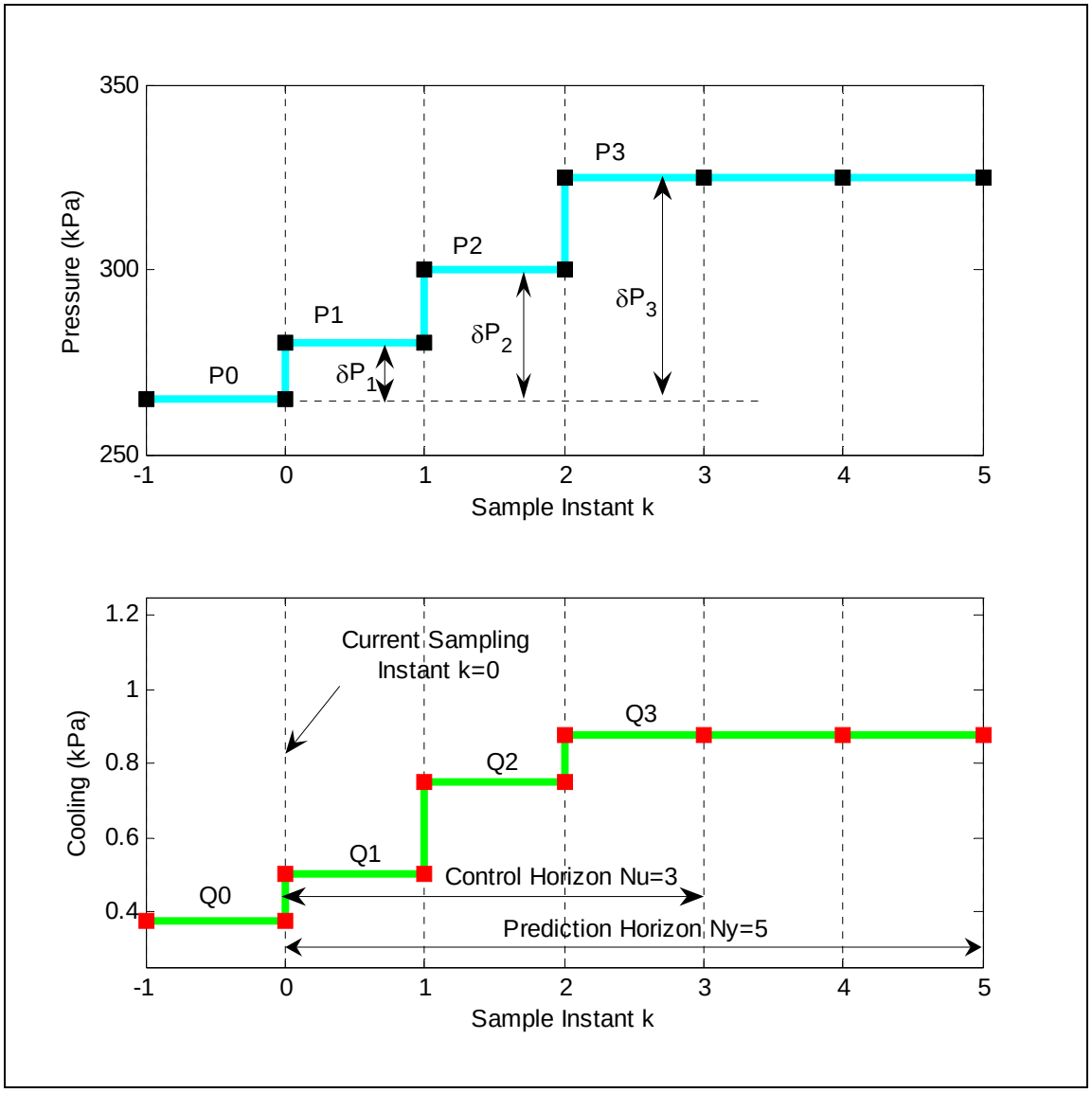

Fig. 5.3 Global controller conventions

The development of the global control law consists primarily of using the system conditions to derive the ***R*** and ***A*** matrices, as well as the ***f*** vector, in the optimization problem so that the cost function can be minimized on-line. The cooling zone temperature errors and a function describing energy consumption will be developed in the following sections and adapted to fit into the optimization problem.

Energy Efficiency Terms

The first step in devising this global control law is developing a function that expresses energy efficiency as a function of the operating conditions of the evaporators; if this function alone were used to determine the setpoints of the local controllers, it would select the pressure and cooling setpoints for each evaporator that would minimize this function. A common way of expressing the efficiency of VCC cycles is the Coefficient of Performance (COP). The COP is normally defined as [2]:

$$\beta = \frac{Q_{TOTAL}}{W_{TOTAL}}$$

Where Q_{TOTAL} is the total cooling performed, and W_{TOTAL} is the work input required to perform this cooling, including compressor work and fan work. Throughout this chapter, both cooling and work are expressed in terms of kilowatts (kW). The COP increases with increasing efficiency; however, the control law being developed will seek to minimize a cost function. Therefore, an Inverse Coefficient of Performance (ICOP) will be used, and be defined as:

$$\Phi \equiv \Phi({}^1Q, {}^2Q, {}^1P, {}^2P) = \frac{W_{COMP} + {}^1W_{FAN} + {}^2W_{FAN}}{{}^1Q + {}^2Q}$$

This portion of the cost function will cause the global controller to select the cooling and pressure setpoints that minimize this ICOP function. In order to predict the efficiency of a calculated control profile, the numerator terms must be estimated as functions of the evaporator pressure and cooling setpoints. Therefore, a mathematical relationship between the evaporator conditions and the compressor power consumption

is required. Additionally, a simulated fan work function will be needed. In order to develop these relationships for the experimental system, a series of test runs was performed to map out the range of operation for a single evaporator (in this case, evaporator #1). The second evaporator was closed off for this set of tests.

Compressor Power Function

First, the range of testing was determined. In order to find the range, the compressor speed was increased through a range of 2000 through 3000 RPM. A PI controller was used with the EEV to regulate pressure at 250 kilopascals (kPa). Plotting this result in Cartesian space, with the EEV as the ordinate and the compressor speed as the abscissa, gives the left hand side of the operating range. A similar experiment was performed using the EEV to regulate superheat at 5° C. This gave the right hand side of the operating range. Least squares curve fitting to the data from these experiments gave two linear functions demarcating the envelope of operation for the compressor mapping test in EEV-Compressor space. Figure 5.4 shows this envelope.

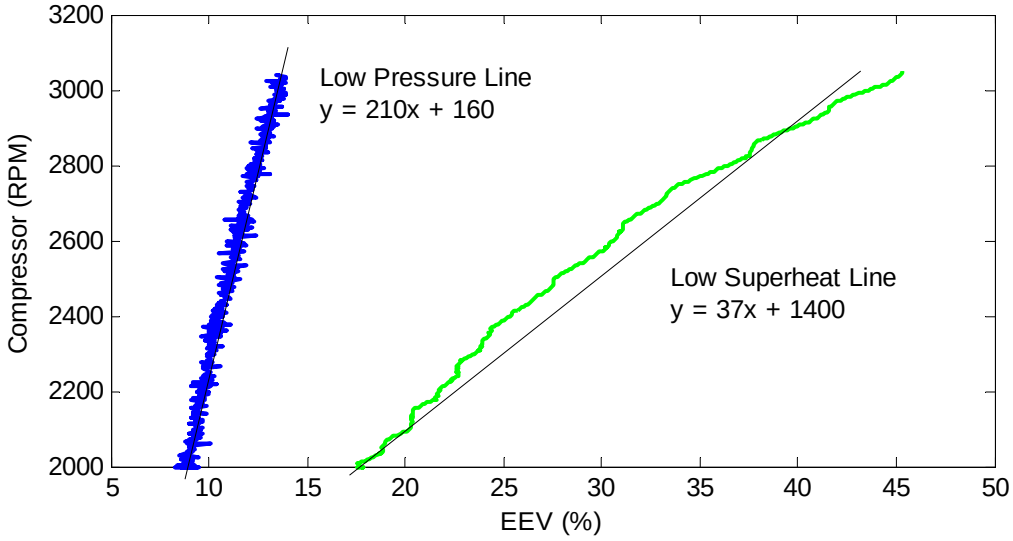

Fig. 5.4 Operating envelope

Now that a range of operation was developed, the evaporator was walked through this range very slowly, simulating a steady state condition. The condenser and evaporator outlet waters were mixed after cooling, and the condenser water cooler turned on, so that inlet water temperature for both heat exchangers remained constant over the test. Water flow rate was held constant at maximum flow. From data collected for this test, compressor work as a function of evaporator cooling and pressure could be developed using a least squares fit. Figure 5.5 shows the walkthrough. Figures 5.6 and 5.7 show the resulting data points and the least-squares curve, respectively.

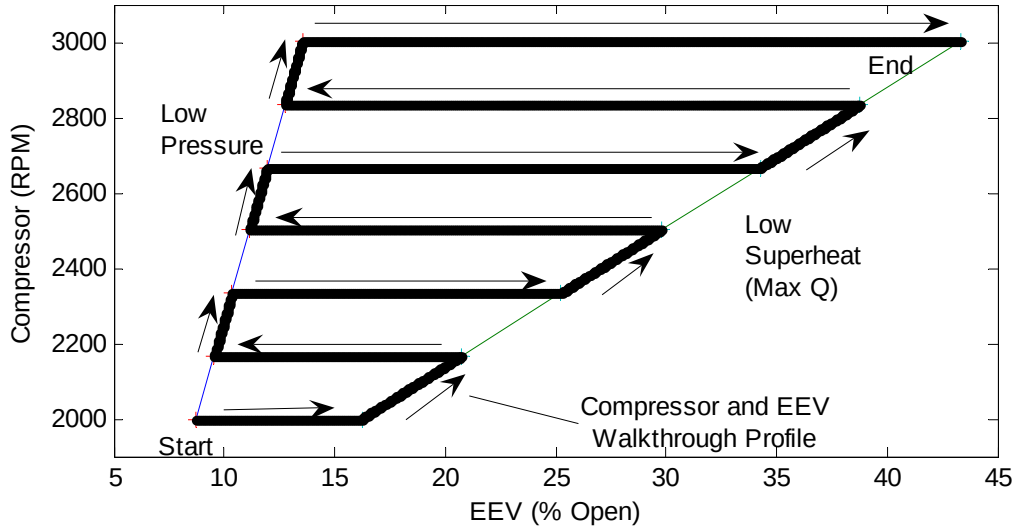

Fig. 5.5 Command profile for compressor/EEV walkthrough

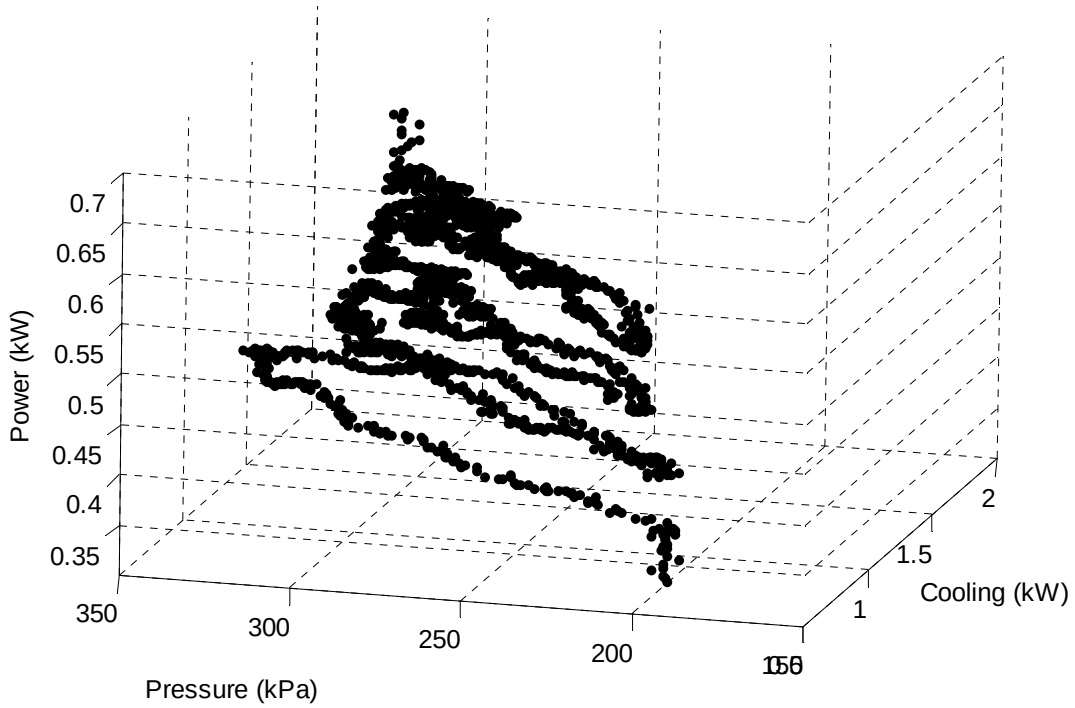

Fig. 5.6 Compressor/EEV walkthrough data points

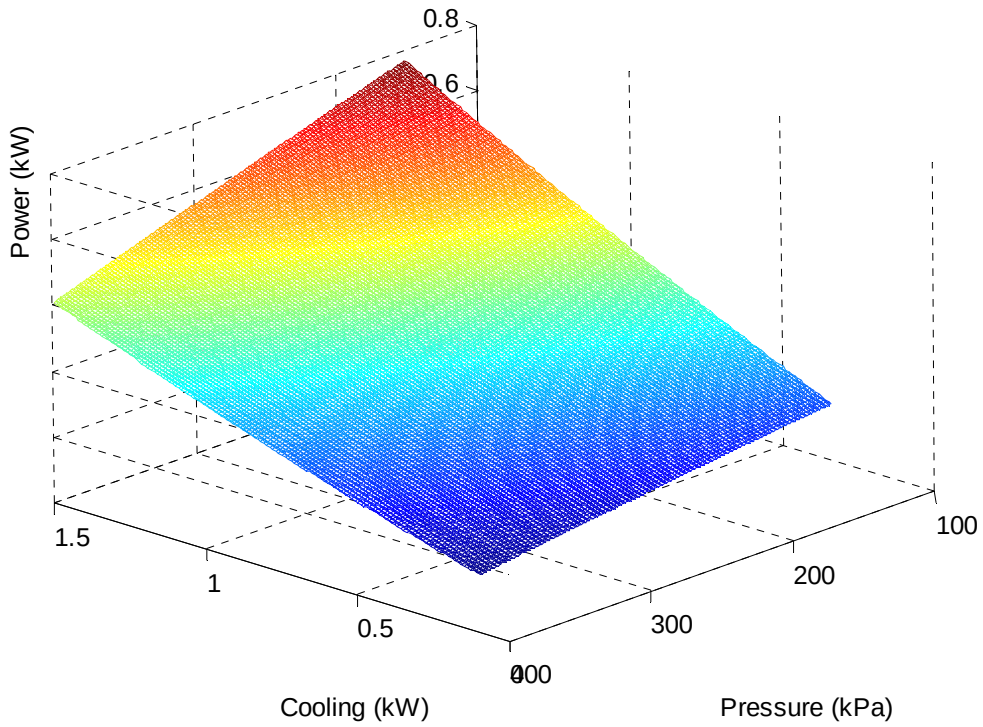

Fig. 5.7 Fit curve: of compressor power as a function of evaporator cooling and pressure

The function derived from this approach is:

$$W_{comp} = 0.1369 - 0.0004P + 0.49576Q - 0.0006PQ + 0.04Q^2$$

Therefore, we can now estimate compressor work as a function of the evaporator pressure and cooling.

Fan/Pump Power Function

In the experimental apparatus used, no energy is consumed to move the water through the evaporators, since all of the heat exchangers are gravity fed. However, this is not typical of most VCC systems, which generally use fans or pumps to create secondary fluid flow. Moreover, the selection of the operating speed of the fan or pump

is an important consideration for the system efficiency; a higher fan speed can allow for a slower compressor speed, or vice versa, in order to get the same system performance for less energy consumed, as established by Jakobsen (and cited by Leducq in [38]). Therefore, an energy consumption term—expressed as fan work—for the water flow must be developed in order to make the global controller more realistic.

In order to develop a fan work approximation for the water flow, first approximate the equivalent amount of air needed for the same amount of cooling and the same amount of temperature drop under the same refrigerant conditions. Note that the cooling is calculated on the secondary loop side as:

$$\dot{Q}_s = \dot{m}_s C_s \Delta T_s$$

Where:

$\dot{Q}_s$ ≡ Cooling on secondary loop side (air or water)

$\dot{m}_s$ ≡ Mass flow of secondary fluid across evaporator

C_s ≡ Specific heat of secondary fluid

ΔT_s ≡ Change in temperature of secondary fluid

The specific heats are:

C_s= 4.186 $\frac{kJ}{kgK}$ for water

C_s= 1.005 $\frac{kJ}{kgK}$ for air at 27°C, 1 atmosphere pressure, assuming ideal gas

Multiplying the range of water mass flow rates by the ratio of heat transfer coefficients will therefore give the range of air mass flow rates needed to get the same

drop in temperature and the same amount of cooling as that of the water based system; this can be converted to volumetric flow of air. Thus, since the water flow rates vary from 0.1 kg/s to 0.3 kg/s, the fictional fan would need to have a range of 748 to 2245 cubic feet per minute (cfm), under the same assumptions for air as before.

A DC-powered fan manufactured by Kansas Wind Power is used as the model for the system fan [53]. From their fan data, a fan power function can be least-squares curve fit that generates fan power as a cubic function of water mass flow. This fan power function will be used in the ICOP function detailed earlier. Figure 5.8 shows the calculated curve with the data points supplied by the manufacturer. The formula is as follows (fan work is in kW, water flow in kg/s):

$$W_{fan} = 0.2249\dot{m} - 1.3016\dot{m}^2 + 6.8447\dot{m}^3$$

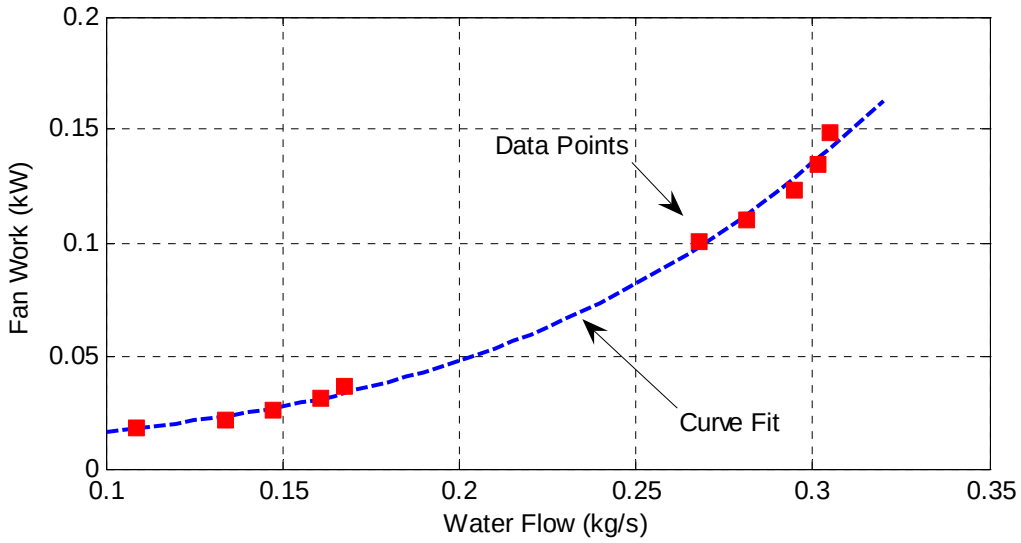

Fig. 5.8 Fan power curve

In order to implement the fan power function into the ICOP function, and thus into the MPC cost minimization problem, it must be expressed as a function of evaporator cooling and pressure, thus:

$$W_{fan} = f(\dot{m}_{water}(Q, P))$$

Experience with the experimental system suggests that for a given pressure, cooling, and superheat, the required water mass flow rate is fixed[1]. Therefore, a relationship can be derived for mass flow as a function of cooling and pressures, assuming constant superheat. This function is experimentally derived in much the same way as the compressor power term found earlier; the water flow function can be plugged into the fan power law, thereby giving the fan power as a function of evaporator pressure and cooling.

Recall that the local MPC controllers keep superheat inside a tight band. In general, the higher the evaporator pressure, the less power the compressor requires; this suggests that the global controller will tend to set high evaporator pressures, which will reduce superheat. This fact, along with the knowledge from Chapter IV with regards to efficient evaporator operation, implies that if the experimental system is operating in an energy efficient manner, superheat will tend towards its lower constraint. Therefore, for the purposes of developing this function, superheat will be fixed near its lower constraint, at 6°C. The EEV will be used to regulate superheat at this low level, as the WFV and compressor are slowly walked through their operating ranges for a single

[1] The effect of the difference between the evaporator refrigerant and water inlet temperatures is ignored, since all of the experiments performed for this research operate with the water inlet temperature in the 18°C to 30°C range.

evaporator. Figure 5.9 shows the walkthrough in WFV-Compressor Cartesian space. Figure 5.10 shows the data points generated, and figure 5.11 shows the surface fit to the data points.

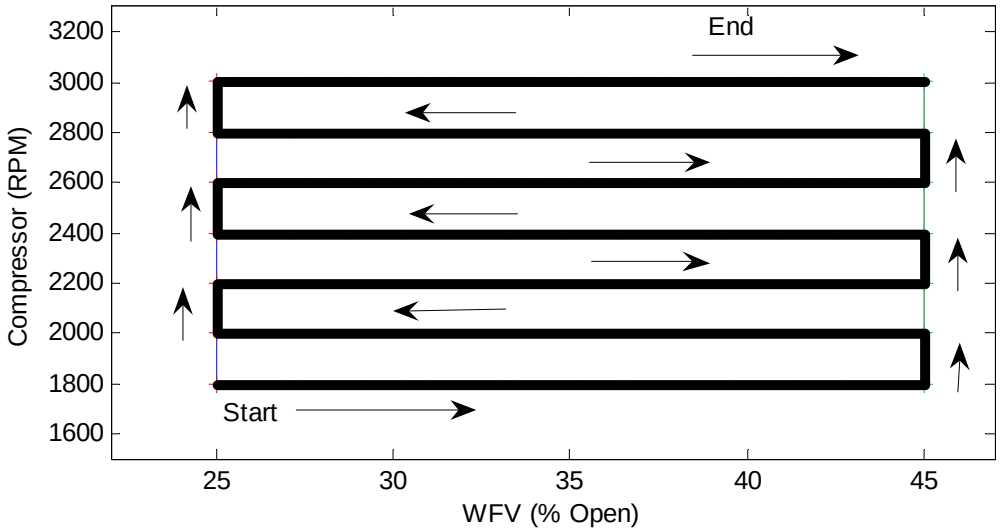

Fig. 5.9 Compressor/WFV walkthrough command profile

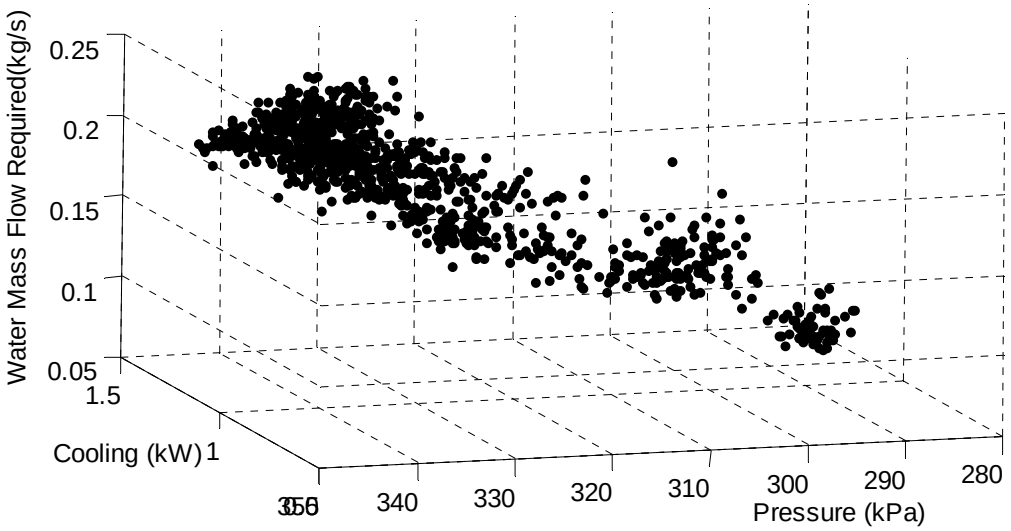

Fig. 5.10 Compressor/WFV walkthrough data points

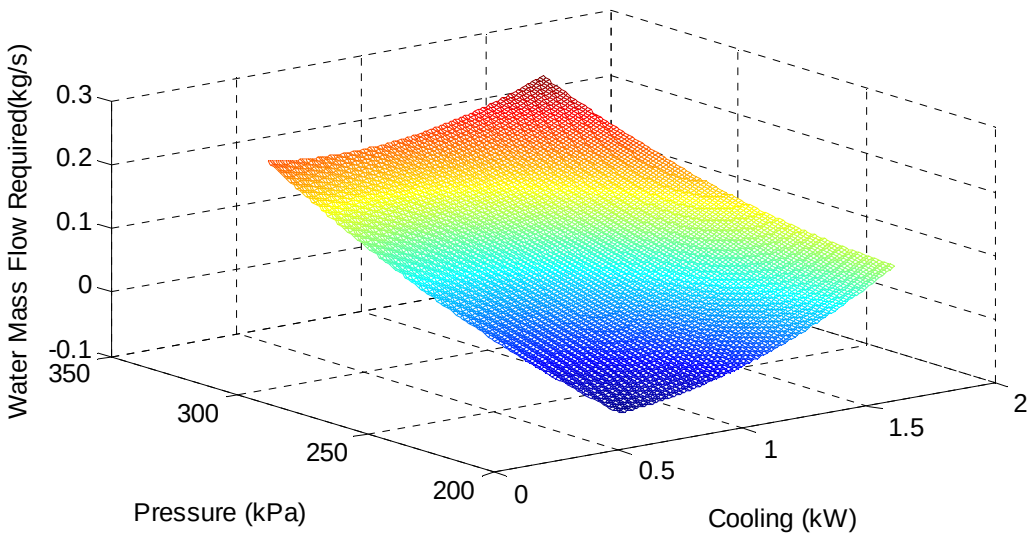

Fig. 5.11 Fit curve: water mass flow as a function of evaporator cooling and pressure

By measuring P and Q, calculating water mass flow through the derived relationship, and plugging this into the Fan work function, we have a direct link between

cooling and pressure setpoints and energy efficiency for use in the predictive controller. The equation derived is (water mass flow is in kg/s):

$$\dot{m}_{water} = -0.0185 - 0.0012P + 0.0561Q - 0.0006PQ + 0.1009Q^2$$

Assembly of ICOP Function and Conversion to Minimization Problem

Thus, we now have fan work and compressor work terms as functions of evaporator cooling and pressure. However, the system has two evaporators but only one compressor; therefore, a method of relating the total cooling performed to the compressor is needed. The compressor work term will be set as a function of the total system cooling ($Q_1 + Q_2$), and the pressure of the first evaporator only. Thus the ICOP function becomes:

$$\Phi({}^1Q, {}^2Q, {}^1P, {}^2P) = \frac{W_{COMP}({}^1Q + {}^2Q, {}^1P) + {}^1W_{FAN}({}^1Q, {}^1P) + {}^2W_{FAN}({}^2Q, {}^2P)}{{}^1Q + {}^2Q}$$

Two experimental runs were performed to justify these assumptions. First, the evaporators were sent cooling setpoints; while the individual setpoints changed, the total system cooling performed remained constant, and the compressor power consumption remained constant as well. This implies that the compressor work is dependent on the total cooling performed, and the proportion of the total that each evaporator performs has a negligible effect on compressor work. Figure 5.12 shows this test result. In addition, another test was run where the second evaporator's pressure was changed while the compressor regulated the first evaporator's pressure. This shows that the compressor power consumption is independent of the second evaporator's pressure. Figure 5.13 shows this result.

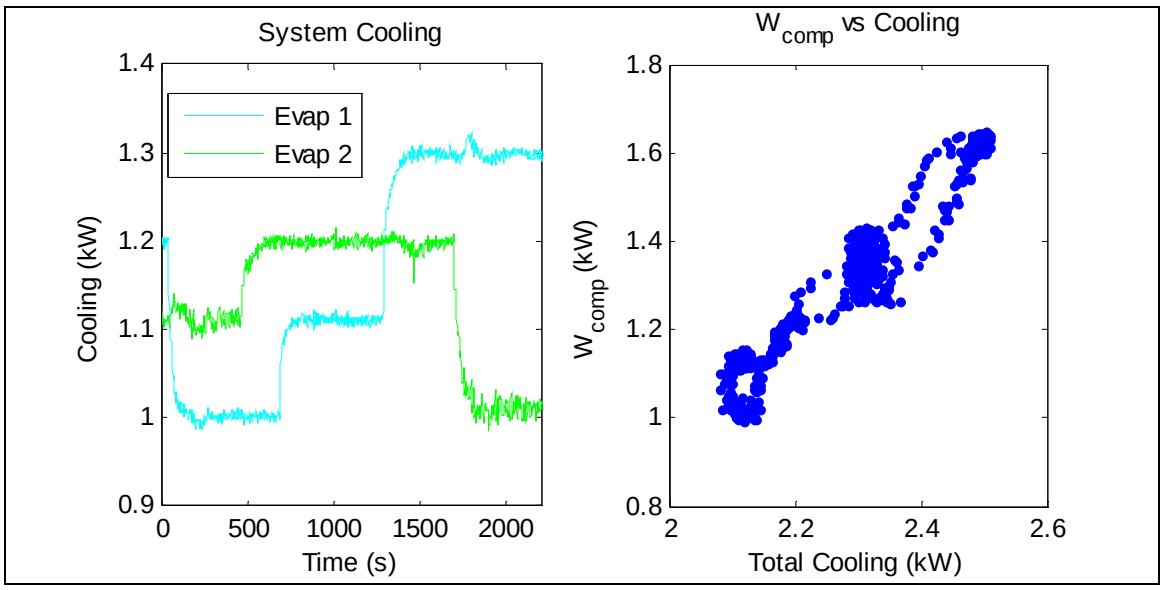

Fig. 5.12 Compressor work vs. total cooling

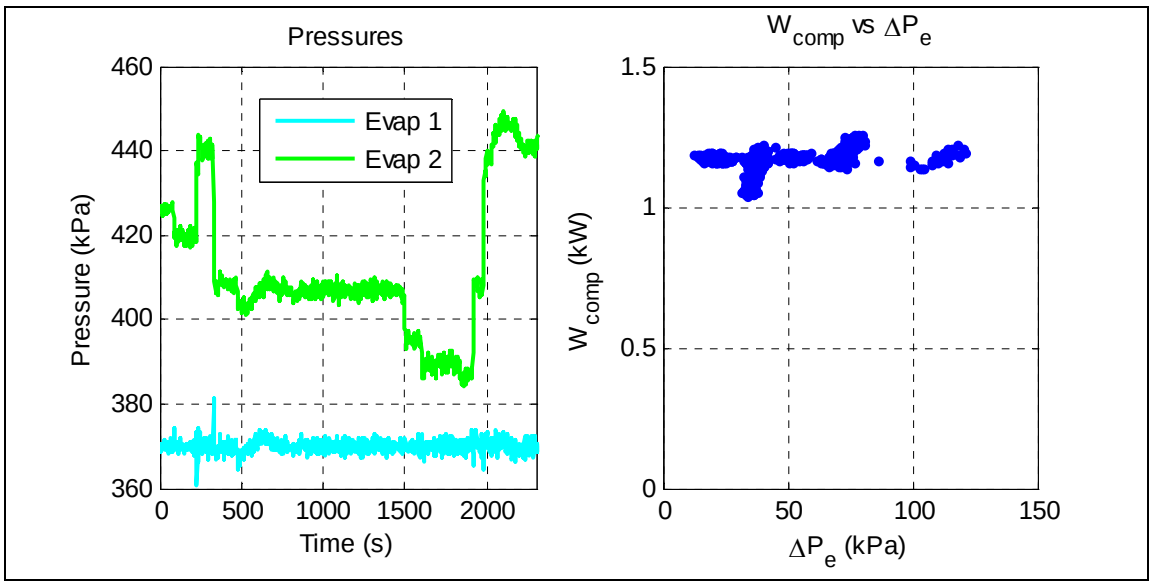

Fig. 5.13 Compressor work vs. evaporator 2 pressure

Now that the ICOP function has been derived for the experimental system, it needs to be converted into a form that can be used in the minimization problem detailed in the earlier section. The first step is linearization about a point using a Taylor series

expansion; the linearization point is be the value of the ICOP function at the current sampling instant as defined for the global controller:

$$\Phi \approx \Phi_0 + \frac{\partial \Phi}{\partial\left({}^1Q\right)}({}^1Q + {}^1\delta Q) + \frac{\partial \Phi}{\partial\left({}^2Q\right)}({}^2Q + {}^2\delta Q) + \frac{\partial \Phi}{\partial\left({}^1P\right)}({}^1P + {}^1\delta P) + \frac{\partial \Phi}{\partial\left({}^2P\right)}({}^2P + {}^2\delta P)$$

Assuming the ICOP function is convex allows ignoring of the constant terms in the above, leading to the following:

$$\Phi' = \begin{bmatrix} \frac{\partial \Phi}{\partial\left({}^1Q\right)} & \frac{\partial \Phi}{\partial\left({}^2Q\right)} & \frac{\partial \Phi}{\partial\left({}^1P\right)} & \frac{\partial \Phi}{\partial\left({}^2P\right)} \end{bmatrix} \begin{bmatrix} {}^1\delta Q \\ {}^2\delta Q \\ {}^1\delta P \\ {}^2\delta P \end{bmatrix}$$

This function is in exactly the form of the linear component of the minimization function detailed earlier, with a control horizon of 1. Since the control horizon will not generally be 1, assume that the respective gradients in the row vector above will not change over the control horizon as the controller moves the setpoints. This assumption is partially justified by keeping the control horizon small; in addition, the earlier assumption of convexity implies that the gradients of Φ will not change drastically in nature as the controller moves along the 4-dimensional manifold. This leads to an expansion of the above equation thus:

$$\Phi' = \left[\frac{\partial \Phi}{\partial \left({}^{1}Q \right)} \cdots \frac{\partial \Phi}{\partial \left({}^{1}Q \right)}, \quad \frac{\partial \Phi}{\partial \left({}^{2}Q \right)} \cdots \frac{\partial \Phi}{\partial \left({}^{2}Q \right)}, \quad \frac{\partial \Phi}{\partial \left({}^{1}P \right)} \cdots \frac{\partial \Phi}{\partial \left({}^{1}P \right)}, \quad \frac{\partial \Phi}{\partial \left({}^{2}P \right)} \cdots \frac{\partial \Phi}{\partial \left({}^{2}P \right)} \right]_{1 \times 4Nu} \begin{bmatrix} {}^{1}\delta Q_{1} \\ \vdots \\ {}^{1}\delta Q_{Nu} \\ {}^{2}\delta Q_{1} \\ \vdots \\ {}^{2}\delta Q_{Nu} \\ {}^{1}\delta P_{1} \\ \vdots \\ {}^{1}\delta P_{Nu} \\ {}^{2}\delta P_{1} \\ \vdots \\ {}^{2}\delta P_{Nu} \end{bmatrix}_{4Nu \times 1}$$

$$\Phi' = f_{\Phi}^{T} \Delta U$$

In addition, a weight is added to this term so that the competing requirements of efficiency and performance can be balanced:

$$\Phi' = \lambda_{\Phi} f_{\Phi}^{T} \Delta U$$

Therefore, by plugging the gradient terms into the linear part of the cost function, energy efficiency will be maximized as the cost function is minimized. Figure 5.14 shows an example function, plotted in two dimensional space, that illustrates this principle. If starting at point A, the gradient is negative; moving to the right will tend to minimize the function, since increasing x will decrease $x\nabla f$. Similarly, if starting at point B, where the gradient is positive, moving to the left will tend to minimize the function. This is the method that will be used by the global controller.

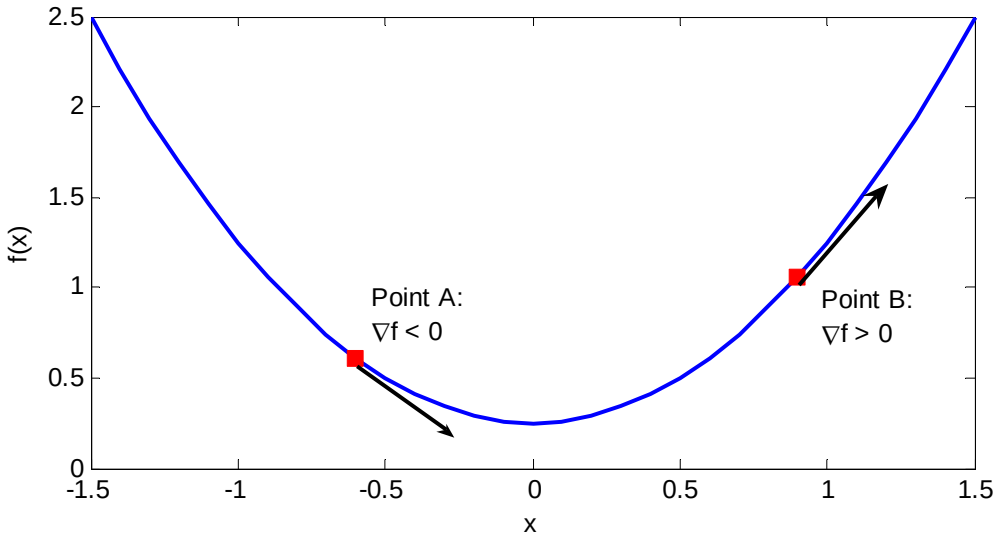

Fig. 5.14 Sample efficiency function

Cooling Zone Temperature Errors

We have developed an efficiency function that gets smaller as the system operates more efficiently. If the developed ICOP function were the only consideration for the control law, the system would simply operate at the conditions that minimize ICOP and never leave. However, VCC systems have a larger role to play—namely, keeping temperature of a body of fluid at a desired level. Therefore, the error—defined in this case as the difference between the desired and actual temperatures of a tank of water—must also play a role in the development of the control law. We start with the error definition for the i^{th} evaporator:

$$^{i}e_0 = {}^{i}T_S - {}^{i}T_0$$

In this equation, T_s is the water temperature setpoint, T_0 is the temperature at the current sampling instant, and e_0 is the error at the current sampling instant. For the sake of clarity, the evaporator number superscripts will be left off the variables henceforth during this derivation only. At each future instant, the future errors will change linearly with respect to the future levels of cooling:

$$
\begin{aligned}
e_0 &= T_S - T_0 \\
e_1 &= T_S - T_0 + \tfrac{k}{mc} Q_1 \\
e_2 &= T_S - T_0 + \tfrac{k}{mc} Q_1 + \tfrac{k}{mc} Q_2 \\
e_3 &= T_s - T_0 + \tfrac{k}{mc} Q_1 + \tfrac{k}{mc} Q_2 + \tfrac{k}{mc} Q_3 \\
&\vdots \\
e_{Ny} &= T_s - T_0 + \tfrac{k}{mc} \sum_{i=1}^{Ny} Q_i
\end{aligned}
$$

In these equations, m is the mass of the water in the "cabin," k is the sample time, and c is the specific heat of water. These are the same conventions laid out in Figure 5.3. As before, N_u is the control horizon and N_y is the output prediction horizon. This set of equations can be expressed in vector form as $e = e_0 v_1 + MQ$, where:

$$e \equiv \begin{bmatrix} e_1 \\ \vdots \\ e_{Ny} \end{bmatrix} \qquad v_1 \equiv \begin{bmatrix} 1 \\ \vdots \\ 1 \end{bmatrix}_{Ny\times 1} \qquad Q \equiv \begin{bmatrix} Q_1 \\ \vdots \\ Q_{Nu} \end{bmatrix}_{Nu\times 1}$$

$$M \equiv \frac{k}{mc} \begin{bmatrix} 1 & 0 & 0 & \cdots & 0 \\ 1 & 1 & \ddots & \ddots & \vdots \\ 1 & 1 & 1 & \ddots & 0 \\ \vdots & \ddots & \ddots & \ddots & 0 \\ 1 & \ldots & 1 & 1 & 1 \\ 1 & 1 & \cdots & 1 & 2 \\ 1 & 1 & \cdots & 1 & 3 \\ \vdots & \vdots & \cdots & \vdots & \vdots \\ 1 & 1 & \cdots & 1 & 1+Nu-Ny \end{bmatrix}_{Ny\times Nu}$$

Now define a weighting matrix: $R = \lambda I_{Ny\times Ny}$ This will be a symmetric, nonsingular, positive definite matrix, since we require λ>0. Squaring the error vector ***e*** and scaling it with the weighting matrix ***R*** yields a quadratic term:

$$\begin{aligned} e^T Re &= \left(e_0 v_1 + MQ\right)^T R\left(e_0 v_1 + MQ\right) \\ &= {e_0}^2 {v_1}^T R v_1 + e_0 {v_1}^T RMQ + e_0 Q^T M^T R^T v_1 + Q^T M^T RMQ \end{aligned}$$

Note that the second and third terms in the equality are scalars, so the above simplifies into a quadratic equation in ***Q***:

$$e^T Re = {e_0}^2 {v_1}^T R v_1 + 2e_0 {v_1}^T RMQ + Q^T M^T RMQ$$

Define the terms of the $\boldsymbol{Q}$ vector as the variations from the initial cooling condition $\boldsymbol{Q_0}$:

$$Q = Q_0 w_1 + \Delta Q$$

$$w_1 = \begin{bmatrix} 1 \\ \vdots \\ 1 \end{bmatrix}_{Nu \times 1} \qquad \Delta Q = \begin{bmatrix} \delta Q_1 \\ \vdots \\ \delta Q_{Nu} \end{bmatrix}_{Nu \times 1}$$

Substitution of this into the quadratic form for $\boldsymbol{e^T Re}$ yields:

$$\begin{aligned} e^T Re &= e_0{}^2 v_1{}^T R v_1 + 2 e_0 v_1{}^T RM \left(Q_0 w_1 + \Delta Q\right) + \left(Q_0 w_1 + \Delta Q\right)^T M^T RM \left(Q_0 w_1 + \Delta Q\right) \\ &= e_0{}^2 v_1{}^T R v_1 + 2 e_0 v_1{}^T RM Q_0 w_1 + 2 e_0 v_1{}^T RM \Delta Q + Q_0{}^2 w_1{}^T M^T RM w_1 \\ &\qquad + 2 Q_0 w_1{}^T M^T RM \Delta Q + \Delta Q^T M^T RM \Delta Q \\ &= \varepsilon + f_e^T \Delta Q + \frac{1}{2} \Delta Q^T H_e \Delta Q \end{aligned}$$

where:

$$\varepsilon = e_0{}^2 v_1{}^T R v_1 + 2 e_0 Q_0 v_1{}^T RM w_1 + Q_0{}^2 w_1{}^T M^T RM w_1$$

$$f_e^T = 2 e_0 v_1{}^T RM + 2 Q_0 w_1{}^T M^T RM$$

$$H_e = 2 M^T RM$$

Thus we now have a quadratic function in $\boldsymbol{\Delta Q}$ that is equal to the weighted sum of squares of the water temperature errors over the prediction horizon of the controller. Minimizing the sum of squares of the errors is equivalent to minimizing the sums of the errors. Therefore, it can be used in the cost function $\boldsymbol{J}$ derived earlier. Each evaporator will have one of these equations, as will be seen in the assembly of the cost function.

Assembly of Optimization Problem

Cost Function

In the earlier sections, we derived terms for the Inverse Coefficient of Performance and the water temperature errors that were either linear or quadratic in terms of the changes in control inputs, where the changes are measured from the command profile at the sampling instant of the global controller. Now these terms must be assembled into a cost function that will be used by the global controller. Recall the defined cost function:

$$\begin{aligned} \underset{\min(x)}{J} &= \frac{1}{2} x^T H x + f^T x \\ &= \frac{1}{2} \Delta u^T H \Delta u + f^T \Delta u \end{aligned}$$

$$x \equiv \Delta u = \begin{bmatrix} {}^1\delta Q_1 \\ \vdots \\ {}^1\delta Q1_{Nu} \\ {}^2\delta Q_1 \\ \vdots \\ {}^2\delta Q_{Nu} \\ {}^1\delta P_1 \\ \vdots \\ {}^1\delta P_{Nu} \\ {}^2\delta P_1 \\ \vdots \\ {}^2\delta P_{Nu} \end{bmatrix}_{4Nu \times 1} = \begin{bmatrix} {}^1\Delta Q \\ {}^2\Delta Q \\ {}^1\Delta P \\ {}^2\Delta P \end{bmatrix}$$

Inserting the temperature error terms into the cost function yields the following (note that the upper left hand superscripts on $\boldsymbol{H_e}$ and $\boldsymbol{f_e}$ denote the cooling zone/evaporator number):

$$J = \frac{1}{2}\begin{bmatrix} {}^1\Delta Q & {}^2\Delta Q & {}^1\Delta P & {}^2\Delta P \end{bmatrix}\begin{bmatrix} {}^1H_e & 0 & 0 & 0 \\ 0 & {}^2H_e & 0 & 0 \\ 0 & 0 & 0 & 0 \\ 0 & 0 & 0 & 0 \end{bmatrix}\begin{bmatrix} \Delta Q_1 \\ \Delta Q_2 \\ \Delta P_1 \\ \Delta P_2 \end{bmatrix} + \begin{bmatrix} {}^1f_e & {}^2f_e & 0 & 0 \end{bmatrix}\begin{bmatrix} {}^1\Delta Q \\ {}^2\Delta Q \\ {}^1\Delta P \\ {}^2\Delta P \end{bmatrix}$$

Now add the Φ' terms derived from the ICOP function:

$$J = \frac{1}{2}\Delta u^T \begin{bmatrix} {}^1H_e & 0 & 0 & 0 \\ 0 & {}^2H_e & 0 & 0 \\ 0 & 0 & 0 & 0 \\ 0 & 0 & 0 & 0 \end{bmatrix}\Delta u$$
$$+\begin{bmatrix} {}^1f^T{}_e + \lambda_\Phi \frac{\partial \Phi}{\partial\left({}^1Q\right)} w_1^T, & {}^2f_e^T + \lambda_\Phi \frac{\partial \Phi}{\partial\left({}^2Q\right)} w_1^T, & \lambda_\Phi \frac{\partial \Phi}{\partial\left({}^1P\right)} w_1^T, & \lambda_\Phi \frac{\partial \Phi}{\partial\left({}^2P\right)} w_1^T \end{bmatrix}\Delta u$$

Note that the matrix in the quadratic term is not invertible; define $\boldsymbol{I}$ as the $Nu \times Nu$ identity matrix, and add a very small term μ to the diagonal entries in this matrix that are currently zero:

$$J = \frac{1}{2}\Delta u^T \begin{bmatrix} {}^1H_e & 0 & 0 & 0 \\ 0 & {}^2H_e & 0 & 0 \\ 0 & 0 & \mu I & 0 \\ 0 & 0 & 0 & \mu I \end{bmatrix}\Delta u$$
$$+\begin{bmatrix} {}^1f^T{}_e + \lambda_\Phi \frac{\partial \Phi}{\partial\left({}^1Q\right)} w_1^T, & {}^2f_e^T + \lambda_\Phi \frac{\partial \Phi}{\partial\left({}^2Q\right)} w_1^T, & \lambda_\Phi \frac{\partial \Phi}{\partial\left({}^1P\right)} w_1^T, & \lambda_\Phi \frac{\partial \Phi}{\partial\left({}^2P\right)} w_1^T \end{bmatrix}\Delta u$$

Finally, as with any controller, a smooth control profile is desirable; that is, some damping on the controller is necessary so that the setpoints do not oscillate wildly. Recall that the terms in Δu are themselves changes in the control action; therefore, simply adding an additional weight to the terms in the quadratic matrix will provide controller damping. Define λ_Q and λ_P as the rate weights assigned to changes in cooling and pressure, respectively, and add to the quadratic matrix thus:

$$J = \frac{1}{2}\Delta u^T \begin{bmatrix} {}^1H_e + \lambda_Q I & 0 & 0 & 0 \\ 0 & {}^2H_e + \lambda_Q I & 0 & 0 \\ 0 & 0 & (\mu + \lambda_P) I & 0 \\ 0 & 0 & 0 & (\mu + \lambda_P) I \end{bmatrix} \Delta u$$
$$+ \left[{}^1f_e{}^T + \lambda_\Phi \frac{\partial \Phi}{\partial Q_1} w_1^T, \quad {}^2f^T{}_e + \lambda_\Phi \frac{\partial \Phi}{\partial Q_2} w_1^T, \quad \lambda_\Phi \frac{\partial \Phi}{\partial P_1} w_1^T, \quad \lambda_\Phi \frac{\partial \Phi}{\partial P_2} w_1^T \right] \Delta u$$

This is the quadratic cost function that the global controller will minimize; it balances the cooling demand with energy efficiency according to the weights assigned to each by the user, and can be tuned to achieve desired performance characteristics. Now a set of constraints can be built into the solution; the development of these constraints is detailed in the next section.

Constraint Matrix Development

Recall that the constraints in the quadratic programming problem must be put in the following format:

$$A\Delta u \le b$$
$$\Delta u \ge \Delta u_{\min}$$

In this equation $\boldsymbol{A}$ is a constraint matrix of dimension $Nc \times 4Nu$, where Nc is the number of constraints, $\boldsymbol{b}$ is a constraint vector of length Nc, and Δu is a $4Nu$ vector containing the command profile through the control horizon Nu.

The constraints themselves are strictly of the input type, i.e. they are limitations on the requests that the global controller makes of the local level controllers. This allows the global controller to account for the maximum cooling that the evaporators are capable of delivering, as well as a reasonable range of evaporator pressures. It also can add a maximum slew rate to the change in setpoints; if the change in cooling and pressure requirements is limited, the local level controllers can settle quickly to meet the setpoints, reducing the chances of unstable behavior and keeping transient dynamics to a minimum. The global constraints chosen are detailed in Table 5.1.

Table 5.1 Global constraints

Constraint	Variable	Value
1	Evaporator Maximum Cooling	1 kW
2	Evaporator Minimum Cooling	0.6 kW
3	Evaporator Maximum Pressure	350 kPa
4	Evaporator Minimum Pressure	200 kPa
5	Maximum Pressure Slew Rate	40 kPa/sample
6	Maximum Evap Pressure Differential, P2 - P1	100 kPa
7	Minimum Evap Pressure Differential, P2 - P1	0 kPa

These constraints are used to generate the constraint matrices. In the global controller implementation, each of these constraints is combined with the conditions at the sampling instant to create a constraint in terms of the maximum change of the control

input. Therefore the maximum cooling change for a given evaporator (Constraint #1 from Table 5.1) is calculated thus:

$$
\begin{aligned}
&{}^{i}Q_0 + {}^{i}\delta Q \le Q_{\max} \\
&\Downarrow \\
&{}^{i}\delta Q \le Q_{\max} - {}^{i}Q_0
\end{aligned}
$$

Similarly, the maximum pressure change for a given evaporator (Constraint #3) is constrained by:

$$
\begin{aligned}
&{}^{i}P_0 + {}^{i}\delta P \le P_{\max} \\
&\Downarrow \\
&{}^{i}\delta P \le P_{\max} - {}^{i}P_0
\end{aligned}
$$

Additionally, a slew rate limit is imposed (Constraint #5):

$$
{}^{i}\delta P \le \delta P_{\max}
$$

The maximum change in pressure differential between the evaporators (Constraint #6) is calculated thus:

$$
\begin{aligned}
&{}^{2}P_0 + {}^{2}\delta Q - ({}^{1}P_0 + {}^{1}\delta Q) \le \Delta Pe_{\max} \\
&\Downarrow \\
&-{}^{1}\delta P + {}^{2}\delta P \le \Delta Pe_{\max} + {}^{1}P_0 - {}^{2}P_0
\end{aligned}
$$

The construction of the experimental systems requires that the pressure of evaporator 2 is always greater than or equal to than that of evaporator 1 (Constraint #7):

$$
\begin{aligned}
&{}^{1}P_0 + {}^{1}\delta P - ({}^{2}P_0 + {}^{2}\delta P) \le \Delta Pe_{\min} = 0 \\
&\Downarrow \\
&{}^{1}\delta P - {}^{2}\delta P \le -{}^{1}P_0 + {}^{2}P_0
\end{aligned}
$$

The left sides of each of the preceding inequalities are used to construct the $\boldsymbol{A}$ matrix in the first constraint equation. The right sides of each are used as the elements of the $\boldsymbol{b}$ vector in the same equation. For example, if the control horizon $Nu = 1$, the constraint equation becomes:

$$\begin{bmatrix} 1 & 0 & 0 & 0 \\ 0 & 1 & 0 & 0 \\ 0 & 0 & 1 & 0 \\ 0 & 0 & 1 & 0 \\ 0 & 0 & 0 & 1 \\ 0 & 0 & 0 & 1 \\ 0 & 0 & -1 & 1 \\ 0 & 0 & 1 & -1 \end{bmatrix} \begin{bmatrix} {}^{1}\delta Q_1 \\ {}^{2}\delta Q_1 \\ {}^{1}\delta P_1 \\ {}^{2}\delta P_1 \end{bmatrix} \leq \begin{bmatrix} Q_{\max} - {}^{1}Q_0 \\ Q_{\max} - {}^{2}Q_0 \\ P_{\max} - {}^{1}P_0 \\ \delta P_{\max} \\ P_{\max} - {}^{2}P_0 \\ \delta P_{\max} \\ \Delta Pe_{\max} + {}^{1}P_0 - {}^{2}P_0 \\ -{}^{1}P_0 + {}^{2}P_0 \end{bmatrix}$$

For the general case, this becomes:

$$\begin{bmatrix} I & 0 & 0 & 0 \\ 0 & I & 0 & 0 \\ 0 & 0 & I & 0 \\ 0 & 0 & I & 0 \\ 0 & 0 & 0 & I \\ 0 & 0 & 0 & I \\ 0 & 0 & -I & I \\ 0 & 0 & I & -I \end{bmatrix}_{8Nu \times 4Nu} \begin{bmatrix} {}^{1}\delta Q_1 \\ \vdots \\ {}^{1}\delta Q_{Nu} \\ {}^{2}\delta Q_1 \\ \vdots \\ {}^{2}\delta Q_{Nu} \\ {}^{1}\delta P_1 \\ \vdots \\ {}^{1}\delta P_{Nu} \\ {}^{2}\delta P_1 \\ \vdots \\ {}^{2}\delta P_{Nu} \end{bmatrix}_{4Nu \times 1} \leq \begin{bmatrix} \left(Q_{\max} - {}^{1}Q_0\right) w_1 \\ \left(Q_{\max} - {}^{2}Q_0\right) w_1 \\ \left(P_{\max} - {}^{1}P_0\right) w_1 \\ \delta P_{\max} w_1 \\ \left(P_{\max} - {}^{2}P_0\right) w_1 \\ \delta P_{\max} w_1 \\ \left(\Delta Pe_{\max} + {}^{1}P_0 - {}^{2}P_0\right) w_1 \\ \left(-{}^{1}P_0 + {}^{2}P_0\right) w_1 \end{bmatrix}$$

Where, as before, Nu is the control horizon, $\boldsymbol{I}$ is the $Nu \times Nu$ identity matrix, and $\boldsymbol{w_1}$ is the $Nu \times 1$ vector wherein every element is the number 1. Note that if the number

of constraints per sample time *Nc* was different than 8, the first matrix would be *NcNu* × 4*Nu* in size.

A similar approach is used to calculate the $\boldsymbol{x_{min}}$ vector. Constraints #2 and #4 from Table 5.1 lead to the following:

$$
\begin{aligned}
&{}^{i}Q_0 + {}^{i}\delta Q \geq Q_{\min} \\
&\Downarrow \\
&{}^{i}\delta Q \geq Q_{\min} - {}^{i}Q_0
\end{aligned}
$$

$$
\begin{aligned}
&{}^{i}P_0 + {}^{i}\delta P \geq P_{\min} \\
&\Downarrow \\
&{}^{i}\delta P \geq P_{\min} - P_0
\end{aligned}
$$

The minimum constraint requirement is therefore constructed thus:

$$
\begin{bmatrix}
{}^{1}\delta Q_1 \\
\vdots \\
{}^{1}\delta Q_{Nu} \\
{}^{2}\delta Q_1 \\
\vdots \\
{}^{2}\delta Q_{Nu} \\
{}^{1}\delta P_1 \\
\vdots \\
{}^{1}\delta P_{Nu} \\
{}^{2}\delta P_1 \\
\vdots \\
{}^{2}\delta P_{Nu}
\end{bmatrix}_{4Nu\times 1}
\geq x_{\min} =
\begin{bmatrix}
\left(Q_{\min} - {}^{1}Q_0\right) w_1 \\
\left(Q_{\min} - {}^{2}Q_0\right) w_1 \\
\left(P_{\min} - {}^{1}P_0\right) w_1 \\
\left(P_{\min} - {}^{2}P_0\right) w_1
\end{bmatrix}
$$

Controller Implementation

The controller was implemented in Simulink, in conjunction with the local controllers detailed in Chapter IV. The quadratic programming software used is the QPDANTZ program, which is included in the MatLab Model Predictive Control Toolbox. This program uses the Wolfe-Dantzig quadratic programming (QP) algorithm to solve the QP problem [51, 54]. System conditions are measured and transformed into a format useable by the QPDANTZ program by a combination of embedded MatLab functions and S-functions coded in the programming language ***C***. These coded functions were adapted from the MatLab code supplied with the MPC Toolbox. An m-file program was also written to allow the user to set the various weights and parameters and set up the Simulink file for compilation into the WinCon real-time software.

Global Controller Development and Experimental Results

A testing program was performed subjecting the implementing controller to a series of conditions to verify that the controller is designed correctly and that it does indeed tend to the most efficient operating condition. Experimentation with the controller resulted in a baseline set of parameters for which the system works well; these parameters are found in Table 5.2.

Table 5.2 Global controller MPC parameters

Parameter	Description	Value
Ts	Sample Time	150 s
Nu	Control Horizon	3
Ny	Prediction Horizon	5

Test 1: Baseline Case with Global Controller

For the first test shown, the entire control system was run to bring the water temperature down to a desired setpoint as shown. During this test, a small amount of condenser water was mixed into the evaporator water; due to the system construction, the same amount of mixed evaporator water overflows into the condenser water tank. This has the effect of adding a disturbance to the plant; namely, heating at an unknown rate is added to the water in addition to the cooling performed by the system. For this test, the parameters are found in Table 5.3. Cooling and water temperatures are shown in Figure 5.15.

Table 5.3 Test 1 parameters

Parameter	Description	Value
Ts	Sample Time	150 s
Nu	Control Horizon	3
Ny	Prediction Horizon	5
λ_e	Temperature Error Weight	1.0
λ_Φ	ICOP Weight	2000
λ_Q	Cooling Slew Weight	4.0
λ_P	Pressure Slew Weight	4.0

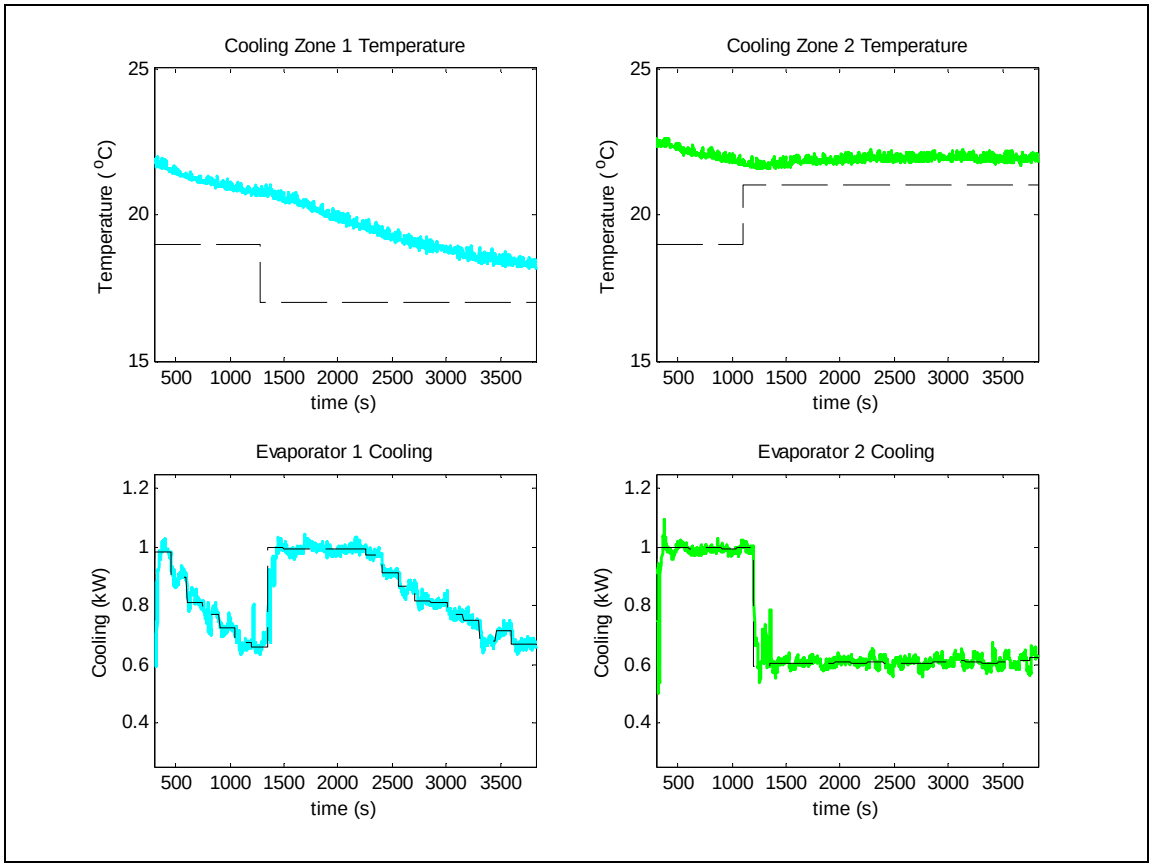

Fig. 5.15 Test 1 cooling zone temperatures and cooling

This figure displays some of the functionality of the control architecture. At the beginning of the experimental run, the zone 1 error is approximately 3 °C; as the water is chilled, the error decreases, and the global controller begins to allow cooling to decrease, as the dominance of the error term in the cost function decreases. At approximately 1200 seconds, the setpoint is decreased, increasing the error significantly; this time, the controller responds by increasing cooling to the maximum value allowed. Again, as the error decreases, the cooling setpoint decreases, resulting in an asymptotic approach to final temperature by the cooling zone temperature. Cooling zone 2 shows a different example of the controller behavior during the same run. As the setpoint is increased at

approximately 1100 seconds, the controller reduces cooling to its minimum of 0.6 kW. Due to the disturbance added, which can be surmised to be approximately 0.6 kW, the cooling zone temperature remains almost constant throughout the run. This displays the effect of the weight attached to the ICOP term in the cost function; the steady state error of approximately 1 °C is acceptable to the controller. Later experiments will explore the effects of changing the ICOP weight.

Figure 5.16 shows the superheat during this experimental run. Note that except for some transients, the local controllers successfully keep superheat within a band of 6 to 12 °C as required.

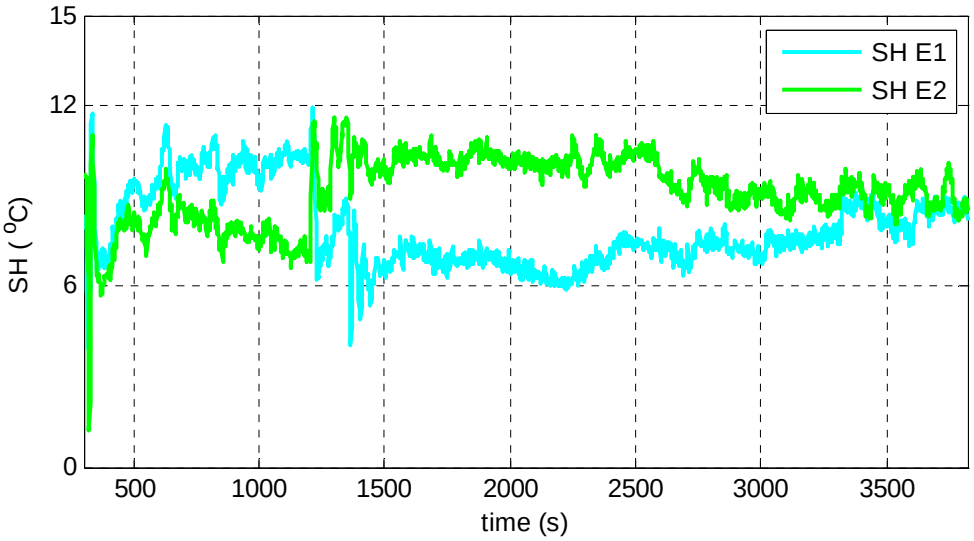

Fig. 5.16 Test 1 superheat

Figure 5.17 shows the pressure during the experimental run; the controller brings both pressures to the same value; they oscillate about 325 kPa over the course of the test. A future data run will show the effect of making one fan more expensive than another.

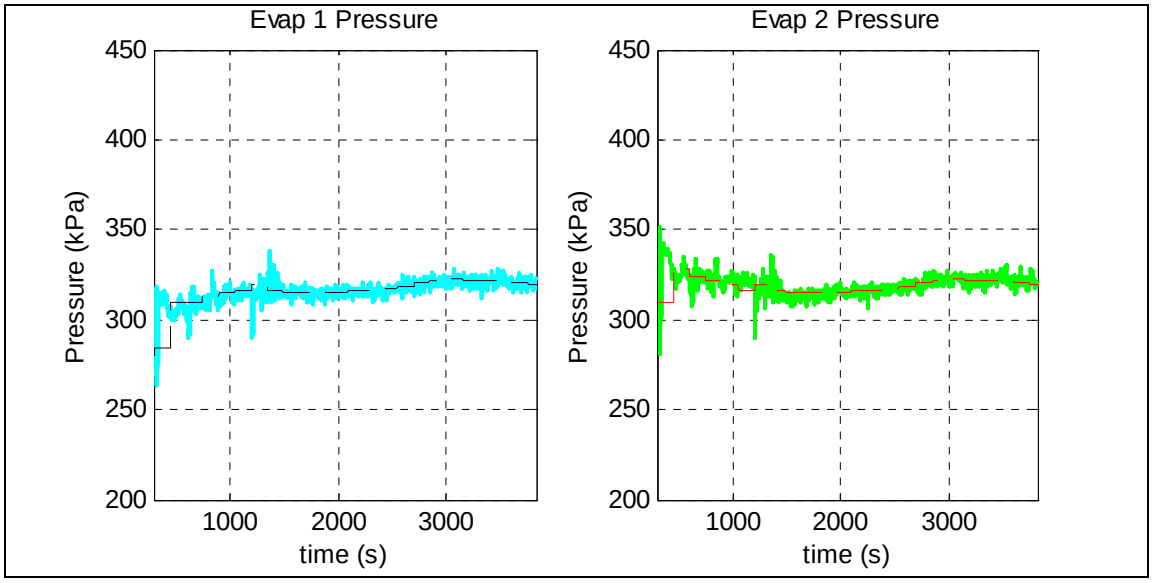

Fig. 5.17 Test 1 evaporator pressures

Finally, figures 5.18 and 5.19 show the power consumption and Coefficient of Performance, respectively. Note that more fan work is required as more cooling is needed. Additionally, the COP drifts upward slightly as the experiment progresses, implying that the system is tending towards more efficient operation.

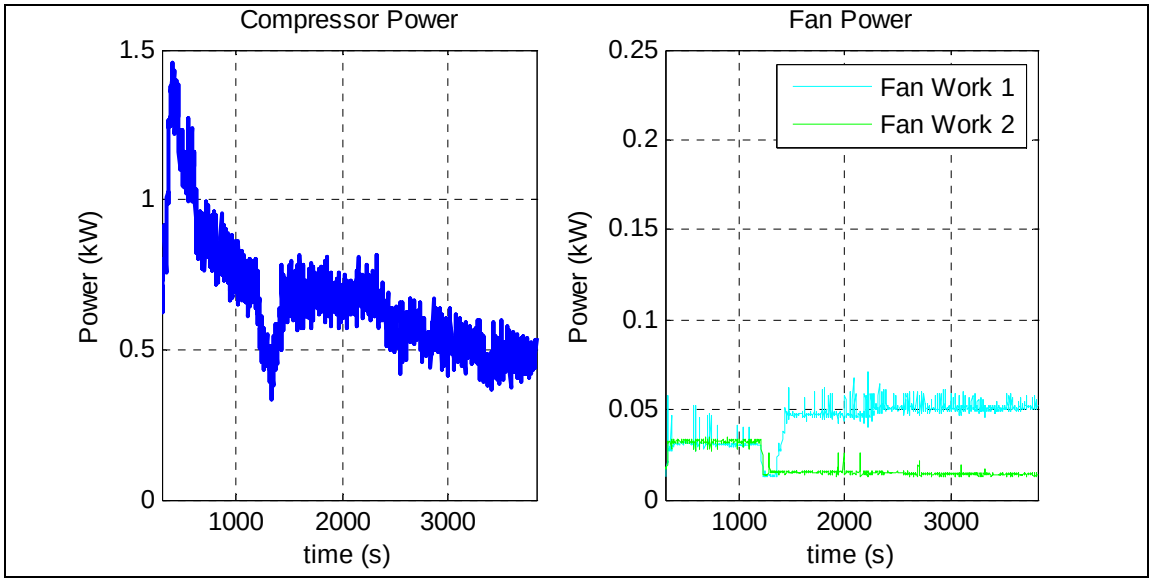

Fig. 5.18 Test 1 component power consumption

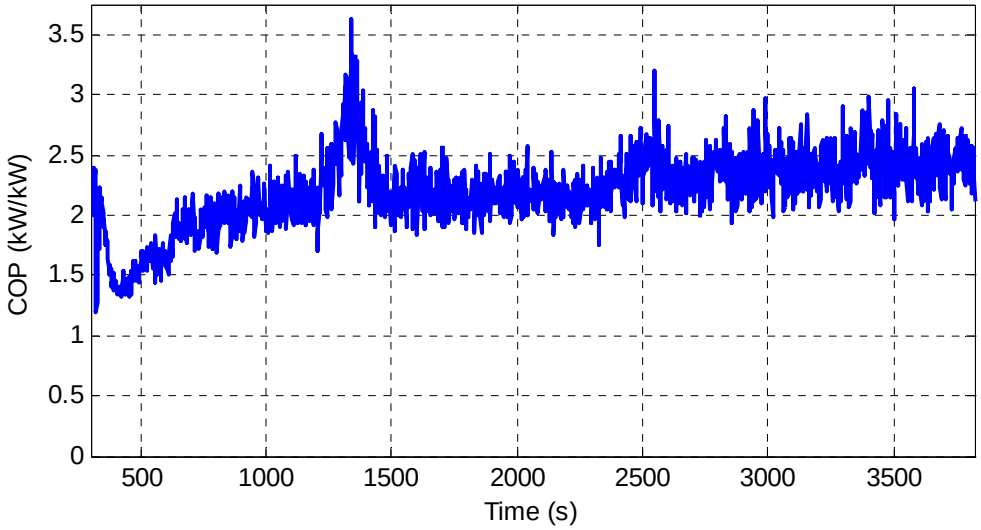

Fig. 5.19 Test 1 coefficient of performance

Test 2: Decreased ICOP Weight

For this second experimental run, the ICOP weight was decreased from 2000 to 750. The results of the first test imply that as the ICOP weight is decreased relative to the error weight, the steady state error that the controller will tolerate also decreases. The purpose of this experiment is to test the validity of that implication. Table 5.4 shows the test parameters. Figure 5.20 shows the temperatures and cooling setpoints; note that a constant disturbance was added to both zones starting at approximately 5000 seconds.

Table 5.4 Test 2 parameters

Parameter	Description	Value
Ts	Sample Time	150 s
Nu	Control Horizon	3
Ny	Prediction Horizon	5
λ_e	Temperature Error Weight	1.0
λ_Φ	ICOP Weight	750
λ_Q	Cooling Slew Weight	4.0
λ_P	Pressure Slew Weight	2.0

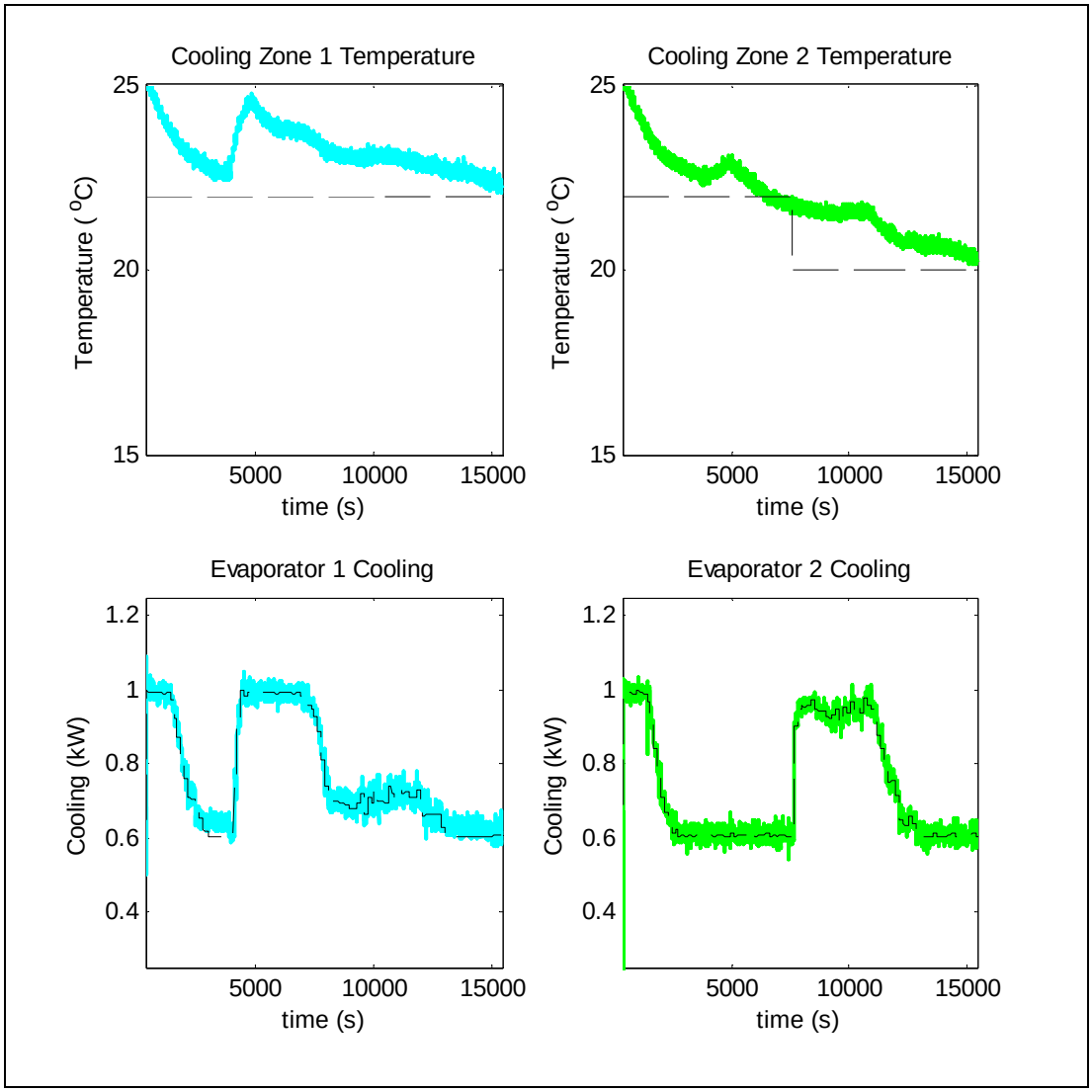

Fig. 5.20 Test 2 cooling zone temperatures and cooling

The results of this test show that with the lower weight, the setpoint is indeed reached even in the presence of disturbances. To better illustrate this idea, figure 5.21 shows a clear trend that for the case where the ICOP weight is higher, the controller requires a larger error before assigning a particular amount of cooling to the evaporator.

This agrees with an intuitive sense of the role the relative weights play in tuning the global controller. The black points are from Test 2; the green squares are from Test 1.

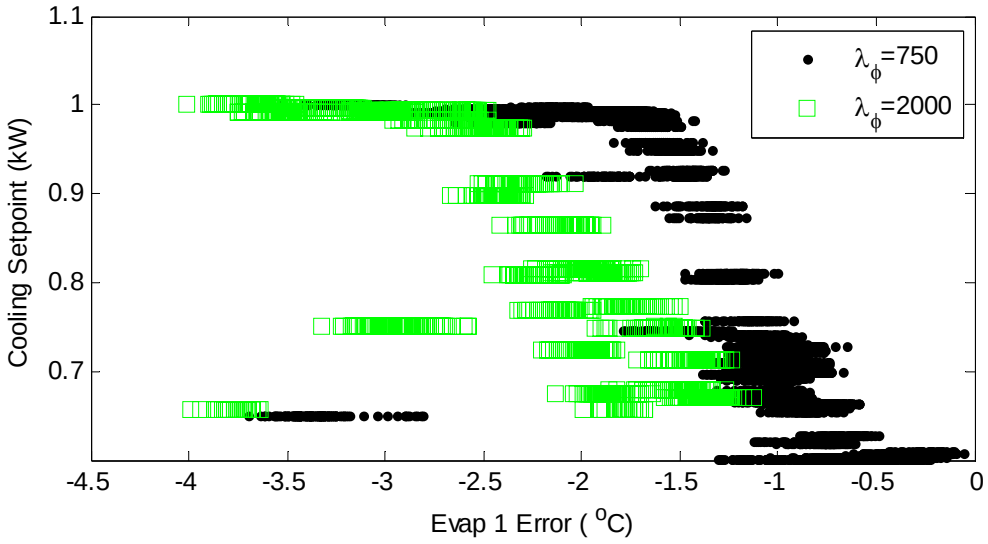

Fig. 5.21 The effects of λ_Φ on cooling setpoints

Figure 5.22 shows the pressures during this test run. Note that the pressures again oscillate about the 325 kPa mark. This seems to be a point where the compressor and fan consumptions balance each other. Figure 5.23 illustrates this. In this figure, the values of the ICOP function are plotted as functions of evaporator 1 cooling for various pressures. Pressures 1 and 2 are kept identical for this graph, and evaporator 2 cooling is held constant at 0.6 kW. As evaporator pressure increases past 325 kPa, the fans have to move more fluid in order to keep superheat above the minimum value; clearly, the global controller is seeking an energy-optimal pressure for the evaporators.

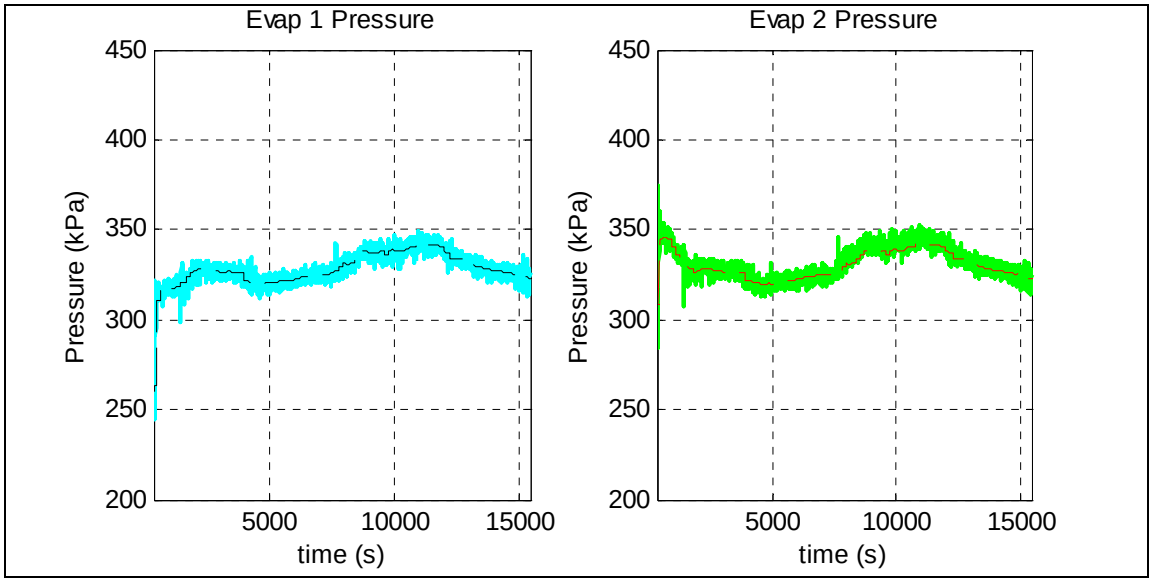

Fig. 5.22 Test 2 pressures

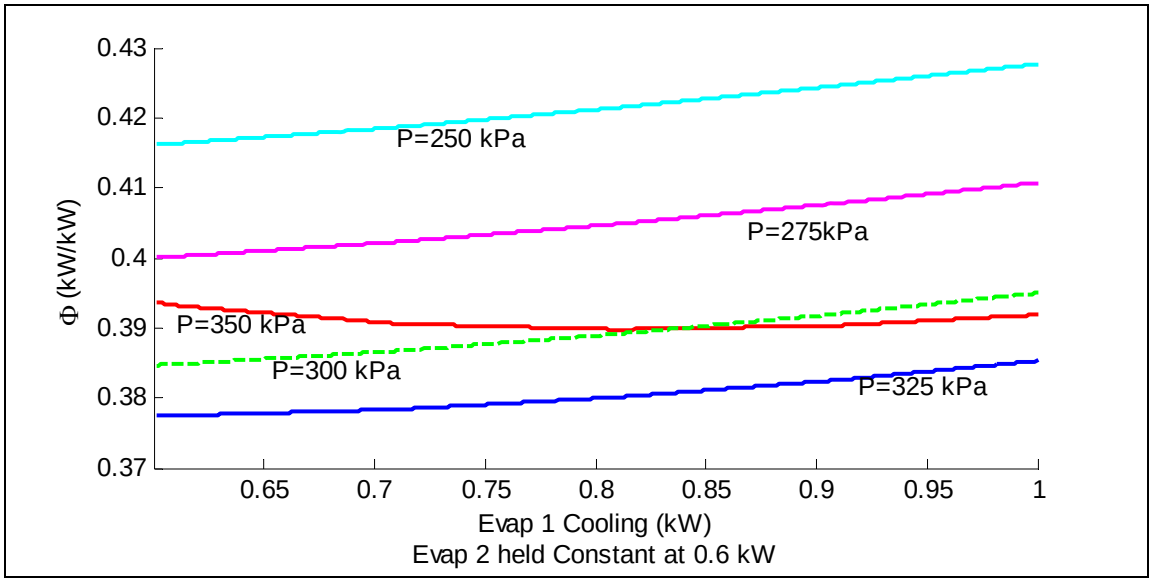

Fig. 5.23 ICOP as a function of evaporator 1 cooling for different pressures

Test 3: Increased ICOP weight

For this test, the weight placed on ICOP was increased to 3000; all other parameters are the same as those in Table 5.4. This resulted in undesirable limit cycle behavior, as shown in Figure 5.24. Additionally, the system was not able to drive the cooling zone temperatures down to the setpoint in the presence of a disturbance.

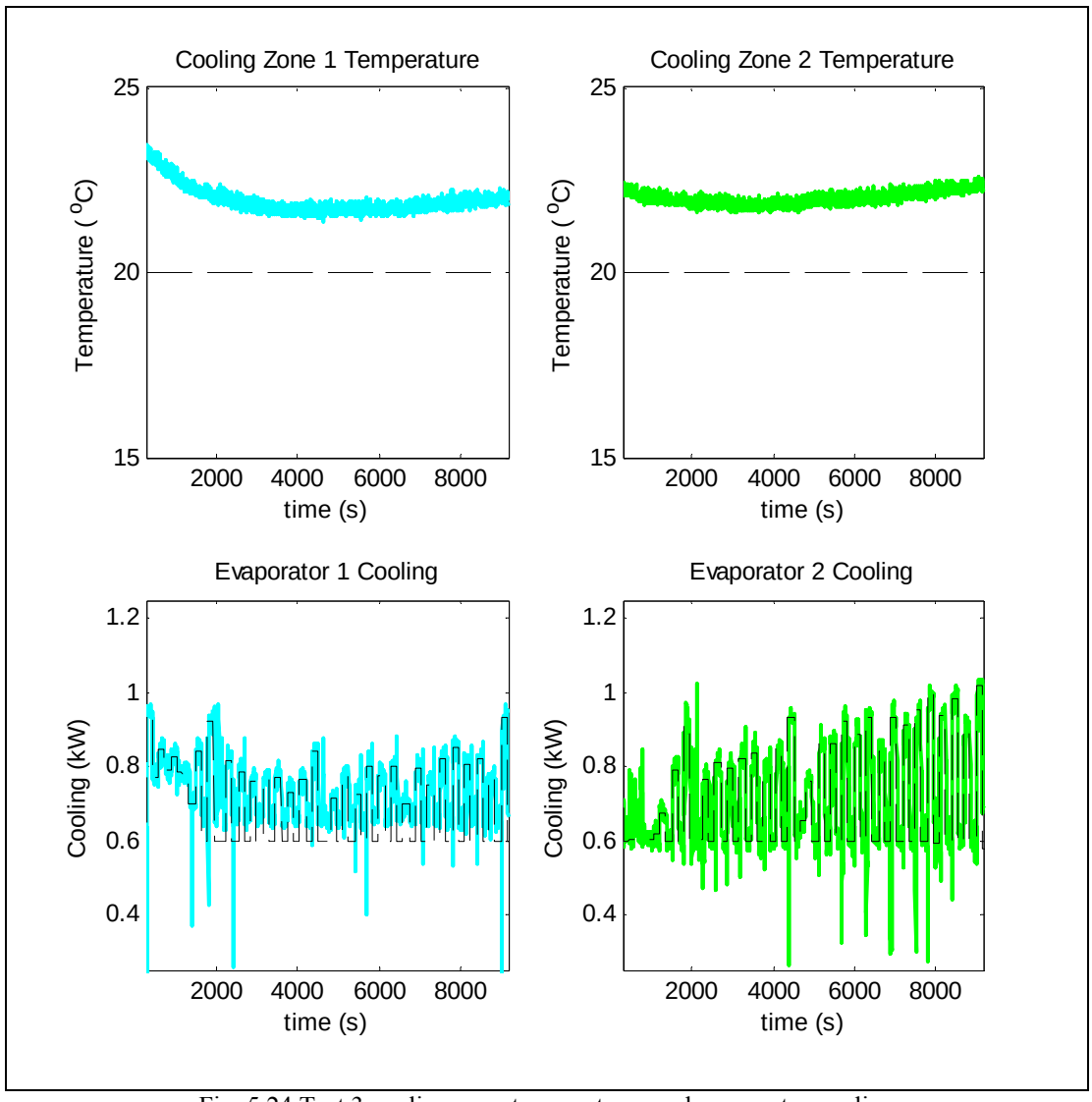

Fig. 5.24 Test 3 cooling zone temperatures and evaporator cooling

Test 4: Verification that Global Controller will Improve Efficiency

The purpose of this third test is to provide some verification that the controller will move the system from a randomly chosen set of operating points to a more energy efficient one. At the start of this test, the system was allowed to come to a steady state where the evaporator cooling and the disturbance were balanced, thereby maintaining a constant water temperature. Then the global controller was activated at approximately 1200 seconds, which brought the pressure and cooling setpoints to a more efficient operating condition. Figures 5.25 and 5.26 show the temperature/cooling and pressure results, respectively. Figure 5.27 shows how superheat decreases, implying more efficient operation. Figure 5.28 shows the 9.5% increase in COP as a result of the controller's actions. In each figure arrows indicate when the global controller was activated. The parameters for the test are the same as those in Table 5.4.

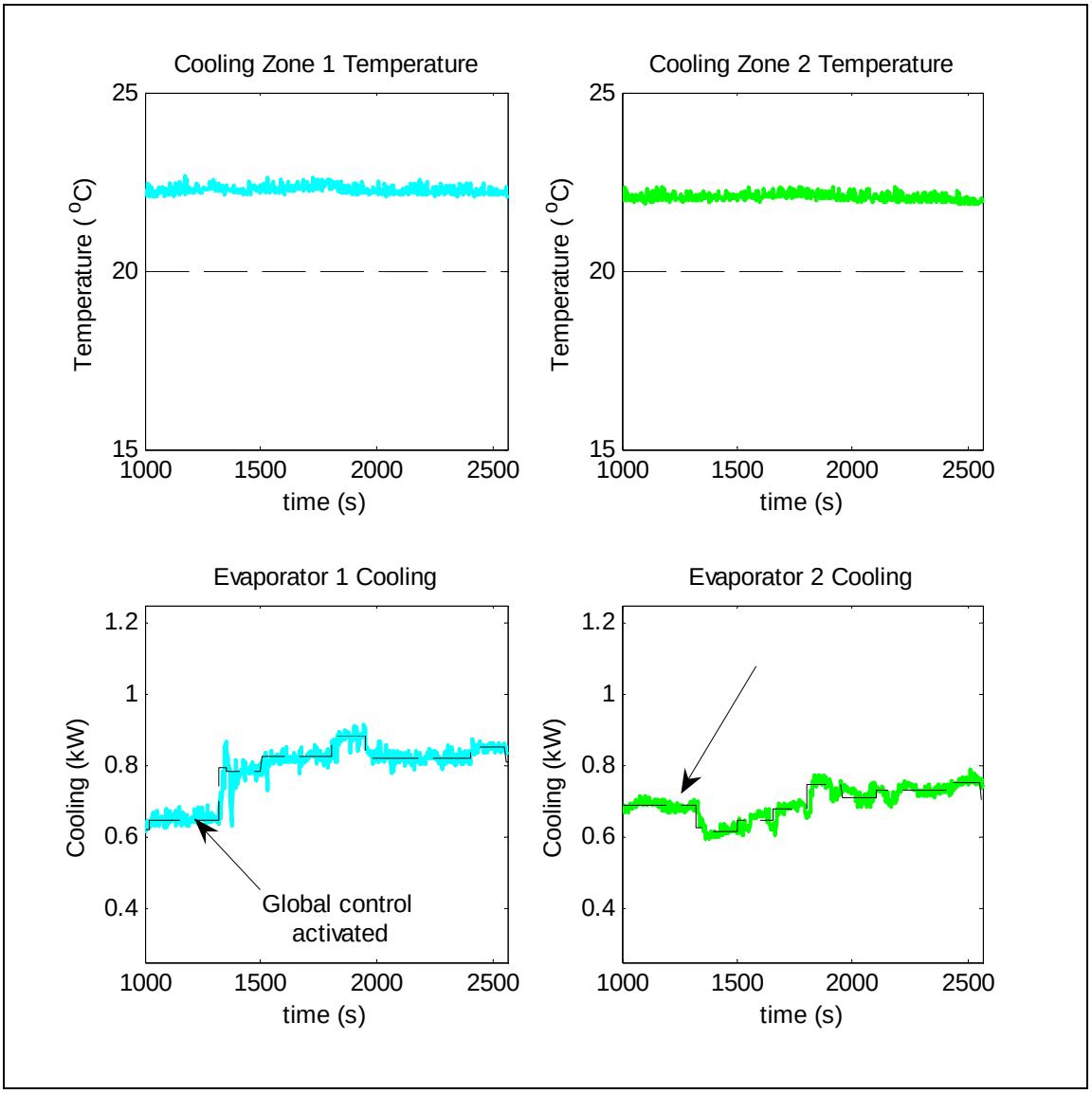

Fig. 5.25 Test 4 cooling zone temperatures and cooling

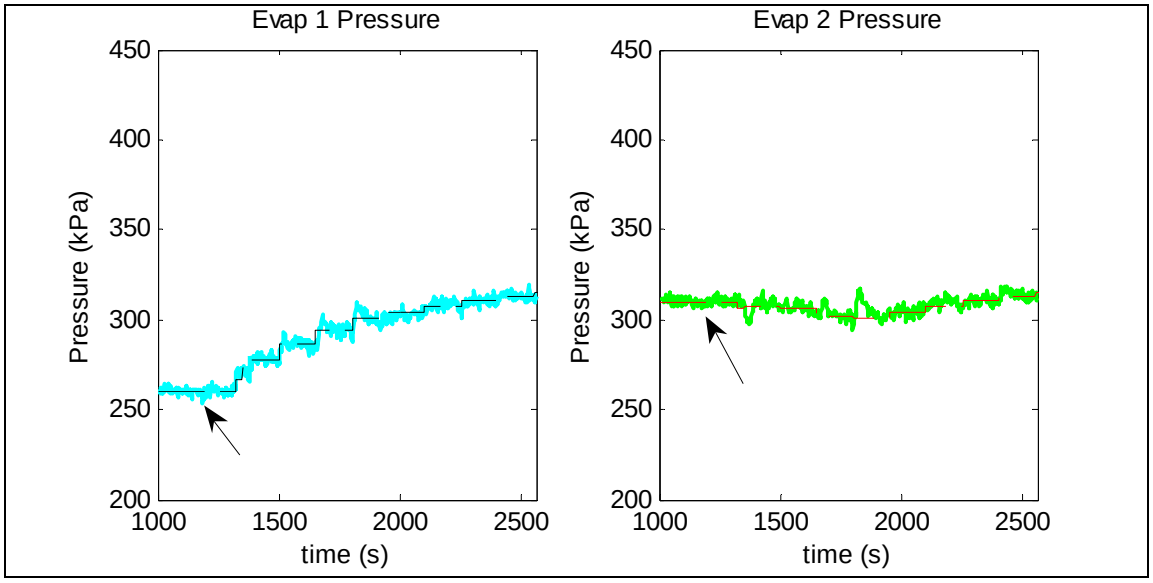

Fig. 5.26 Test 4 pressures

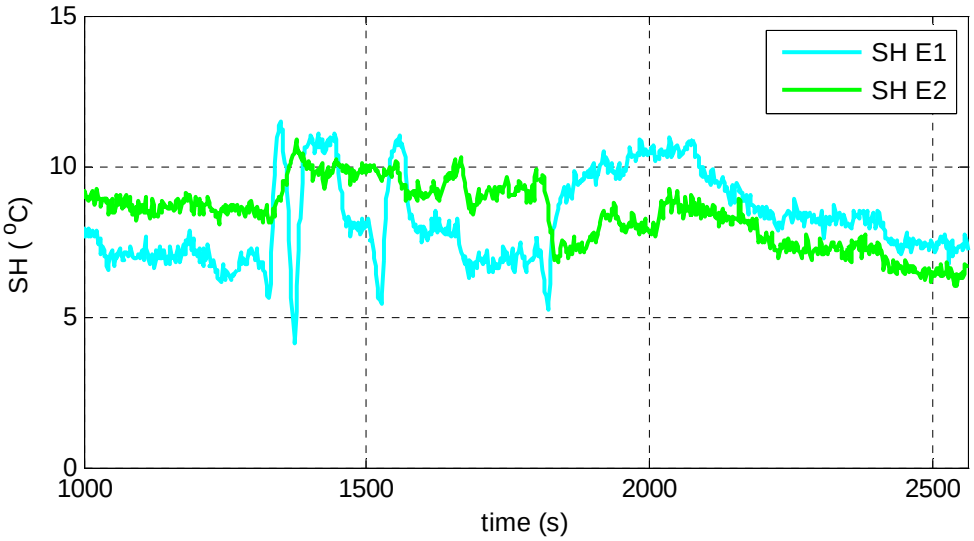

Fig. 5.27 Test 4 superheats

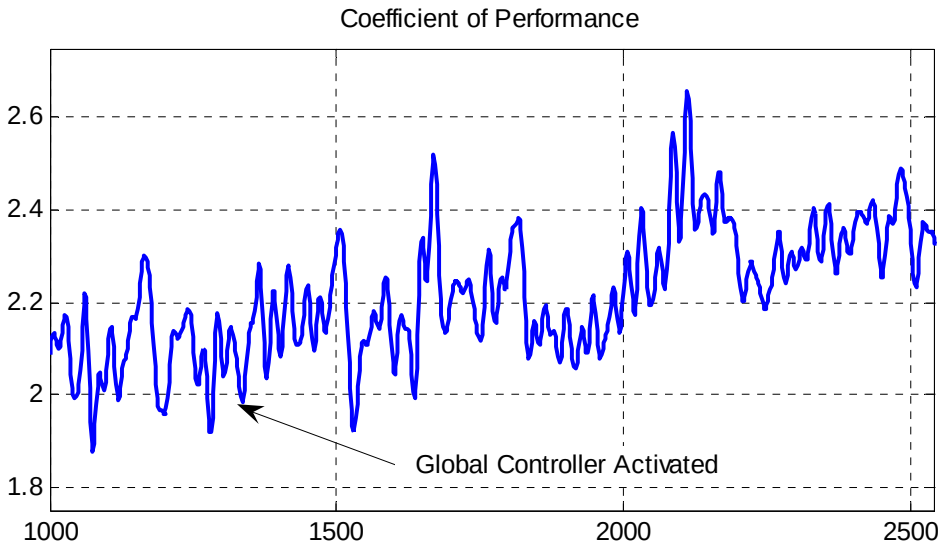

Fig. 5.28 Test 4 coefficient of performance

Test 5: More Expensive Fan Law

This final test exploits the modularity and adaptability built into the design approach. The ICOP function is modified so that the first evaporator's "fan" consumes twice as much energy as the default. The second evaporator's fan is left unchanged. Test parameters are the same as those in Table 5.4. A disturbance was added to the second evaporator so that it tracked its setpoint with its cooling at a minimum. Figure 5.29 shows the cooling zone temperatures and evaporator cooling.

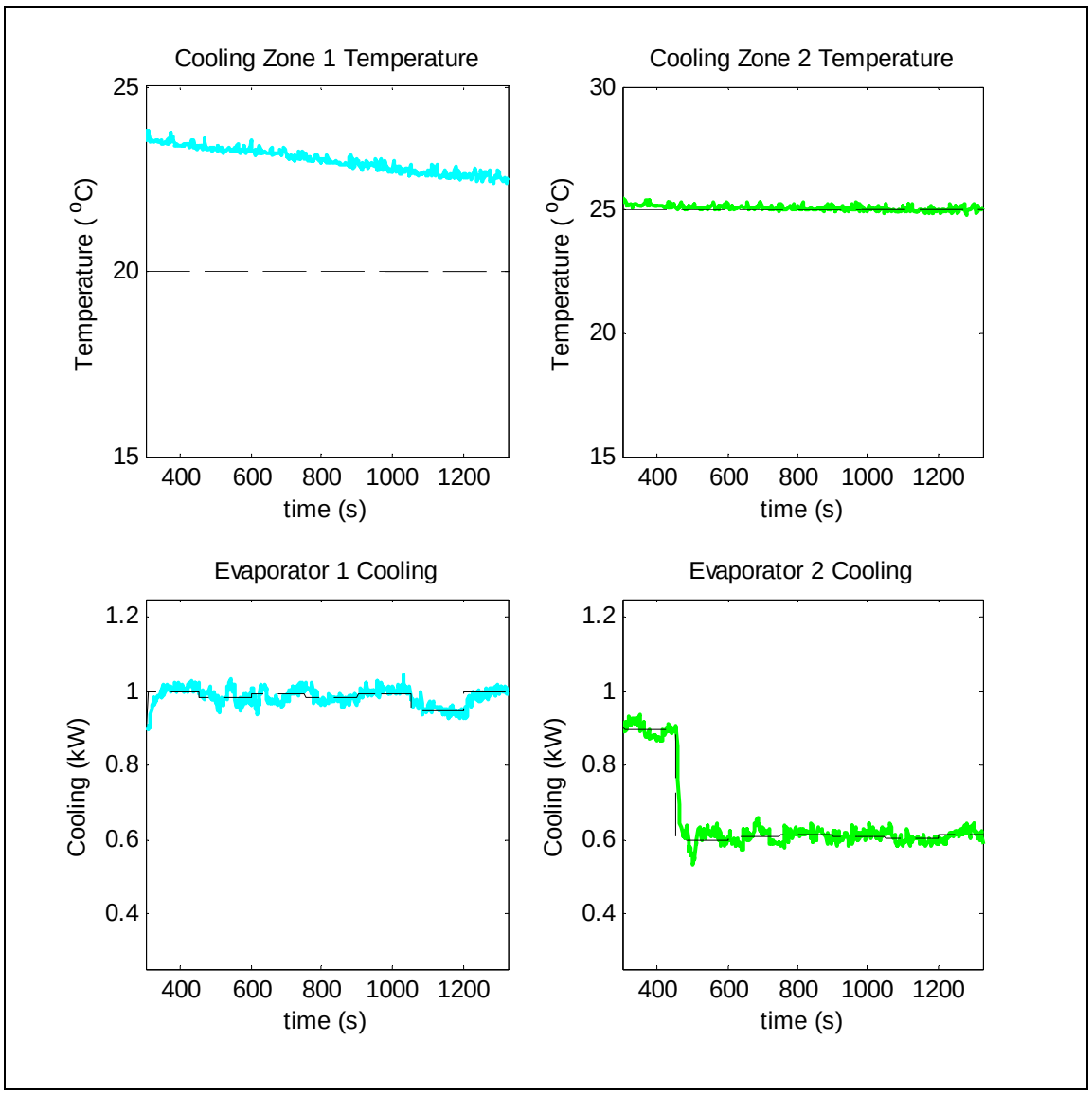

Fig. 5.29 Test 5 cooling zone temperatures and evaporator cooling

As a result of the first fan being more expensive, the controller drives the first evaporator's pressure down, since it becomes more expensive to maintain superheat at higher pressures. Figure 5.30 shows the pressures; figure 5.31 shows the component work. Figure 5.32 is similar to the earlier plot of the ICOP function with varying cooling, except using the expensive fan for the first evaporator. In this case, keeping the

second evaporator's pressure constant at 350 kPa, the ICOP function will seek to drive the first evaporator's pressure down to a minimum value.

This example indicates the possibility that the control approach presented can be an effective design tool; combinations of fans and compressors can be explored to help ensure an energy efficient design and component selection.

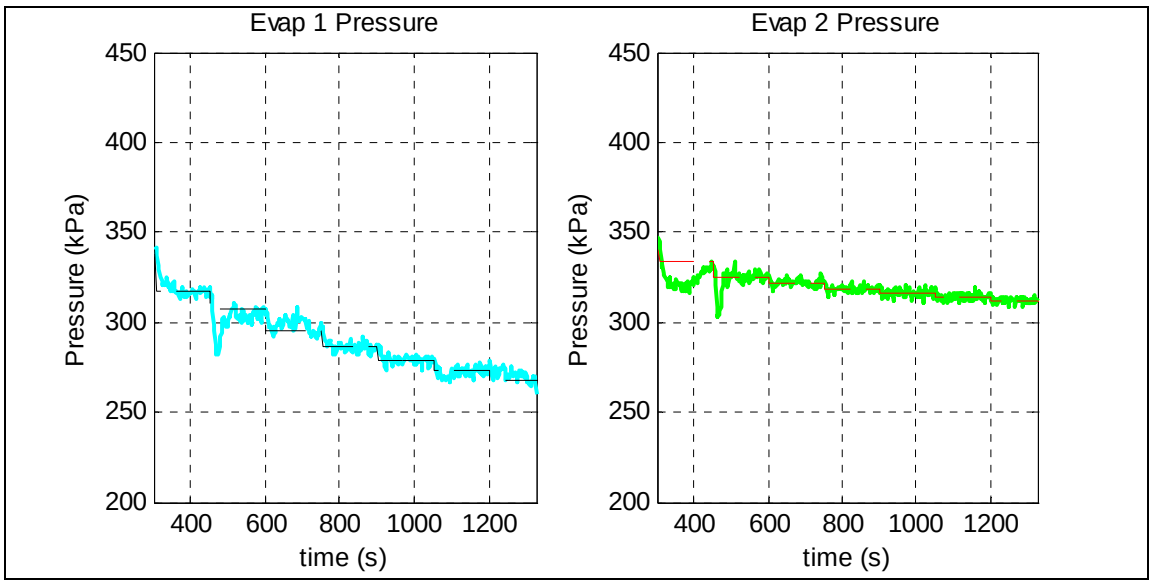

Fig. 5.30 Test 5 pressures

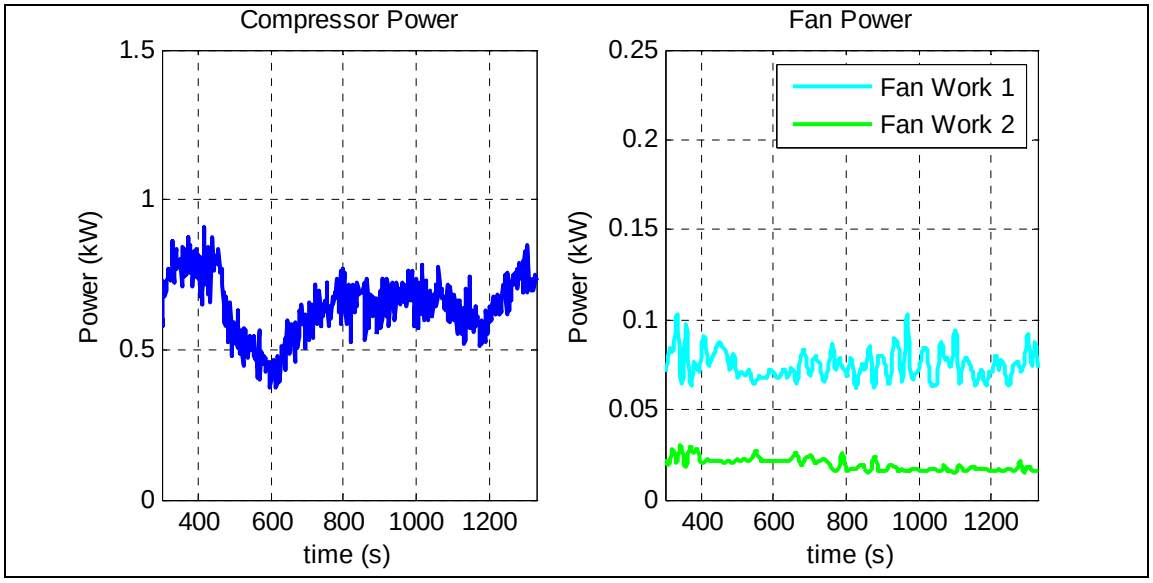

Fig. 5.31 Test 5 component power consumption

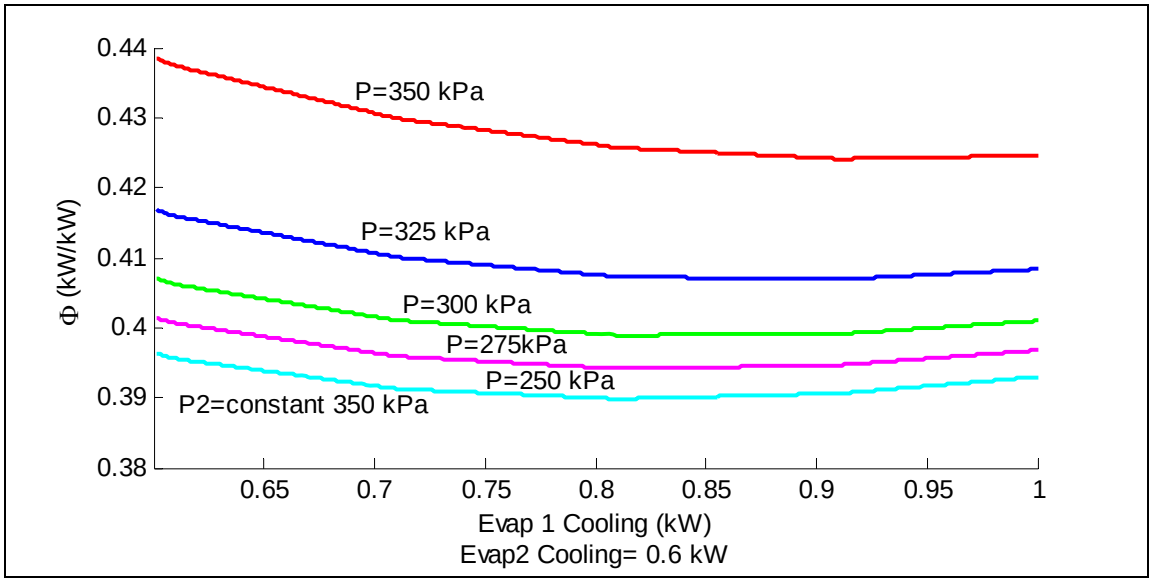

Fig. 5.32 ICOP as a function of evaporator 1 cooling for different pressures, modified fan law

Conclusion

In this chapter, a new global control approach was derived to regulate the setpoints of the local controller architecture designed in Chapter IV. This architecture seeks to drive the temperature of a cooling zone to a setpoint in an energy efficient manner. The controller has knowledge of the energy consumption characteristics of the system components; furthermore, it can be tuned to assign different weights to errors and energy efficiency. This allows the user to select weights that reflect the criticality of temperature regulation, or the cost of energy consumed in operating the cooling system. The controller is also shown to be flexible and modular, and can be used as a design tool while selecting components for a cooling system.

CHAPTER VI

CONCLUSION

Results

This thesis presents a novel control architecture for multiple evaporator cooling systems. The architecture is a flexible, two-level structure that uses model predictive control methods at both levels to achieve the respective goals of each controller. The global controller seeks to regulate the temperatures of two different cooling zones serviced by the same vapor compression cycle, while maximizing energy efficiency in the process. It achieves this by calculating the pressure and cooling values for the evaporators that minimize a tunable quadratic cost function, subject to a set of constraints. These pressure and cooling values are sent as setpoints to the local component controllers. These local controllers are distributed among the components and use a combination of MPC and PID controllers to regulate evaporator cooling and pressure while ensuring that superheat stays within a band for all evaporators.

The control architecture presented was shown to be effective in achieving the control objectives. The global controller was shown to seek the minimum energy consumption condition, and can be tuned to place different weights on setpoint error and on energy consumption. This flexibility means the control algorithm can be adapted for different situations depending on the user's need. Additionally, the global control algorithm was shown to be adaptable to different equipment configurations; thus, if the

energy consumption characteristics of the individual components change, the global law can be adapted to reflect these changes.

Local Controllers

At the local control level, 2 x 2 MIMO MPC controllers are implemented on each evaporator. The inputs for these controllers are the EEV and WFV; the outputs are evaporator cooling and superheat. Zero weight is placed on the superheat output, but it is constrained within a band. Using an MPC framework with a MIMO controller allows explicit handling of the superheat constraint. The result of this approach is that no control effort is expended to explicitly track superheat, although it is kept above a specified minimum for safety and below a specified maximum for efficiency. This is different from the industrially standard method of using the expansion device to control superheat explicitly, which is really an indirect method of controlling cooling. This frees the controller to pursue the primary goal of the evaporator, which is cooling of a secondary fluid.

The pressure in the first evaporator is controlled with the compressor. In this way, pressure serves as the signal to the compressor that cooling demand is changing. For example, if the cooling increases, the valve opens, and pressure increases. The compressor then increases in speed to bring the pressure back to its setpoint. The secondary evaporator's pressure is controlled with the SDR, which tracks the difference in pressure setpoints between the second and first evaporators.

Global Controller

For the global controller, an Inverse Coefficient of Performance function was derived for the system; the value of this function decreases in magnitude as the system operates more efficiently. Due to a set of simplifying assumptions, the ICOP function can be expressed solely as a function of each evaporator's cooling and pressure setpoints over a prediction horizon. In addition, the error in the cooling zones' temperatures over a prediction horizon can be expressed as a function of each evaporator's cooling setpoints over a control horizon. The error function and the ICOP function are combined into a tunable quadratic cost function that is minimized subject to a set of constraints; the optimal solution to this function gives the pressure and cooling setpoints that are communicated to the local controllers.

Future Work

There are many potential avenues for future research along the lines opened up in this thesis—as with any research, more questions are revealed in these pages than are answered. General investigations can include demand shedding and fault detection with the current system. Additionally, further development of the global controller and exploration of larger, distributed systems are possible. A few specific areas of inquiry are listed next.

Demand Shedding and Variable Weight Tuning

If the total cooling demand is too high for the system, or is deemed too expensive to meet, the controllers can use their MPC-based logic to limit the total cooling actually performed by the system. In effect, excess demand is ignored and a lower level of cooling is performed. If handled by the local controllers, a limit can be placed on cooling delivered. If handled by the global controller, either a limit can be placed on the setpoints, or additional cost placed on cooling, such that more weight is placed on energy consumption. This would be very useful if electricity were priced based upon the time of day.

Fault Detection Using the Global Law

Logic can be placed in the global controller that would monitor the actual system performance; if the actual performance falls outside certain set boundaries, this can signify a problem with the system. For example, if a certain level of cooling is asked for but not received, it might signal a problem with the evaporator such as a non-functioning fan or a refrigerant leak. The global controller could respond by shutting down the evaporator in question and notifying maintenance personnel. Phenomena such as power spikes could also be monitored.

Adaptation of Global Law

The global law was derived with a set of simplifying assumptions, some of which were with regards to water temperatures. An adaptation algorithm that changes the ICOP function as the water temperature changes, for example, could be very useful in

developing a controller that performs optimally with respect to energy consumption for all situations. Alternatively, a multiple model approach could be used, where different ICOP functions are used in different operating conditions. Another possibility for adaptive control would be adapting the ICOP function by comparing the values of the function with the actual system responses; this would allow the function to evolve with time and different conditions, such as a change in seasons.

Nonlinear Local Control

In general, a better model for use in the local controllers is desirable. Additionally, the local components are limited to a fairly small set of operating conditions; in order to achieve a larger operating envelope and better local performance, a method of dealing with the inherent nonlinearities is required. This method might involve a multiple model MPC approach, where the controller switches between models as system conditions change. This should allow for better control of the local components, including perhaps tightening of the superheat band and decreasing the minimum superheat required. This would improve the operating efficiency of the system overall.

Expansion of Approach

Expansion of the system to a larger cooling network—for example, 6 evaporators with 2 compressors—would provide a bevy of technical challenges in adapting this approach. When should each compressor be used? Do physical distances play a role in the behavior of the system overall, and how should these be implemented into the global

law? Also, can the global law derivation be generalized from VCC systems to any system that transports energy and mass from one place to another?

Guarantees of Stability

A guarantee of stability is one of the most important goals in designing a control system, and would present an interesting challenge in further development of the approach. One possibility is guaranteeing passivity of the subsystems and local controllers, thereby guaranteeing the passivity and thus stability of the entire system; this is a possible fruitful avenue, especially since all of the system components except for the compressor are themselves passive, in that they dissipate energy.

REFERENCES

[1] U.S. Department of Energy website. "End-Use Consumption of Electricity by End Use and Appliance." (Accessed June 3 2008). Available: http://www.eia.doe.gov/emeu/recs/recs2001/enduse2001/enduse2001.html

[2] M. J. Moran and H. N. Shapiro, *Fundamentals of Engineering Thermodynamics*, 3rd ed. New York: John Wiley & Sons, 1996.

[3] J. Rossiter, *Model-Based Predictive Control: A Practical Approach*. Boca Raton, FL: CRC Press, 2003.

[4] P. M. T. Broersen and M. F. G. van der Jagt, "Hunting of evaporators controlled by a thermostatic expansion valve," *ASME Journal of Dynamic Systems Measurement & Control*, vol. 102, pp. 130-135, Jun. 1980.

[5] W. Gruhle and R. Isermann, "Modeling and control of a refrigerant evaporator," *ASME Journal of Dynamic Systems Measurement & Control*, vol. 107, pp. 235-240, Dec. 1985.

[6] G.A. Ibrahim, "Effect of sudden changes in evaporator external parameters on a refrigeration system with an evaporator controlled by a thermostatic expansion valve," *International Journal of Refrigeration*, vol. 24, pp. 566-576, 2001.

[7] K. James and R. James, "Transient analysis of thermostatic expansion valves for refrigeration system evaporators using mathematical models," *Transactions of the Institute of Measurement & Control*, vol. 9, pp. 198-205, 1987.

[8] W. Chen, C. Zhijiu, Z. Ruiqi, and W. Yezheng, "Experimental investigation of a minimum stable superheat control system of an evaporator," *International Journal of Refrigeration*, vol. 25, pp. 1137-1142, 2002.

[9] A. Outtagarts, P. Haberschill, and M. Lallemand, "The transient response of an evaporator fed through an electronic expansion valve," *International Journal of Energy Research*, vol. 21, pp. 793-807, 1997.

[10] D.P. Finn and C.J. Doyle, "Control and optimization issues associated with algorithm-controlled refrigerant throttling devices," *ASHRAE Transactions*, vol. 106, pp. 524-533, Jul. 2000.

[11] H. Rasmussen, C. Thybo, and L. Larsen, "Nonlinear superheat and evaporation temperature control of a refrigeration plant," in *Proc. 2006 IFAC Workshop on Energy Saving Control in Plants and Buildings*, Bansko, Bulgaria, Oct. 2006, pp. 251-254.

[12] X. He, S. Liu, and H. Asada, "Modeling of vapor compression cycles for multivariable feedback control of HVAC systems," *Journal of Dynamic Systems Measurement and Control*, vol.119, pp.183-191, Jun. 1997.

[13] D. Parnitzki, "Digital control of heat pumps with minimized power consumption," *International Journal of Energy Research*, vol. 13, pp. 167-179, 1989.

[14] X. He, S. Liu, H. Asada, and H. Itoh, "Multivariable control of vapor compression systems," *HVAC&R Research*, vol.4, no. 3, pp.205-230, Jul. 1998.

[15] T. Cheng and X. He, "Nonlinear observer design for two-phase flow heat exchangers of air conditioning system," in *Proc. 2004 American Control Conf.*, Boston, MA, 2004, pp. 1534-1539.

[16] T. Cheng, X. He, H. Asada, and S. Kasahara, "Heat exchanger dynamic observer design," *ASHRAE Transactions,* vol. 111, no. 1, pp. 328-335, 2005.

[17] J. Lin and T. Yeh, "Modeling, identification and control of air-conditioning systems," *International Journal of Refrigeration*, vol. 30, pp. 209-220, 2007.

[18] R. Shah, B. Rasmussen, and A. Alleyne, "Application of a multivariable adaptive control strategy to automotive air conditioning systems," *International Journal of. Adaptive Control and Signal Processing,* vol. 18, pp. 199-221, 2004.

[19] G. Singh, M. Zaheer-uddin, and R. Patel, "Adaptive control of multivariable thermal processes in HVAC systems," *Energy Conversion and Management,* vol. 41, pp. 1671-1685, 2000.

[20] S. Skogestad and I. Postlethwaite, *Multiple Feedback Control: Analysis and Design*, 2nd ed. West Sussex, England: John Wiley & Sons, Ltd., 2005.

[21] E. Camacho and C. Bordons, *Model Predictive Control*. London, UK: Springer, 1999.

[22] C. Garcia, D. Prett, M. Morari, "Model predictive control: theory and practice—a survey," *Automatica*, vol. 25, no. 3, pp. 335-348, 1989.

[23] S. Qin and T. Badgwell, "A survey of model predictive control technology," *Control Engineering Practice*, vol. 11, pp. 733-764, 2003.

[24] D. Mayne, J. Rawlings, C. Rao, and P. Scokaert, "Constrained model predictive control: stability and optimality," *Automatica,* vol. 36, no. 6, pp. 789-814, 2000.

[25] J. Bordeneuve-Guibe and C. Vaucoret, "Robust multivariable predictive control: an application to an industrial test stand," *IEEE Control Systems Magazine*, vol. 21, no. 2, pp. 54-65, Apr. 2001.

[26] Z. Wu, M. Rajamani, J. Rawlings, and J. Stoustrup, "Model predictive control of thermal comfort and indoor air quality in livestock stable," in *Proc. European Controls Conference*, Kos, Greece, Jul. 2007, pp. 4746 - 4751.

[27] J. Rawlings, "Tutorial overview of model predictive control," *IEEE Control Systems Magazine*, vol. 20, no. 3, pp. 38-52, Jun. 2000.

[28] D. Clarke, Ed., *Advances in Model-Based Predictive Control*. Oxford: Oxford University Press, 1994.

[29] S.J. Qin and T.A. Badgwell, "An overview of nonlinear model predictive control applications," in *Nonlinear Model Predictive Control,* F. Allgower and A. Zheng, Eds. Basel, Switzerland: Birkhauser Verlag, 2000, pp. 369–392.

[30] F. Allgower and Zheng, Eds., *Nonlinear Model Predictive Control* (Progress in Systems and Control Theory, vol. 26). Basel, Switzerland: Birkhauser Verlag, 2000.

[31] B. Aufderheide, V. Prasad, and B. Bequette, "A comparison of fundamental model-based and multiple model predictive control," in *Proc. 40th IEEE Conf on Decision and Control*, Orlando FL, 2001, pp. 4863-4868.

[32] M. He, W. Cai, and S. Li, "Multiple fuzzy model-based temperature predictive control for HVAC systems," *Information Sciences*, vol. 169, pp. 155-174, 2005.

[33] M. Xu, S. Li, W. Cai, and L. Lu, "Effects of a GPC-PID control strategy with hierarchical structure for a cooling coil unit," *Energy Conversion and Management*, vol. 46, pp. 132-145, Jan. 2006.

[34] M. Xu, S. Li, and W. Cai, "Practical receding-horizon optimization control of the air handling unit in HVAC systems," *Industrial & Engineering Chemistry Research*, vol. 44, no. 8, pp. 2848-2855, 2005.

[35] J. MacArthur and M. Woessner, "Receding horizon control: a model-based policy for HVAC applications," *ASHRAE Transactions*, vol. 99, no. 1, pp. 139-148, Jan. 1993.

[36] A. Dexter and P. Haves, "A robust self-tuning predictive controller for HVAC applications," *ASHRAE Transactions*, vol. 95, no. 2, pp. 431-437, 1989.

[37] J. Sousa, R. Babuska, and H. Verbruggen, "Fuzzy predictive control applied to an air-conditioning system," *Control Engineering Practice*, vol. 5, no. 10, pp. 1395-1406, 1997.

[38] D. Leducq, J. Guilpart, and G. Trystam, "Non-linear predictive control of a vapour compression cycle," *International Journal of Refrigeration*, vol. 29, pp. 761-772, Aug. 2006.

[39] W. Goetzler, K. Roth, and J. Brodrick, "Variable flow and volume refrigerant system," *ASHRAE Journal Magazine*, vol. 46, no. 1, January 2004, pp. 164-165.

[40] J. Choi and Y. Kim, "Capacity modulation of an inverter-driven multi-air conditioner using electronic expansion valves," *Energy*, vol. 28, pp. 141-155, 2003.

[41] Y. Park, Y. Kim, and M. Min, "Performance Analysis on a multi-type inverter air conditioner," *Energy Conversion and Management*, vol. 42, pp. 1607-1621, 2001.

[42] X. He and H. Asada, "A new feedback linearization approach to advanced control of multi-unit HVAC systems," in *Proc. American Control Conf.*, Denver, CO, 2003, pp. 2311-2316.

[43] G. Lee, M. Kim, and Y. Cho, "An experimental study of the capacity control of multi-type heat pump system using predictive control logic," in *Proc. of 7th Intl. Energy Agency Heat Pump Conference 2002*, Beijing, China, 2002, pp. 158-165.

[44] R. Shah, A. Alleyne, and C. Bullard, "Dynamic modeling and control of multi-evaporator air-conditioning systems," *ASHRAE Transactions*, vol. 110, pp. 109-119, 2004.

[45] C.B. Chiou, C.H. Chiou, C.M. Chu, and S.L. Lin, "The application of fuzzy control on energy saving for multi-unit room air-conditioners," *Applied Thermal Engineering*, to be published. Available online (Accessed June 15 2008): http://www.sciencedirect.com/science/journal/13594311

[46] L. Ljung, *System Identification: Theory for the User*, 2nd ed. Upper Saddle River, NJ: Prentice Hall PTR, 1999.

[47] P. Overschee and B. De Moor, "N4SID: subspace algorithms for the identification of combined deterministic stochastic systems," *Automatica*, vol. 30, no. 1, pp. 75-93, Jan 1994.

[48] MATLAB System Identification Toolbox Documentation. (Accessed June 3 2008). Available: http://www.mathworks.com/access/helpdesk/help/toolbox/ident/

[49] K. Ogata, *Modern Control Engineering*, 4th ed. Upper Saddle River, NJ: Prentice Hall Inc., 2002.

[50] G. Franklin, J. Powell, and A. Emami-Naeini, *Feedback Control of Dynamic Systems*, 4th ed. Upper Saddle River, NJ: Prentice Hall Inc., 2002.

[51] MATLAB Model Predictive Control Toolbox Documentation. (Accessed June 3 2008). Available: http://www.mathworks.com/access/helpdesk/help/toolbox/mpc/

[52] D. Clarke, C. Mohtadi, and P. Tuffs, "Generalized predictive control—Part I. the basic algorithm," *Automatica*, vol. 23, no. 2, pp.137-148, 1987.

[53] Kansas Wind Power, Inc., website. (Accessed June 3 2008). Available: http://www.kansaswindpower.net/

[54] R. Fletcher, *Practical Methods of Optimization*, vol. 2. New York, NY: John Wiley & Sons, 1981.

APPENDIX

SENSOR WIRING SCHEMATICS

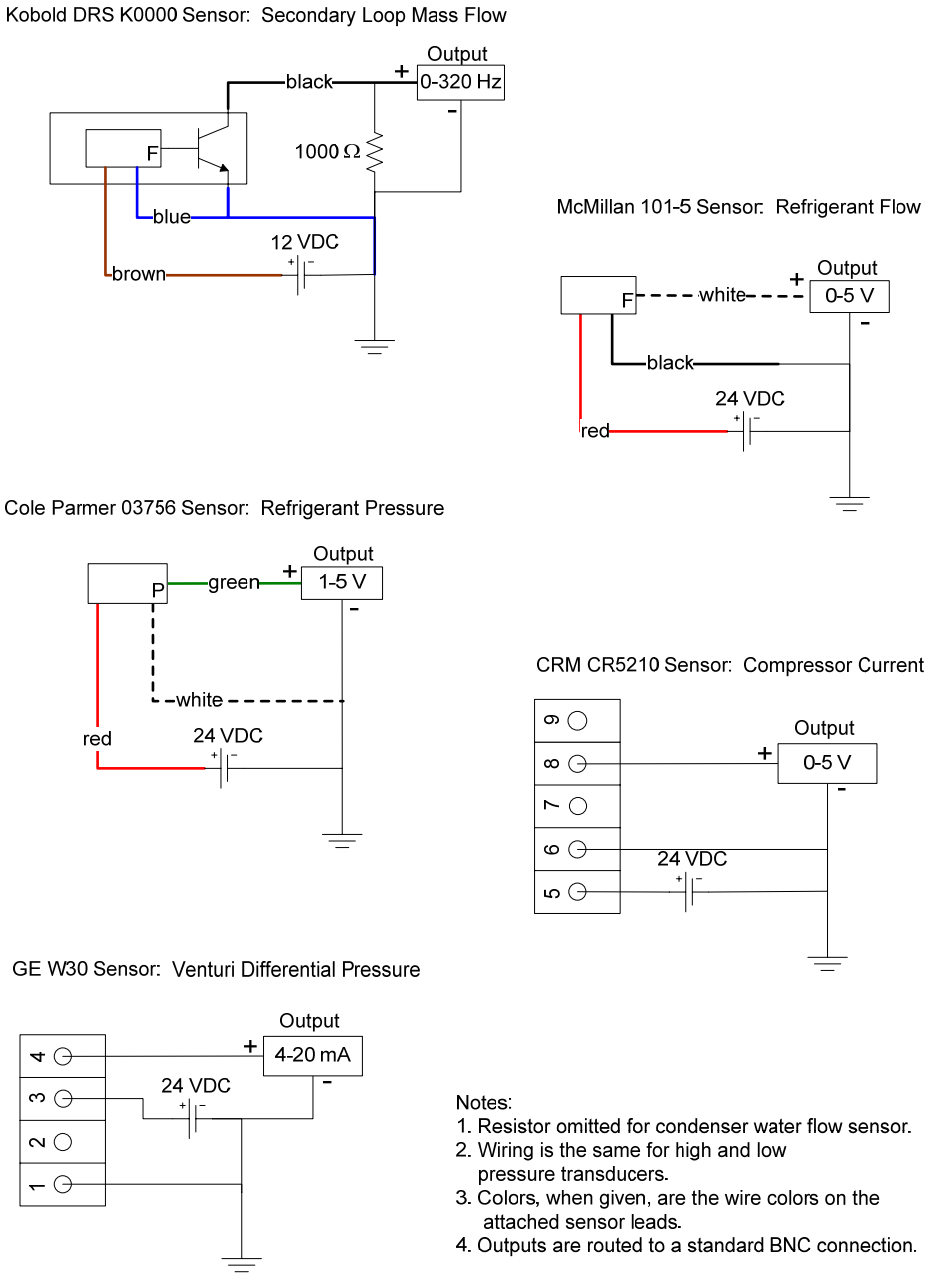

Fig. A.1 Sensor wiring schematics

Wiring Schematic For Compressor Power Supply

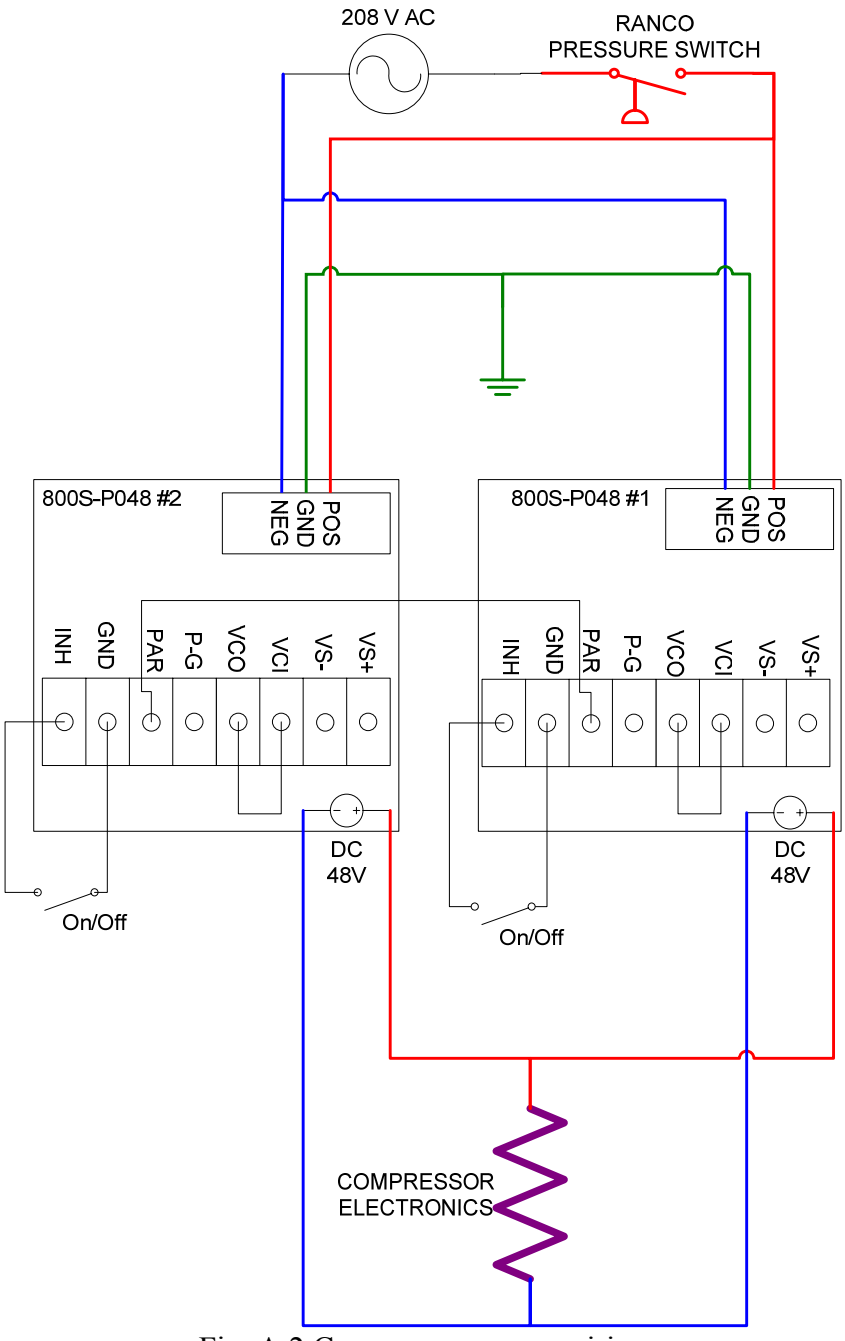

Fig. A.2 Compressor power wiring

POWER SUPPLY –120 VAC COMPONENTS

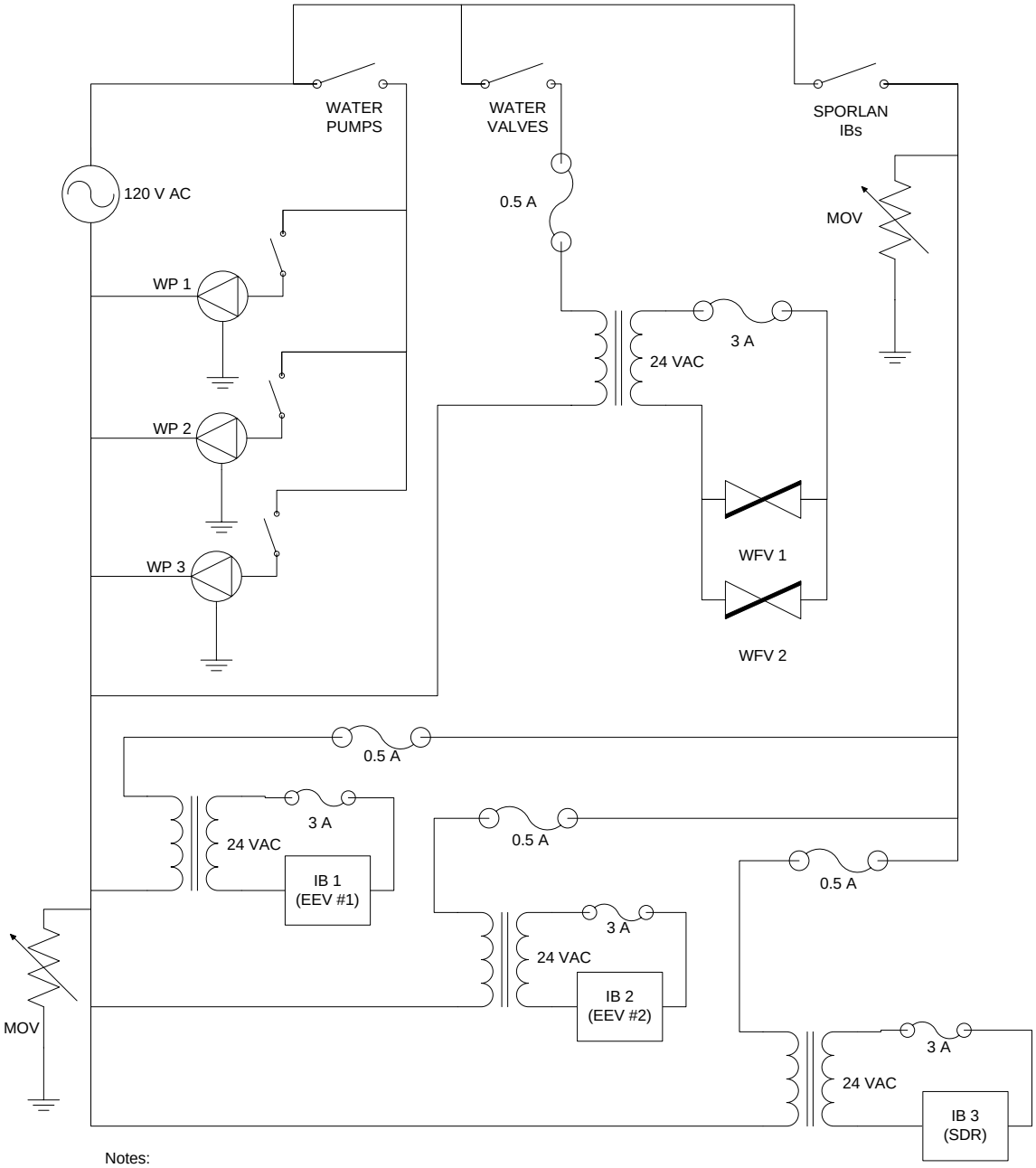

Notes:
1. MOV = Metal Oxide Varistor; supplied by Sporlan (IB Mfr.)

Fig. A.3 120VAC wiring

Table A.1: Part numbers and supplier info, part 1

Description	Qty	Manufacturer	Part Number	Supplier	Contact
PRIMARY LOOP					
Electric Expansion Valve (EEV)	2	Sporlan	SEI 0.5-10-S	Parker Hannefin	www.parker.com
Discharge Valve (SDR)	1	Sporlan	SDR-3X	Parker Hannefin	www.parker.com
Manual Shutoff Valve, 1/4"	8	Mueller	A14833	ACR Supply	(979) 774-7371
Manual Shutoff Valve, 3/8"	4	Mueller	A14835	ACR Supply	(979) 774-7371
3-way Ball Valve, 3/8"	1	ValveWorx	536503	Industrial Automation	www.valvestore.com
Compressor	1	Masterflux	Sierra 03-0982Y3	Masterflux	www.masterflux.com
Liquid Receiver	1	Henry Technologies	S-8060	ACR Supply	(979) 774-7371
Sight Glass	1	Emerson	AMI 1FM2	ACR Supply	(979) 774-7371
Filter Drier	1	Alco	EK-032	South Side Control Supply	www.southsidecontrol.com
Venturi	1	Lambda Square	VU-0.5-0.148	Lambda Square	www.lambdasquare.com
High Pressure Gage	1	Omega	PGC-25L-300	Omega	www.omega.com
Low Pressure Gage	1	Omega	PGC-25L-160	Omega	www.omega.com
Pressure Shutoff Switch	1	Ranco	012-1594-70	Ebay	www.ebay.com
SECONDARY LOOP					
Water Flow Valve (WFV)	2	Erie	APA23A000	Energy Equipment and Control	www.energyequipment.com
Manual Water Valves	19	various	various	U.S. Plastics	www.usplastics.com
Manual Water Valves	3	various	various	U.S. Plastics	www.usplastics.com
Water Pumps	3	Laing	SM-1212-T-26	McMaster-Carr	www.mcmaster.com
Condenser Water Chiller	1	Haier	HWF05XC5T	Ebay	www.ebay.com
Condenser Water Tanks	2	Tamco	6314	U.S. Plastics	www.usplastics.com
Evaporator Water Tanks	4	Tamco	6305	U.S. Plastics	www.usplastics.com
TRANSDUCERS					
Water Flow	3	Kobold	DRS-0380-N5-K000	Kobold	www.kobold.com
Thermocouples	12	Omega	GTMQSS-062U-6	Omega	www.omega.com
Evaporator Pressure	2	Cole-Parmer	07356-03	Cole-Parmer	www.coleparmer.com
Condenser Pressure	1	Cole-Parmer	07356-04	Cole-Parmer	www.coleparmer.com
Differential Pressure	1	GE General Eastern	Modus W30-31E-1-T	TTI Instruments	www.instrumart.com
Refrigerant Flow	2	McMillan	102-5-E-Q-B4-NIST	McMillan	www.mcmillan.com
Compressor Current	1	CR Magnetics	CR5210	CR Magnetics	www.crmagnetics.com
Tachometer	1	Masterflux	--	Masterflux	www.masterflux.com

Table A.2: Part numbers and supplier info, part 2

Description	Qty	Manufacturer	Part Number	Supplier	Contact
POWER COMPONENTS					
Transformer, 24 VAC	4	Honeywell	AT72D-1683	Patriot Supply	www.patriot-supply.com
Power Supply, 48 VDC	2	Cotek	800S-P048	Power Supplies Unlimited, Inc.	www.psui.com
Power Supply, 24 VDC	1	Traco	TML 15124C	Power Supplies Unlimited, Inc.	www.psui.com
Power Supply, 12 VDC	1	Control Engineering Co.	31053	Ebay	www.ebay.com
Power Supply, 5 VDC	1	Traco	TML 15105C	Power Supplies Unlimited, Inc.	www.psui.com
SIGNAL CONDITIONING					
0-3000 Hz in, 0-5 V out	1	Omega	OM5-IKI-3K-C	Omega	www.omega.com
0-500 Hz in, 0-5 V out	1	Analog Devices	5B45-01	Measurement Computing	www.measurementcomputing.com
0-500 Hz in, 0-5 V out	2	Dataforth	SCM 5B45-01	Measurement Computing	www.measurementcomputing.com
4-20 mA in, 0-5 V out	1	Omega	OM5-11-4/20-C	Omega	www.omega.com
-10 to +10 V in, 0-5 V out	1	Omega	OM5-IV-10B-C	Omega	www.omega.com
0-5 V in, 4-20 mA out	2	Analog Devices	5B39-01	Measurement Computing	www.measurementcomputing.com
0-5 V in, 4-20 mA out	3	Dataforth	SCM5B39-01	Measurement Computing	www.measurementcomputing.com
5B Backplane	2	Analog Devices	5B01	Measurement Computing	www.measurementcomputing.com
DATA ACQUISITION BOARDS					
Thermocouple Board	1	Measurement Computing	PCI-DAS-TC	Measurement Computing	www.measurementcomputing.com
Analog Output Board	1	Measurement Computing	PCI-DDI-08	Measurement Computing	www.measurementcomputing.com
Analog Input Board	2	National Instruments	E-6023	National Instruments	www.ni.com
MISCELLANEOUS TOOLS AND FITTINGS					
Compression Fittings	n/a	Swagelok	varies	North Houston Valve and Fitting	www.swagelok.com
SAE Fittings	n/a	varies	varies	Fittings and Valves Unlimited	www.fittingsandmore.com
PVC Fittings	n/a	varies	varies	Sprinkler.com	www.sprinkler.com
Vacuum pump	n/a	Robinair	15300	Ebay	www.ebay.com
Refrigerant, refrigerant tools, etc.	n/a	varies	varies	Discount Refrigerants, Inc.	www.discountrefrigerants.com
Copper Tubing	n/a	varies	varies	ACR Supply	(979) 774-7371

Table A.3: BNC numbers

BNC #	Signal Cond.	Slot	Board	Ch.	Desc.
1	1	0	AO	0	RPM
2	1	2	AO	2	EEV 1
3	1	3	AO	3	WFV 1
4	1	4	AO	4	EEV 2
5	1	5	AO	5	SDR
6	1	6	AO	6	WFV 2
7	NOT USED				
8	NOT USED				
9	2	0	AI 0	0	E1 water flow
10	2	1	AI 0	1	Compressor Tachometer
11	2	4	AI 0	4	Vapor flow dP
12	NOT USED				
13	N/A		AI 1	0	E1 Pressure
14	N/A		AI 1	2	E1 refrig. Flow
15	NOT USED				
16	N/A		AI 1	6	Condenser Pressure
17	2	3	AI 0	3	Condenser water flow
18	2	2	AI 0	5	E2 water flow
19	NOT USED				
20	NOT USED				
21	N/A		AI 1	3	E2 refrig. Flow
22	N/A		AI 1	1	E2 Pressure
23	N/A		AI 1	4	Current
24	NOT USED				

Table A.4 Schematic reference, part 1

Schematic Reference	Description	Abbrev.	Item Type
A1	Compressor	K	Actuator
A2	Evap 1 Expansion Valve	EEV1	Actuator
A3	Evap 2 Expansion Valve	EEV2	Actuator
A4	Evap 2 Discharge Valve	SDR	Actuator
A5	Evap 1 Water Flow Valve	WFV1	Actuator
A6	Evap 2 Water Flow Valve	WFV2	Actuator
AEV-E2	Evap 2 Auxilary Expansion Valve--AEV	AEV	Auxilary
G1	High Pressure Gauge	G1	Gauge
G2	Low Pressure Gauge	G2	Gauge
M1	Venturi	V	Miscellaneous
M2	Liquid Receiver	LR	Miscellaneous
M3	Filter Drier	FD	Miscellaneous
M4	Condenser Water Chiller	CWC	Miscellaneous
MV1	Liquid Receiver Inlet Shutoff	LRI	Manual
MV10	Evap 2 Discharge Shutoff	E2-4-D	Manual
MV11	Evaporator Manifold Discharge Shutoff	E-1	Manual
MV12	Low Pressure Access (Suction/Fill)	K-1	Manual
MV13	Evap 2 Auxilary Expansion Valve Selector	E2-6	Manual
MV14	Evap 2 Auxilary Expansion Valve Shutoff	E2-5	Manual
MV2	Liquid Receiver Bypass Valve	LRB	Manual
MV3	Liquid Receiver Outlet Shutoff	LRO	Manual
MV4	Evap 1 Inlet Shutoff (EEV)	E1-1	Manual
MV5	Evap 1 Auxilary Expansion Valve Inlet Shutoff	E1-2	Manual
MV6	Evap 1 Discharge Shutoff	E1-3-D	Manual
MV7	Evap 2 Inlet Shutoff (EEV)	E2-1	Manual
MV8	Evap 2 TXV Inlet Shutoff	E2-2	Manual
MV9	Evap 2 AEV Inlet Shutoff	E2-3	Manual

Table A.5 Schematic reference, part 2

Schematic Reference	Description	Abbrev.	Item Type
MWV01	Water System Drain (Condenser Tank)	MWV1	Water Flow
MWV02	WP1 Inlet Shutoff	MWV2	Water Flow
MWV03	WP1 Outlet Shutoff	MWV3	Water Flow
MWV04	Condenser Top Tank Overflow Shutoff	MWV4	Water Flow
MWV05	Condenser Water Line Air Bleed (1/2")	MWV5	Water Flow
MWV06	Condenser Water Flow Valve (Manual)	MWV6	Water Flow
MWV07	Condenser Discharge Diverter--Evap 1	MWV7	Water Flow
MWV08	Condenser Discharge Diverter--Evap 2	MWV8	Water Flow
MWV09	WP2 Inlet Shutoff	MWV9	Water Flow
MWV10	WP2 Outlet Shutoff	MWV10	Water Flow
MWV11	Evap 1 Top Tank Overflow Shutoff	MWV11	Water Flow
MWV12	Evap 1 Water Line Air Bleed (1/2")	MWV12	Water Flow
MWV13	Evap 1 Water Discharge Shutoff	MWV13	Water Flow
MWV14	WP3 Inlet Shutoff	MWV14	Water Flow
MWV15	WP3 Outlet Shutoff	MWV15	Water Flow
MWV16	Evap 2 Top Tank Overflow Shutoff	MWV16	Water Flow
MWV17	Evap 2 Water Line Air Bleed (1/2")	MWV17	Water Flow
MWV18	Evap 2 Water Discharge Shutoff	MWV18	Water Flow
MWV19	Condenser Water Line Fill Access Valve	MWV19	Water Flow
MWV20	Evap 1 Water Line Fill Access Valve	MWV20	Water Flow
MWV21	Evap 2 Water Line Fill Access Valve	MWV21	Water Flow
MWV22	Water System Fill Access Valve	MWV22	Water Flow

Table A.6 Schematic reference, part 3

Schematic Reference	Description	Abbrev.	Item Type
S02	Differential Pressure (Vapor mass flow)	C_RM	Transducer
S03	Condenser Pressure	PCRO	Transducer
S04	Evap 1 Refrigerant Mass Flow	E1_RM	Transducer
S05	Evap 1 Pressure	PERO1	Transducer
S06	Condenser Water Mass Flow	C_WM	Transducer
S07	Evap 1 Water Mass Flow	E1_WM	Transducer
S08	Evap 2 Water Mass Flow	E2_WM	Transducer
S09	Evap 2 Refrigerant Mass Flow	E2_RM	Transducer
S11	Evap 2 Pressure	PERO2	Transducer
T01	Condenser Refrigerant Inlet Temperature	TCRI	Thermocouple
T02	Condenser Refrigerant Outlet Temperature	TCRO	Thermocouple
T03	Evap 1 Refrigerant Inlet Temp.	TERI1	Thermocouple
T04	Evap 1 Refrigerant Outlet Temp.	TERO1	Thermocouple
T05	Evap 2 Refrigerant Inlet Temp.	TERI2	Thermocouple
T06	Evap 2 Refrigerant Outlet Temp.	TERO2	Thermocouple
T07	Condenser Water Inlet Temperature	TCWI	Thermocouple
T08	Condenser Water Outlet Temperature	TCWO	Thermocouple
T09	Evap 1 Water Inlet Temp.	TEWI1	Thermocouple
T10	Evap 1 Water Outlet Temp.	TEWO1	Thermocouple
T11	Evap 2 Water Inlet Temp.	TEWI2	Thermocouple
T12	Evap 2 Water Outlet Temp.	TEWO2	Thermocouple
TXV-E2	Evap 2 Auxilary Expansion Valve--TXV	TXV	Auxilary
WP1	Condenser Water Pump	WP1	Water Flow
WP2	Evap 1 Water Pump	WP2	Water Flow
WP3	Evap 2 Water Pump	WP3	Water Flow

Table A.7 Figure to data file cross reference

Figure	Data File (*.mat)
2.29	Data_Proc_04_25_08_T4
3.7	Data_Proc__SYSID_08_08_07_T1_RPM
3.8	Data_Proc__SYSID_08_08_07_T1_RPM
3.9	Data_Proc__SYSID_08_08_07_T1_RPM
3.10	Data_Proc__SYSID_08_08_07_T1_RPM
3.11	Data_Proc__SYSID_08_08_07_T1_RPM
3.12	Data_Proc__SYSID_08_08_07_T1_EEV
3.13	Data_Proc__SYSID_08_09_07_T2_SDR
3.14	Data_Proc__SYSID_08_14_07_T1_H2O1
3.15	Data_Proc_01_25_08_T1
3.16	Data_Proc_01_25_08_T1
3.17	Data_Proc__SYSID_08_08_07_T1_EEV, Data_Proc__SYSID_08_08_07_T1_RPM, Data_Proc__SYSID_08_14_07_T1_H2O1
3.18	Data_Proc__SYSID_08_08_07_T1_EEV, Data_Proc__SYSID_08_08_07_T1_RPM
3.19	Data_Proc__SYSID_08_08_07_T1_EEV, Data_Proc__SYSID_08_08_07_T1_RPM, Data_Proc__SYSID_08_14_07_T1_H2O1
4.1	Data_Proc_01_25_08_T1
4.3	Data_Proc_04_30_08_T2
4.4	Data_Proc_04_30_08_T2
4.5	Data_Proc_04_30_08_T2
4.6	Data_Proc_04_30_08_T1
4.7	Data_Proc_04_30_08_T1
4.8	Data_Proc_04_30_08_T1
4.10	Data_Proc_04_17_08_T3
4.11	Data_Proc_04_17_08_T3
4.12	Data_Proc_04_17_08_T3
4.13	Data_Proc_04_21_08_T2
4.14	Data_Proc_04_21_08_T2
4.15	Data_Proc_04_21_08_T2
4.16	Data_Proc_04_21_08_T2
4.17	Data_Proc_04_21_08_T2
5.4	Data_Proc_02_29_08_T1, Data_Proc_03_06_08_T1
5.6	Data_Proc_03_10_08_T5
5.10	Data_Proc_04_21_08_T1
5.12	Data_Proc_10_17_07_T1
5.13	Data_Proc_10_17_07_T2
5.15	Data_Proc_04_21_08_T3
5.16	Data_Proc_04_21_08_T3
5.17	Data_Proc_04_21_08_T3
5.18	Data_Proc_04_21_08_T3
5.19	Data_Proc_04_21_08_T3
5.20	Data_Proc_04_25_08_T1, Data_Proc_04_25_08_T2, Data_Proc_04_25_08_T3, Data_Proc_04_21_08_T3
5.21	Data_Proc_04_25_08_T1, Data_Proc_04_25_08_T2, Data_Proc_04_25_08_T3
5.22	Data_Proc_04_25_08_T1, Data_Proc_04_25_08_T2, Data_Proc_04_25_08_T3
5.24	Data_Proc_04_25_08_T4, Data_Proc_04_25_08_T5
5.25	Data_Proc_04_21_08_T4
5.26	Data_Proc_04_21_08_T4
5.27	Data_Proc_04_21_08_T4
5.28	Data_Proc_04_21_08_T4
5.29	Data_Proc_04_28_08_T1, Data_Proc_04_28_08_T2
5.30	Data_Proc_04_28_08_T1, Data_Proc_04_28_08_T2
5.31	Data_Proc_04_28_08_T1, Data_Proc_04_28_08_T2

VITA

Name: Matthew Stuart Elliott
Address: TAMU 3123, College Station, TX, 77843

Email Address: matt.elliott@gmail.com

Education: B.S., Mechanical Engineering, Texas A&M University, 2000
M.S., Mechanical Engineering, Texas A&M University, 2008

Experience: Graduate Assistant—Research, TAMU Dept. of Mech. Engr.
8/2006-present, College Station, Texas.

Graduate Assistant—Teaching, TAMU Dept. of Mech. Engr.
1/2006-8/2006. College Station, Texas.

Product Engineer, Oil States Industries.
1/2002-1/2006. Houston, Texas.

Project Engineer, Unifab International West.
4/2001-12/2001. Lake Charles, Louisiana.

Project Engineer, AER Manufacturing.
6/2000-4/2001. Carrollton, Texas.

Affiliations: ASME, 1994-present.

ASHRAE, 2006-present.

IEEE, 2006-present.

Engineer-in-Training, State of Texas, #32396.